ANALYSIS OF WATER LEVEL MEASUREMENTS USING GPS

DISSERTATION

Presented in Partial Fulfillment of the Requirements for

the Degree Doctor of Philosophy in the Graduate

School of The Ohio State University

By

Kai-chien Cheng, M.S.

* * * * *

The Ohio State University
2005

Dissertation Committee:

Professor C. K. Shum, Adviser

Professor Michael Bevis

Doctor Stephane Calmant

Professor Burkhard Schaffrin

Approved by

_____

Adviser

Graduate Program in
Geodetic Science and Surveying

ABSTRACT

Accurate knowledge about sea level and its change is essential to humanity because a large proportion of the Earth's population lives in coastal regions. This study discusses the existing techniques for sea level measurements, including the use of different types of gauges (e.g., water level gauge or tide gauge, and bottom pressure gauge), as well as GPS and satellite altimetry. The GPS water level measurements from a buoy or a vessel are presented and utilized in this study along with other techniques to collect ellipsoidal, geocentric sea surface height measurements for various studies that help improve our knowledge about sea level and its change.

An operational technique of using GPS water level measurement is proposed in this study. The limitation and an upper bound accuracy of the kinematic (epoch-by-epoch) positioning in terms of baseline length are discussed. A set of GPS data in Lake Erie, including buoy data as well as a local GPS network on land, are used to provide the numerical results.

Three main applications of using the GPS water level measurements are presented in this study. They are integration of various data sources in the coastal, satellite radar calibration, and GPS hydrology. The objective of these applications is to demonstrate the potential of the GPS technique in collecting water level measurements. The use of GPS

measurements is also highlighted in connection with the improvement that they may bring to various techniques such as the use of coastal water level gauge and bottom pressure gauge, and satellite altimetry.

The water level gauges are the traditional tools to collect water level data in the coastal areas. A bottom pressure gauge, on the other hand, is deployed away from the shore that senses pressure change in order to infer sea surface variation in terms of depth. Both types of gauges provide only relative measurements, and the land, where they are installed, is subject to the local vertical land movement. In order to take advantage of the large amount of gauge records, a GPS buoy/vessel occupation can be made to link their relative measurements to the global reference frame. This facilitates the integration use of the gauge records to the satellite measurements from altimeters as well as from the GPS technique.

Since studies of global sea level rise using satellite altimetry examine the signal whose magnitude is about 1–2 mm/year, the constant altimeter range bias and the drift should be calibrated and accounted for with the calibration sites around the world. In this study, two calibration sites—the Lake Erie Calibration Site and the South Pacific Calibration Site—were established to support such a global effort for altimeter calibration. The Lake Erie Site uses a coastal water level gauge off the satellite track by 20 km and still produces comparable results compared with others. The establishment of both sites will be address and the instruments for water level measurements involved are: GPS buoys, vessels, satellite altimeters, coastal water level gauge, and bottom pressure gauge.

The GPS water level measurements were also made to provide the river stage height in the Branco River, a tributary of the Amazon River. The stage height along the river is surveyed with a GPS ship. The stage gradient, which is the primary information for quantify sedimentation of the river, is estimated from the GPS ship data. The standard deviation is better than ±0.4 cm/km, which is consistent with other studies in this area.

This study discusses three applications of using GPS water level measurements. They have shown the capabilities of the GPS technique on buoys or vessels to interact with other techniques for making accurate water level measurements. With the water impacts humanity, such measurements have proven to be valuable for better understanding for the coastal environment.

I dedicate this dissertation to my family.

ACKNOWLEDGEMENTS

I would like to express my gratitude to Prof. C. K. Shum, my adviser for the inspiring thoughts, encouragement and generous support throughout this study. I thank Dr. Stephane Calmant of the Laboratoire d'Etudes en Geophysique et Oceanographie Spatiales, Centre National d'Etudes Spatiales for providing the opportunity to work on the MOTEVAS project. I am truly thankful to Profs. Michael Bevis and Burkhard Schaffrin for their constructive comments on this study. I am particularly grateful to Dr. Michael Parke of the College of Engineering for his help building the GPS buoy, sharing field work experience and participation in the GPS buoy campaigns. The help from Dr. Yuchan Yi in providing valuable instructions on the use of altimetric stackfile and from Dr. Gerald Mader of the National Geodetic Survey in permitting the use of Kinematic and Rapid Static (KARS) software is greatly acknowledged. I would also like to thank my colleagues and friends, including: Yiqun Chen, Shengjie Ge, Chung-Yen Kuo, Peter Luk, Doug Martin, Justin Shum, Hong-Zeng Tseng, and Harsh Vangani for their participation in the GPS field work. Also, I acknowledge Kyle Snow for sharing helpful experience on the GPS network adjustment software. Special thanks go to Joktan Kwiatkowski for proof-reading the English writing of this document.

Finally, I would like to express my deepest appreciation to my parents, family members, my dear wife Yu-yun Lin and daughter Jamie for their love, encouragement and support throughout the time of this study.

This research is supported by grants from the Ocean, Ice and Climate Program, Earth Science Enterprise Program (NGA5-12585), Earth Observing System Interdisciplinary Science Program (NAG5-9335) of the National Aeronautics and Space Administration, the Information and Intelligent Systems Digital Government Program (IIS-0091494) of the National Science Foundation, and the Ohio State Sea Grant (No. R/CE-5) via funding from the National Oceanic and Atmospheric Administration.

VITA

October 14, 1969.....Born in Chaiyi, Taiwan.

1992.....B.S. Surveying Engineering, National Cheng Kung University.

1994.....M.S. Surveying Engineering, National Cheng Kung University.

1997.....Specialist, Taipei City Government, Taiwan.

1997–present.....Graduate Research Associate, The Ohio State University.

1999–2002.....Graduate Teaching Associate, The Ohio State University.

2001.....M.S. Geodetic Science, The Ohio State University.

PUBLICATIONS

Research Publication

1. Calmant, S., K. Cheng, G. Jan, C. Kuo, C. Shum, Y. Yi, V. Ballu and M.-N. Bouin. 2004. Comparison of sea surface heights derived from satellite altimetry and from ocean bottom pressure gauges: the SW Pacific MOTEVAS Project. *Marine Geodesy* 27:597–613.

2. Cheng, K. 2004. *GPS Buoy Campaigns for Vertical Datum Improvement and Radar Altimeter Calibration.* Report No. 470. Geodetic Science and Surveying in the Department of Civil and Environmental Engineering and Geodetic Science, the Ohio State University, Columbus, Ohio, USA.

3. Cheng, K. 2004. *Radar Altimeter Absolute Calibration Using GPS Water Level Measurements.* Report No. 469. Geodetic Science and Surveying in the Department of Civil and Environmental Engineering and Geodetic Science, the Ohio State University, Columbus, Ohio, USA.

4. Shum, C., Y. Yi, K. Cheng, C. Kuo, A. Braun, S. Calmant, and D. Chambers. 2003. Calibration of Jason-1 altimeter over Lake Erie. *Marine Geodesy* 26:335–54.

5. Cheng, K., C. Shum, C. Han, Y. Yi, and D. Martin. 2001. Application of GPS-buoy water level instrument for radar altimeter calibration. In *Gravity, Geoid, and Geodynamics 2000 : GGG2000 IAG International Symposium,* International Association of Geodesy Symposa, Sym. 123. Edited by M.G. Sideris. Berlin: Springer.

6. Cheng, K. 2001. Radar altimeter absolute calibration using GPS water level measurements. *Master Thesis.* The Ohio State University, Columbus, Ohio, USA.

7. Cheng, K. 1994. A case study of an operational GIS–A TRTS case. *Master Thesis,* in Chinese, National Cheng Kung University, Tainan, Taiwan.

FIELDS OF STUDY

Major Field: Geodetic Science and Surveying.

TABLE OF CONTENTS

Page

LIST OF TABLES

LIST OF FIGURES

CHAPTER 1

INTRODUCTION

Global sea level fluctuations present a direct influence to those who live near the coast. Sea level rise impacts humanity with the potential to alter ecosystems and habitability in coastal regions, where a large proportion of the worldwide population lives (Douglas, 2001). For example, Cohen et al. (1997) estimated in 1994 that about 2.1 billion people, which represented approximately 37% of the world's population, lived within 100 km of a coast. The importance of monitoring sea level rise is evident. Therefore, various techniques have been employed for sea level or water level measurements such as the coastal water level gauges and satellite altimetry. In this study, it is intended to demonstrate the potential of Global Positioning System (GPS) buoy/vessel water level measurements to complement other techniques such as satellite altimetry and the use of tide gauges or water level gauges. The following sections discuss the background information of the techniques for water level measurements. They include GPS, tide (water level) gauges, and satellite altimetry.

One of the objectives of this study is the development of the challenging technique to collect water level measurements with GPS buoy, or using GPS on a vessel. The current technical limitations of using GPS buoy, including baseline length, along with other issues, will be presented. The information is intended also to benefit planning GPS buoy/vessel campaigns.

Three applications using GPS buoys and vessels will be presented in this study in order to demonstrate their potential. They include: the integrated use of various data sources in the coastal area, satellite altimeter calibration and GPS hydrology. In addition, the choice of the underlying adjustment models for GPS water level data processing will be discussed.

1.1 Global Positioning System

The NAVSTAR GPS (NAVigation System with Time And Ranging/Global Positioning System) is a principal component of the global navigation satellite system (GNSS). It is a satellite-based radio navigation system that provides precise three-dimensional position, navigation and time information to suitably equipped users. It is intended to provide the position at any given location in the world in terms of coordinates defined in a geocentric earth-fixed reference frame such as the International Terrestrial Reference Frame (ITRF).

Other components of GNSS include the Russian GLObal NAvigation Satellite System (GLONASS) and the European GALILEO project. GLONASS is a Russian space-based navigation system comparable to the NAVSTAR GPS (Lebedev, 1998). The deployment of the full constellation of satellites was completed in late 1995 (Andrews Space & Technology, 2001). GALILEO is a European initiative, which provides accurate and guaranteed global positioning services under civilian control with the new L3 civil signal. It is anticipated to be operational in 2008 (European Commission, 2003). All systems are intended to be interoperable with other systems for better accuracy.

1.1.1 GPS constellation

The current GPS constellation consists of 29 operational satellites in six near circular orbital planes, which are evenly spaced with the inclination of 55° with respect to the equator and a 12-hour period. Figure 1.1 presents the artist's rendering of the GPS constellation. The orbital altitudes are 20,200 km above the earth so that there are at least four satellites available simultaneously above the horizon anywhere on the earth, 24 hours a day (Hofmann-Wellenhof et al., 1997).

SVN 13 through 21 are designated for the Block II satellites, which are designed to provide 14 days of operation without the contact from the control segment. SVN 22 through 40 are designated for the Block IIA (A denotes Advanced) satellites. They represent the second series of the operational satellites and are designed to provide 180 days of operation with autonomy. However, the degrading accuracy is evident in the

Figure 1.1. Artist's concept of GPS constellation (Courtesy of R. Rummel).

navigation message near the end of (180 days) autonomy (U.S. Naval Observatory, 2005). SVN 41 through 62 are given to the Block IIR (R denotes Replenishment) satellites. Similar to the previous Block II/IIA satellites, they are designed to provide at least 14 days of operation without the contact from the control segment and up to 180 days of operation when operating in the autonomous navigation mode. The designed life of the Block II/IIA satellites is about 7.3 years and that of the Block IIR is 7.8 years (U.S. Naval Observatory, 2005).

The next generation satellites are in development, including the Block IIR-M (M denotes military-use-only M-code), the Block IIF (F denotes Follow-on), and the Block III. The current implementation plan and the proposed capabilities for these new satellites are listed in Table 1.1. The current status of the Block II/IIA/IIR satellites is provided by the U.S. Naval Observatory online at ftp://tycho.usno.navy.mil/pub/gps/gpstd.txt.

Satellites	Proposed capabilities
Block IIR-M	- 8 satellites - new civilian signal (L2C) on L2 - M-code on L1/L2 - 1st launch is planned to be in fiscal year of 2005
Block IIF	- 12 satellites - IIR-M capabilities with the additional 3rd civilian signal on L5 - 1st launch is planned to be in fiscal year of 2006
Block III	- architecture studies are underway to define the new capabilities - IIF capabilities with increased power/security/accuracy/availability. - future signals (e.g., L1C with anti-jam capability) - 1st launch is planned to be in fiscal year of 2012.

Table 1.1. The proposed next generation GPS satellites (Clark, 2004).

1.1.2 GPS principle and DGPS

The principle of GPS positioning is trilateration. The three-dimensional coordinates of the antenna position and the receiver clock error can be solved for, provided that sufficient (usually more than four) satellites are simultaneously tracked and their positions are accurately provided. The position and velocity vectors of each satellite can be acquired from the broadcast ephemerides. With longer latency, more precise ephemerides are provided by the International GPS Services (IGS). For example, the accuracy of the orbit and of the satellite clock in the final product (~13 days latency) from IGS is less than 5 cm and 0.1 nano (10^{-9}) second, respectively (Neilan et al., 2004). The

positioning accuracy can be improved with more observations either from other satellites that are simultaneously tracked or from the same set of satellites with longer observing time.

The range from an antenna to a satellite can be obtained from two GPS observables: pseudoranges (from codes) and phase ranges. The pseudorange observable is a measure of the distance between the satellite and the receiver's antenna, referring to the epoch of emission and reception of the codes (Leick, 1994). The range can be determined by multiplying the speed of light to the total travel time, which is inferred from correlating the identical pseudo-random noise (PRN) of the received codes to the receiver-generated replica. On the other hand, the range can also be expressed by the total number of waves, including the integer and the fractional parts, multiplied by the wavelength of the carrier wave (Langley, 1993). The phase observable is the fractional part of the phase difference between the received wave and that of the internal receiver oscillator. The integer part of the exact number of carrier waves from each satellite to the antenna, called the initial integer ambiguity, remains unknown and needs to be solved for. Leick (1994) states that the correct ambiguity solution is a key to achieve cm-level accuracy in the kinematic applications. Christensen et al. (1994) mentioned that reliable pseudoranges from codes could be used to constrain ambiguity resolution. It is common to use both code and phase observations, provided that the receiver is equipped with such capabilities.

Both codes and phases are derived from the fundamental frequency of 10.23 MHz. The chip rate of the P-code is the fundamental frequency and that of the C/A (Coarse/Acquisition) code is one tenth of the fundamental frequency (i.e., 1.023 MHz).

The L1 carrier is derived from multiplying the fundamental frequency by 154, whereas the L2 carrier is obtained from multiplication by 120. As a result, the length per chip for the C/A code is about 293 m and that for the P-code is about 29.3 m. On the other hand, the wavelength for the L1 and L2 carriers is about 19 cm and 24 cm, respectively. The phase range is, therefore, more accurate and usually preferred in the applications that demand high precision because of the shorter wavelength of the carrier wave compared with the codes (El-Rabbany, 2002).

The simple setting of the Differential GPS (DGPS) involves the cooperation of two receivers: One is referred to the reference station (whose coordinates are known with the associated variance and covariance); the other is referred to the rover (whose coordinates are to be determined while either being stationary like the reference station, or moving). With both receivers taking data simultaneously, the common errors such as the clock synchronization errors and the tropospheric range delays can frequently be canceled out by differencing the observations of both receivers with respect to the same set of satellites. DGPS provides the rover's coordinates with respect to the reference station due to the differencing; that is, the coordinate components of the relative position vector from the reference station to the rover's positions. In addition, as the separation between the reference station and the rover's position (called the baseline) increases, the fewer common satellites are simultaneously tracked, and also the troposphere condition at both ends of the baseline starts to decorrelate (Goad, 1998). As a result, the differencing can no longer eliminate as much tropospheric range delay error as it would when the rover is near the reference station. Hence, the rover's position accuracy depends on that of

the reference station's coordinates and the baseline length. Seeber (1993) pointed out that the baseline accuracy of DGPS could reach ±(0.5 cm + 1 part per million of the baseline length).

1.1.3 GPS water level measurements

The GPS water level measurements are the GPS observations (codes and phases) collected on floating platforms, which include different types of buoys and vessels. The height of the GPS antenna phase centers above the waterline is strictly maintained in order to refer the GPS solutions to the water surface, on which the buoy or the vessel was deployed. It also involves specifying the correct antenna type in the data processing as incorrect antenna types may result in up to 10 cm error in the height solution (Mader, 1999). Therefore, close attention needs to be paid to the GPS antenna height, to be exact, the height of the antenna reference point (ARP) with respect to the waterline of the buoy or the vessel, in order to accurately refer the APR to the water surface.

Various technical issues about the wave form, the sampling rate, the baseline length and others are addressed in this study. The buoy (or vessel), is positioned using the DGPS technique in the kinematic mode with respect to the onshore reference stations, whose coordinates and associated variances and covariances are known. Therefore, the baseline lengths as well as the accuracy of the reference stations are crucial to the kinematic positioning accuracy. In this study, the buoy solutions from different reference stations are employed in order to compare and analyze the impact of the baseline length.

The GPS water level measurements collected by a buoy system is still a new technique especially in the application of satellite altimeter absolute calibration (Schöne, 2000). Its design and implementation vary, but it is generally used to observe geocentric ssh and other oceanic phenomena such as wave heights, sea states, tides, water depths, and the surface topography. The potential applications of GPS water level measurements include satellite altimeter calibration (e.g., Shum et al., 2004; Calmant et al., 2004), the verification of GPS reflection applications (Cardellach et al., 2000), validation of water storage for large river (e.g., Frappart et al., 2005), and determination of the boundary conditions for numerical models (Mader et al., 2001).

1.2 Water level gauge

This section clarifies the terminology of tide (or water level) gauge and introduces two types of them used in this study: the coastal tide (or water level) gauge, and the bottom pressure gauge (BPG).

The water level gauge, illustrated in Figure 1.2, is a device installed onshore and is able to collect a time series of the relative water level with respect to local benchmarks. Emery and Aubrey (1991) mentioned that the early interest in water level was far more concerned with the timing of the tide than with its height. This is so, in part, because in the past it was important to know the time of high tides in order to navigate large ships into the port. The gauges that were developed for that reason are rightly called tide gauges, since they provide the timing of the tides that were of principal interest then.

However, the concern about the magnitude of water level change has recently raised more interest. Studies using long-term (~100 years) island and coastal gauge records indicate a global sea level rising rate of 1.8 to 1.9 mm/year for the last century (e.g., Douglas, 1997; Trupin and Wahr, 1990). The gauges used in these studies collect water level heights (which contain tidal information) to determine the changing magnitude, and are thus called water level gauges, especially for those operating in the lakes (e.g., Great Lakes), which have negligible or little tides. This concept of naming is advocated by NOAA and is adapted in this study also. The reader should keep in mind that the terminology is the same as "tide gauge" found in part of the literatures.

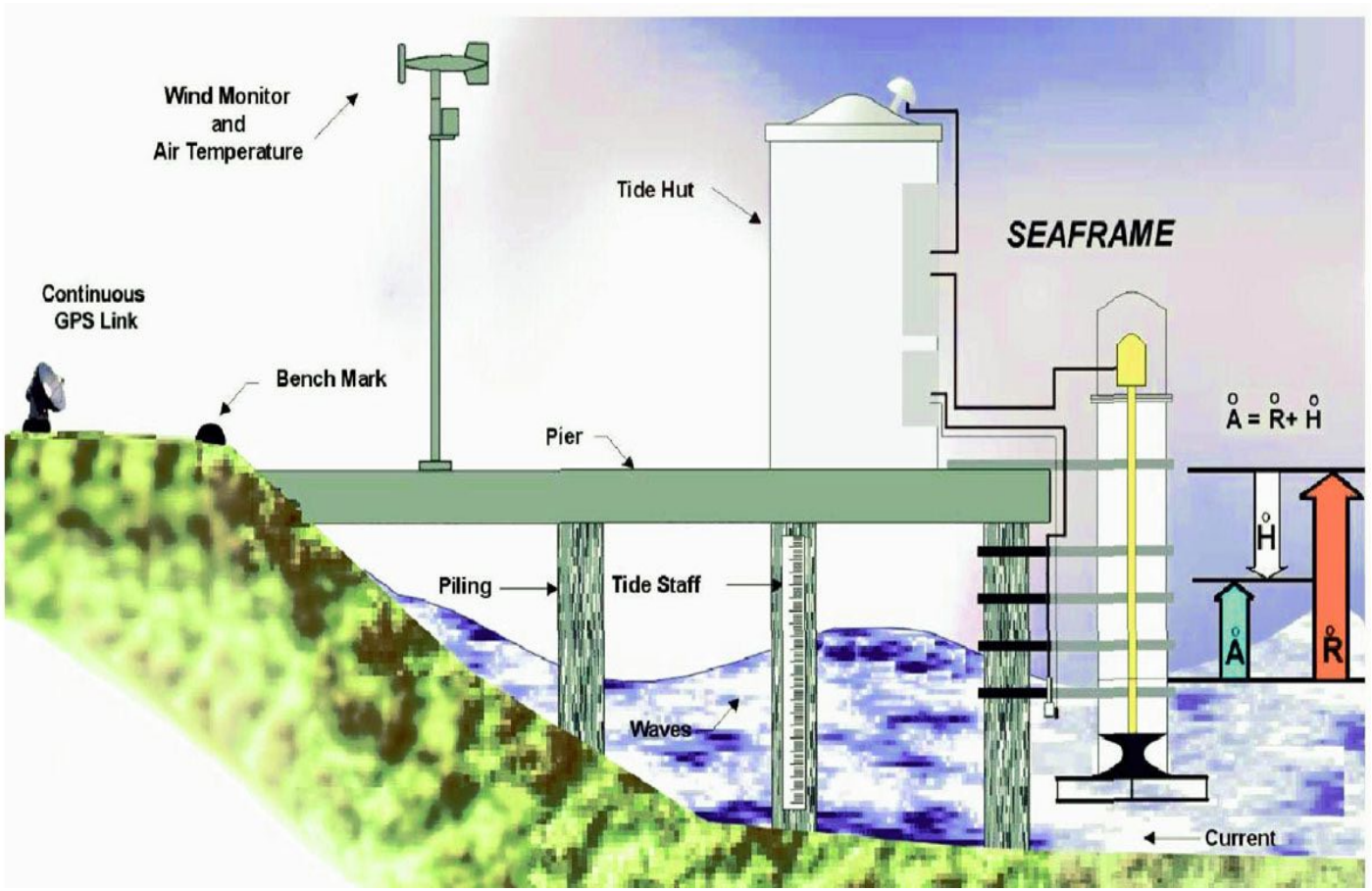

Figure 1.2. The coastal water level (tide) gauge diagram (courtesy of J. Luick).

The coastal water level gauge is a common instrument for measuring water levels. It provides a time series of the water level which, at some places, covers several decades. As shown in Figure 1.2: *A* denotes the water level measurements with respect to the instrumental zero point. *R* denotes the offset from the benchmark to the zero point. As a result, the water level measurements with respect to the benchmark, *H*, can be obtained. One problem of using the water level gauge is that it is based on a relative measurements. The vertical movement of the benchmark is not easy to identify from the gauge record. Recently, continuous GPS (CGPS) observations at the site of a water level gauge have been proposed in order to observe the vertical movement of the benchmark. In fact, the International Association of Geodesy (IAG) and others have formed a "CGPS at Tide Gauge" (CGPS@TG) joint Working Group to advocate the concept and to experiment with the idea. As a result, the relative water level measurements from a water level gauge can be referenced to the geocentric reference frame, which is claimed to be more stable than the local benchmarks (Bevis et al., 2002).

As opposed to the coastal gauge, a bottom pressure gauge can be deployed off the coast. It senses the total pressure at the bottom of the sea floor, which is the addition of the water and the atmospheric pressure above it. Its auxiliary data include seawater temperature and salinity. It provides the depth and depth variation inferred from a hydrostatic relation. As a result, it is also a tool to indicate the relative water level with respect to its deployed depth. Its relative water level measurements, similar to that of a coastal water level gauge, are subject to the vertical movement of the deployment location.

The bottom pressure gauge has been extensively used in the open ocean to measure tides (Filloux, 1980). However, Christensen et al. (1994) pointed out that one significant error source is the instrumental drift. It is not a practical instrument for sea level measurements unless proper calibration is performed regularly. Its water level variation can be linked to the geocentric reference frame with the GPS buoy/vessel occupation (e.g., Bouin et al., 2003). The detailed procedure will be discussed in Chapter 4.

1.3 Satellite radar altimetry

Satellite radar altimetry is a revolutionary technology in oceanography to map the global ocean surface from space. It is able to observe global oceanic phenomena with unprecedented accuracy of cm-level in ssh. Its temporal resolution is 1–2 weeks, and its spatial resolution is about 50 km (Shum et al., 2003).

The principle of satellite radar altimetry is relatively straightforward. It sends out the electromagnetic radar pulse and collects the reflected signal after the radar pulse is bounced back by the water surface. The one-way signal travel time can be inferred from the power distribution of the reflected radar pulse. Consequently, the range between the satellite and the instantaneous water surface can be determined by multiplying the speed of light with the one-way travel time. If the satellite position is accurately tracked, the ellipsoidal ssh above the geocentric reference ellipsoid can be obtained approximately by subtracting the range from the altitude of the satellite. Radar altimetry is exclusively

designed for oceans because of the favorable reflectivity of the radar signals over large water bodies. Alternate radar waveform retracking algorithms have been developed for measurements of ice sheet, sea ice, river, lakes, and land elevation. Recently, the Ice, Cloud, and land Elevation Satellite (ICESat) laser altimeter mission of the National Aeronautics and Space Administration (NASA) of the United States (U.S.) represents an alternate satellite altimetry with much finer footprint (80 m) compared to that of radar altimeter (km), and capable of providing accurate measurements on various surface types (ice, river, land, and lake) other than ocean (e.g., Braun et al., 2004).

There are three fundamental measurements that can be derived from a satellite radar altimeter: geocentric ssh, wave height, and wind speed. They are all inferred from the waveform analysis of the radar return. Several corrections are applied in order to provide more accurate ssh measurements. These corrections, categorized into instrumental, media, and geophysical corrections, are discussed in detail in Chapter 4.

Satellite altimetry ideally provides the ellipsoidal ssh above the geocentric reference ellipsoid that is not subject to the local vertical motion of the land. Therefore, the comparison of the altimeter ssh measurements to the water level gauge data provides a general idea of the vertical movement of the gauges and of the solid Earth, on which the gauges are installed. For example, Kuo et al. (2004a,b) used altimeter ssh measurements to analyze the vertical movement of the water level gauges and of the solid Earth in the Great Lakes and Fennoscandia, respectively.

1.4 Summary

This chapter introduced the conventional ways of collecting water level measurements. The water level gauge (or tide gauge) is one of the traditional methods, has a long data span, and is valuable for the determination of the long-term sea level trend. The BPG provides depth and depth variation, inferred from the pressure difference between the sea floor bottom and the atmosphere, provided that other auxiliary information such as profiles of salinity and temperature along the water column are available. Also, the instrumental drift of a BPG needs to be regularly calibrated. However, both coastal and bottom pressure gauges are subject to the local vertical movement of the ground, including land uplift/subsidence and glacial isostatic adjustment (GIA), which is the rebound of the solid Earth from the deglaciation since the last Ice Age.

The GPS buoy systems and GPS-equipped vessels also demonstrate their potential in collecting water level measurements. If DGPS is used, the water level measurements are relative to the reference stations. Hence, similar to the water level gauge, the local vertical movements affect the result. In addition, the baseline length plays an important role in DGPS determination of the GPS buoy/vessel locations. Thus the GPS buoy/vessel applications are limited to the coastal area.

Satellite altimetry ideally provides ellipsoidal ssh above the chosen, geocentric reference ellipsoid in oceans and large inland lakes. Its accuracy depends on the instrument and the corrections, which are either obtained by instruments or from other

empirical models. The total time span of the multiple missions are relatively short (a decade or so). However, the combination of satellite altimeters and water level gauges is beneficial: The local vertical motion of the gauge can indirectly be monitored with altimeters, whereas the long-term gauge records help to fill in the time series when the altimeter measurements are unavailable. Moreover, the gauge data are collected near the sore by land, whereas the altimeter measurements are done over the oceans. Thus, they are spatially complementary. The GPS buoy can be utilized to link a gauge datum to the geocentric reference frame, to which altimeters refer. The details are presented in Chapter 3.

The following Chapter 2 discusses GPS buoy data processing, and provides tests for the impact of baseline lengths on the vertical accuracy, with data collected in Lake Erie in 2003. Chapter 3 then presents the idea of linking a water level gauge datum to the geocentric reference frame. The common vertical datums used in the Great Lakes, their conversions, and the associated error budget are also presented. Chapter 4 will introduce the principle of satellite altimetry and the use of GPS water level measurements as *in-situ* data for altimeter absolute calibration. The detailed implementation and the current results from two calibration sites will be reported. The use of GPS in conjunction with other satellite-based techniques such as radar altimetry and the river gauge in the Amazon Basin for a hydrological application is discussed in Chapter 5. Chapter 6 addresses the choice of the adjustment models for the GPS water level data processing. Finally, Chapter 7 provides conclusion for this study.

CHAPTER 2

THE GPS BUOY AND ITS DATA PROCESSING

In this study, a GPS buoy system is defined as a floating buoy equipped with a geodetic GPS receiver, and one or more antennae near-shore occupied at the reference stations, whose coordinates are known with the associated uncertainty in terms of variances and covariances. The GPS buoy is capable of monitoring the buoy's position and velocity as a function of time in a geocentric earth-fixed coordinate system, or within the ITRF, using the GPS satellites. Since the buoy moves with the waves and may drift due to current and wind, its position is often processed on an epoch-by-epoch basis, or in kinematic mode, with DGPS from the onshore reference stations. As a result, a time series of the three-dimensional position vector of the buoy from the reference station can be obtained. Although various system designs exist, the height of the ARP above the waterline of the buoy is strictly maintained in order to accurately reference the vertical solution of the buoy to the water surface.

Depending on the application and the design of the buoy, the data processing scheme may be different. This study, with a small, compact floater-type buoy, focuses on the measurement of mean water surface height above the reference ellipsoid at one

location for applications such as altimeter calibration and determination of the geoid height. Therefore, the buoy is anticipated to be deployed at the desired location for a period of several hours in order to filter out the high fluctuation caused by the waves and the buoy's movement. The boat, to which the buoy is tethered, is usually anchored in order to maintain the position. This type of application requires higher accuracy for the buoy's position so the carrier phase observables are generally favored. Codes are used for determining the initial value of the ambiguities. Since the real-time position of the buoy is not of interest, the data collected by the buoy are post-processed after the fieldwork.

The buoy positioning involves several technical issues such as the accuracy of the reference station coordinates, baseline length, sampling rate, waves, ambiguity determination, and others. The weighted Partial MInimum NOrm LEast Squares Solution (P-MINOLESS) is used to solve for the coordinates and their variances at each station in the GPS network. It selects a number of certain fiducial stations and minimizes the norm of their coordinate increments after having minimized the weighted squared residuals of the observed baseline components. It maintains the inner consistency of the network by allowing the coordinates of each station in the network to change based on the given criteria (Snow, 2002).

Since the buoy's position is determined with the DGPS technique, the accuracy depends on the assumption that the atmospheric condition, especially the tropospheric delay, at both ends of a baseline is similar and will be significantly canceled out in differencing. However, as Goad (1998) pointed out, the atmospheric condition starts to decorrelate as the baseline length increases, and, therefore, complicates the determination of the buoy's location. The accurate ambiguities are also essential for the cm-level

kinematic positioning (Leick, 1994). Therefore, the GPS data from the buoy campaign near Cleveland in Lake Erie, and the data from a regional GPS network were used to analyze these technical issues. Both the GPS network (processed in the static mode) and the buoy position (processed in the epoch-by-epoch, or kinematic, mode) are analyzed with DGPS. A comparison of the epoch-by-epoch solution to the static solution of the GPS network is carried out with the objective of testing the agreement between them with different baselines. In addition, the buoy is positioned with different choices of the reference stations from the GPS network in order to verify the solutions derived from the longer baseline with that from the shorter one. The integer ambiguities of the buoy solution are verified with the multiple reference station approach. The sampling rates of 1-, 2-, and 5-seconds are also analyzed.

Section 2.1 reviews the GPS buoy system and discusses its current applications. Section 2.2 presents the waverider GPS buoy that was used in this study. Its advantages and disadvantages are addressed. Section 2.3 presents two GPS buoy campaigns in Lake Erie conducted as part of this research. The data collected from them were used in Section 2.4 to analyze the technical issues such as the impact of baseline length and sampling rate. Section 2.5 summarizes this chapter.

2.1 Review of GPS buoy applications

Schöne (2000) points out that GPS buoy systems are still a new technology, especially in the absolute calibration of satellite altimetry. The design and implementation vary and the applications include absolute calibration of satellite altimeters, observing oceanic phenomena such as water surface height, coastal circulation, ocean tides, and other coastal applications (Shum and Parke, 1999). The GPS buoy is able to provide ssh in the area where the satellite altimeter passes. The buoy-measured ssh serves as the *in-situ* water level information to be compared with altimeter ssh measurements.

Various GPS buoy designs have been used for satellite altimeter calibration, and their size ranges from a small life-saver type with the receiver and power supply on the tethered boat to a big, ruggedized type that accommodates all of the equipments, including the sensors that provide orientation as well as meteorological and auxiliary data for long-term deployment. The campaign style design requires dedicated personnel to operate it, whereas a ruggedized design, although more complex and expensive, is able to transmit observations automatically to the base station.

GPS buoys have been implemented for altimeter calibration in the past (e.g., Shum et al., 2003; Watson et al., 2003; Haines et al., 2002a, b; Liebsch et al., 2002; Cheng et al., 2001; Kruizinga, 1997; Schutz et al., 1995; Born et al., 1994; Hein et al., 1992; Rocken et al., 1990). Kelecy et al., (1994) showed the equivalent ssh measurements

between a waverider (a life-saver type) and a spar design for absolute altimeter calibration. However, Schöne (2000) notes that an intercomparison of the different designs is still needed.

In addition to the water level measurement, the buoy is capable of observing other oceanic phenomena. For example, Young et al. (1986) demonstrated the buoy's ability in water depth mapping. Hein et al. (1990) observed wave height and sea state with a GPS buoy. Born et al. (1994) analyzed the wave height spectrum with data from a buoy. Key et al. (1998) and Shum et al. (2003) used GPS buoys to determine the mean water surface gradient in the open sea and in large inland lakes, respectively.

The GPS buoy can also be used in geodetic applications. For example, the National Geodetic Survey (NGS) uses buoys for a height modernization project, seeking the use of GPS data on land and oceans to improve the determination of the local geoid height and, thus, promoting GPS applications on measuring elevation, which is traditionally done by spirit leveling. Also, Zilkoski and D'Onofrio (1996) implemented a GPS-equipped ship and a buoy (ruggedized type) in the San Francisco Bay for the NGS height modernization project with an ultimate goal of mapping the bottom of the Bay in a geocentric reference frame such as ITRF, and using GPS on ships in an electronic chart display to transit the Bay and dock during low visibility.

In linking water level gauge records to other data derived from satellite techniques, the buoy can be deployed next to the water level gauge in order to determine the local geoid height, or to link the benchmark of the gauge to the geocentric reference frame. Li et al. (2002) proposed to combine different data sources in the coastal region with a hydrodynamic model, including the ssh measurements from a GPS buoy and from

satellite altimeters, satellite remote sensing images, a digital elevation model (DEM) as well as bathymetry and water level gauge data, to map the shoreline of Lake Erie in a digital format and to integrate different data sources into one reference frame. Gesch and Wilson (2001) and Hess (2001) used the data from a GPS buoy with numerical interpolation methods and a geoid model to link DEM to bathymetric data and to generate a tidal datum in Tampa Bay, respectively. Parker et al. (2003) proposed the expansion of the VDatum (Milbert, 2002), a NOAA vertical datum conversion tool that is currently available for certain areas in the U.S., to a nationwide coverage in order to seamlessly integrate the coastal and offshore spatial datasets. The data from the GPS buoy are among the various data sets that involved. One of the requirements of these coastal applications is the accurate local geoid height when it comes to convert the orthometric height to the ellipsoidal height or vice versa. Shum et al. (2003) collocated a GPS buoy at a water level gauge in Lake Erie simultaneously and measured the lake level with 1 Hz GPS data for 8 hours in order to determine the local geoid height at the gauge. They showed that the root mean square (rms) error was better than 1 cm considering the insignificance of the lake surface topography, and the result was used in the absolute calibration of JASON-1 satellite altimeter. Similar applications for the determination of the local geoid height can be found in, for example, Bisnath et al. (2003).

2.2 Waverider GPS buoys

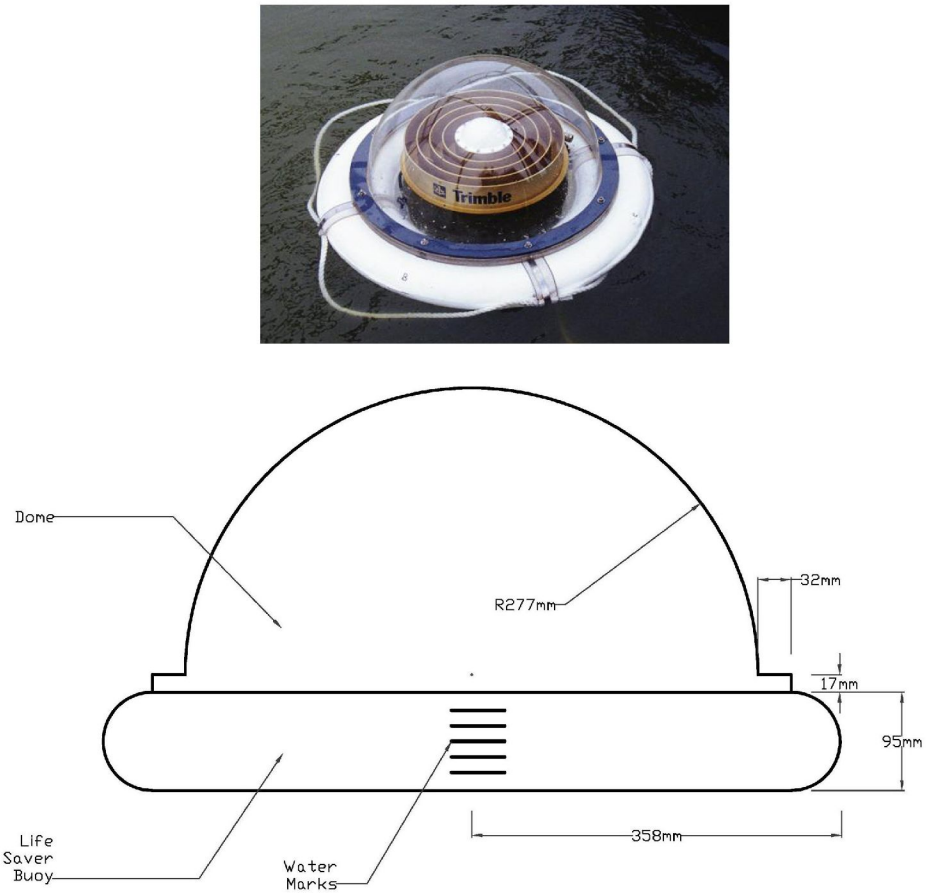

Figure 2.1. The waverider GPS buoy.

The waverider GPS buoy is illustrated in Figure 2.1. As the name indicates, the buoy moves with the wave. It is a fairly simple design: A geodetic grade Dorne/Margolin Element with a Choke Ring antenna and a transparent radome is attached on top of a 2-foot diameter floater buoy. The inner compartment of the buoy is sealed for

waterproofing before the deployment. The GPS receiver and the battery units remain on the ship to which the buoy is tethered. Similar designs can be found, for example, in Key et al. (1998) and Kelecy et al. (1994).

In general, this floater type design is kept close to the waterline to minimize the possible impacts caused by the buoy tilt and multipath. Marks on four sides of the buoy are made and their vertical offsets to the ARP are carefully measured. The operator must keep track of the waterline location from these marks during the data collecting session in order to accurately determine the height of the ARP above the water surface. However, unless water breaks into the central compartment, the waterline location in general does not change significantly. Mader (1999) points out that the misuse of antenna type or offsets could result in 10 cm errors in the vertical. Thus, it is crucial to keep track of the waterline location from these marks. The ARP height of the buoy shown in Figure 2.1 is about 60 mm above the waterline when deployed in the Lake Erie. Cheng (2004) discussed the use of this buoy in Lake Erie and the detailed procedures of operation.

The advantages of the waverider buoy include simplicity, compact size, reusability, and maneuverability in deployment, in contrast to the navigation buoy which is intended to stay longer on the water. In addition, it is economical because it collects the water level measurements equivalent to a more complex and expensive design, as Kelecy et al. (1994) have proved. Also, one can connect a water level gauge to an absolute geocentric reference frame by collocating a similar buoy next to the gauge, simultaneously measuring the water level.

Alternatively, the campaign-style buoy inevitably needs special personnel to deploy and operate it. As opposed to a ruggedized buoy that is designed to stay on the water surface for a longer period of time, it is usually impractical to deploy a campaign-style buoy repeatedly due to its extensive human involvement. Also, a campaign-style buoy is less weather resistant due to safety precautions.

2.3 GPS buoy campaigns in Lake Erie

The Great Lakes area contains well-maintained water level gauges and the NGS Continuously Operating Reference Stations (CORS) network as shown in Figure 2.2a. There are 57 water level gauges (shown in the inset of Figure 2.3) operated by the Center for Operational Oceanographic Products and Services (CO-OPS) of the U.S. and Marine Environmental Data Service (MEDS) of Canada in the Great Lakes, repeatedly recording the water level information every 6 minutes. In addition, the NGS CORS network covers this area with well-maintained continuous GPS observations every 30 seconds. Some stations, established by the Ohio Department of Transportation (ODOT) since late 2001, observe data in a 1-second sampling rate (National Geodetic Survey, 2004). Recently, the Great Lakes Continuous GPS (CGPS) Network (in Figure 2.2b) has been implemented with the cooperative effort from the Ohio State University (OSU), NGS and MEDS. It consists of 18 geodetic-quality GPS stations that are collocated with the water level gauges in the Great Lakes areas (Snay et al., 2002).

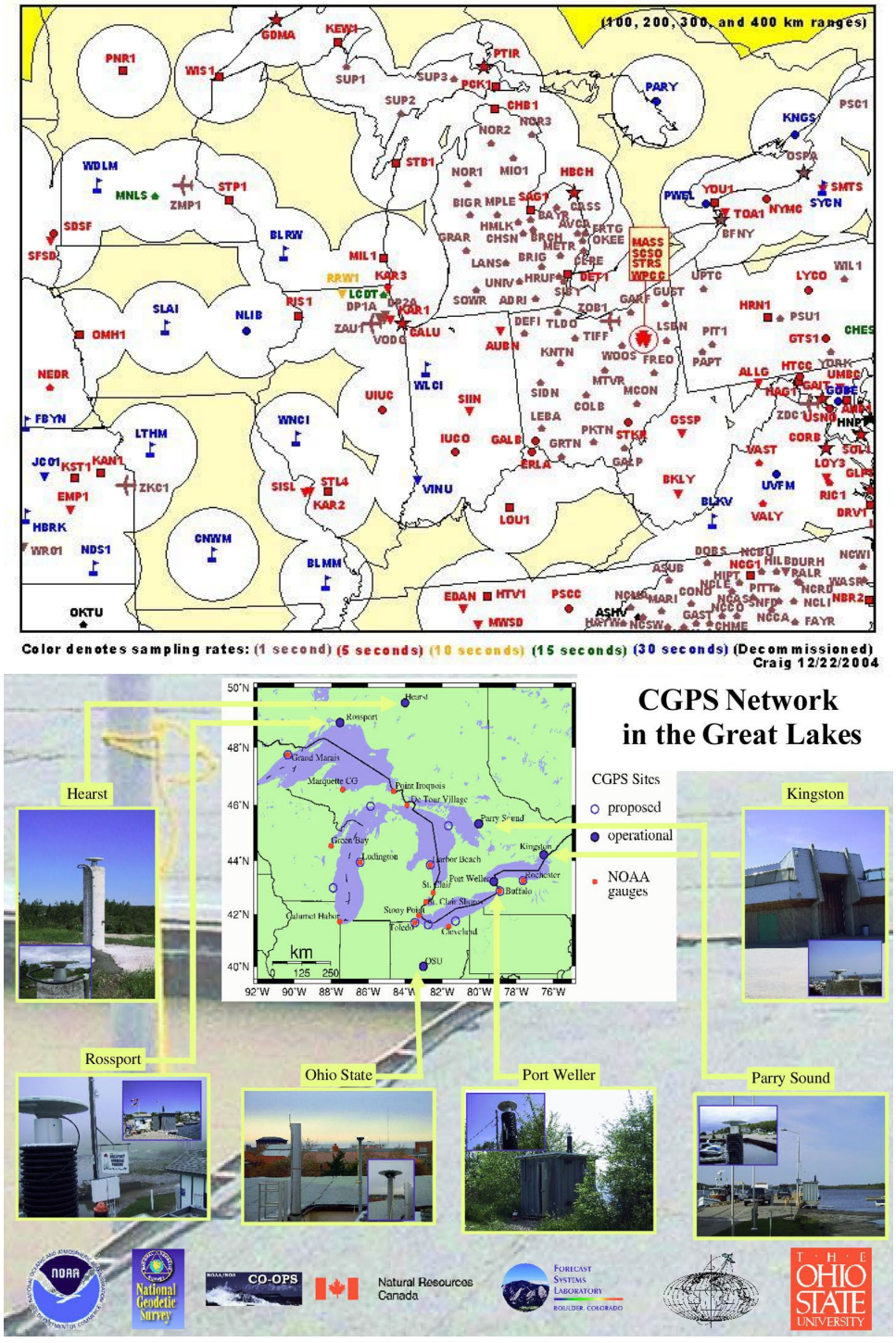

Figure 2.2. (a): The NGS CORS network in the Midwest (Courtesy of the National Geodetic Survey). (b): The CGPS network in the Great Lakes (Snay et al., 2002).

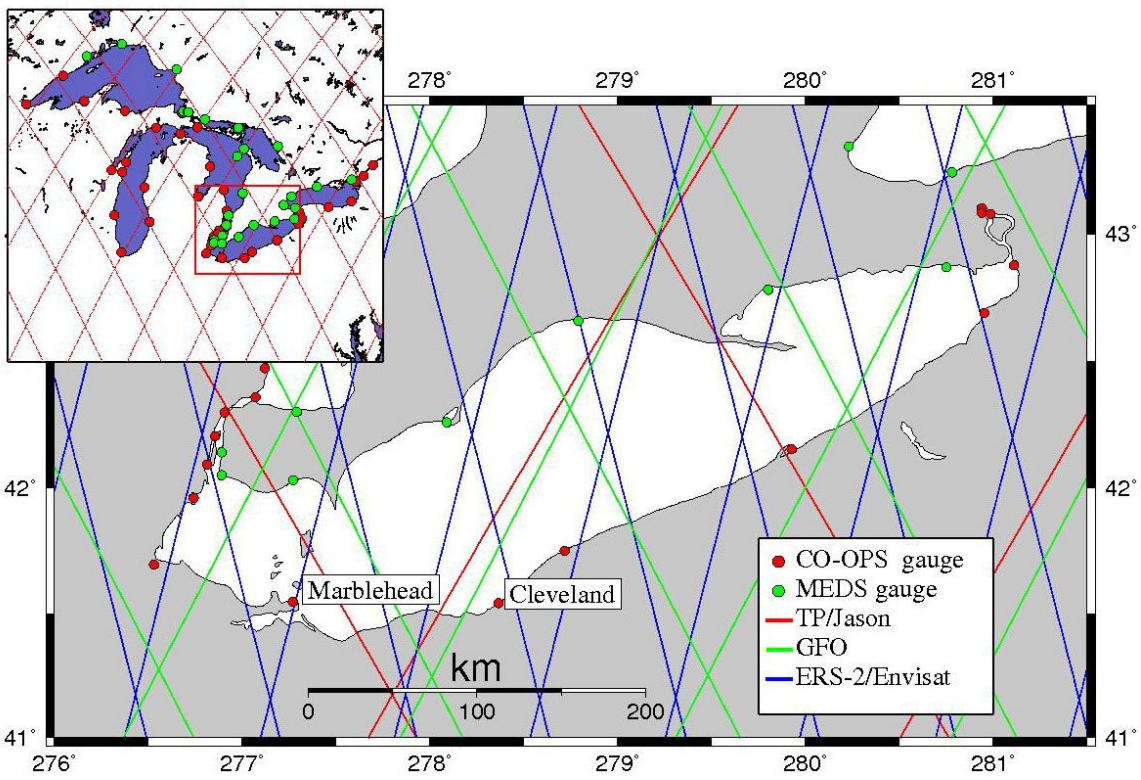

Figure 2.3. The GPS buoy campaigns at Cleveland and Marblehead. The water level gauges from CO-OPS of the U.S. and MEDS of Canada and the ground tracks of multiple satellite altimeters are shown. The ground track of JASON-1 and the gauges in the Great Lakes are shown in the inset.

Two GPS buoy campaigns (Cheng, 2004) were conducted by the Laboratory for Space Geodesy and Remote Sensing of OSU at the Marblehead and Cleveland water level gauges (Figure 2.3). The buoy was deployed next to the water level gauge as well as at a few selected satellite nominal footprints in the lake to measure the instantaneous lake surface height in the 1-second sampling rate. The objective is to link the gauge records to a geocentric reference frame and also to survey the mean lake surface gradient in the area for altimeter calibration.

The Marblehead and Cleveland GPS buoy campaigns were conducted from October 20–21, 2001 and September 17–19, 2003, respectively. The waverider GPS buoy, illustrated in Figure 2.1, was used in both campaigns. Several NGS control points were chosen to serve as reference stations, which were later used to determine the buoy's position with DGPS. They were chosen to be as close to the coast as possible in order to reduce the baseline to the buoy's deployment location. Other criteria for choosing the reference stations include stability, accessibility, and sky visibility. A regional GPS network was established in each campaign with these reference stations as well as a few from the NGS CORS in the vicinity (see Figure 2.4). The NGS CORS serve as the fiducial stations in the GPS network, and the coordinates of these "new" reference stations are determined with minimum norm by weighted P-MINOLESS. The campaign details and the fieldwork log can be found in Cheng (2004).

The fieldwork in Marblehead was carried out with the intention of establishing an absolute altimeter calibration in the inland lake in order to support the worldwide effort for altimeter calibration. Located in the inland lake, its water condition and tides are less complicated compared to those of an ocean (Shum et al., 2003). The details of this part as well as the calibration principle will be discussed in Chapter 4. With the GPS buoy collocated with the water level gauges at both Marblehead and Cleveland, it allows the linking of the gauge record to the geocentric reference frame. These details will be reported in Chapter 3.

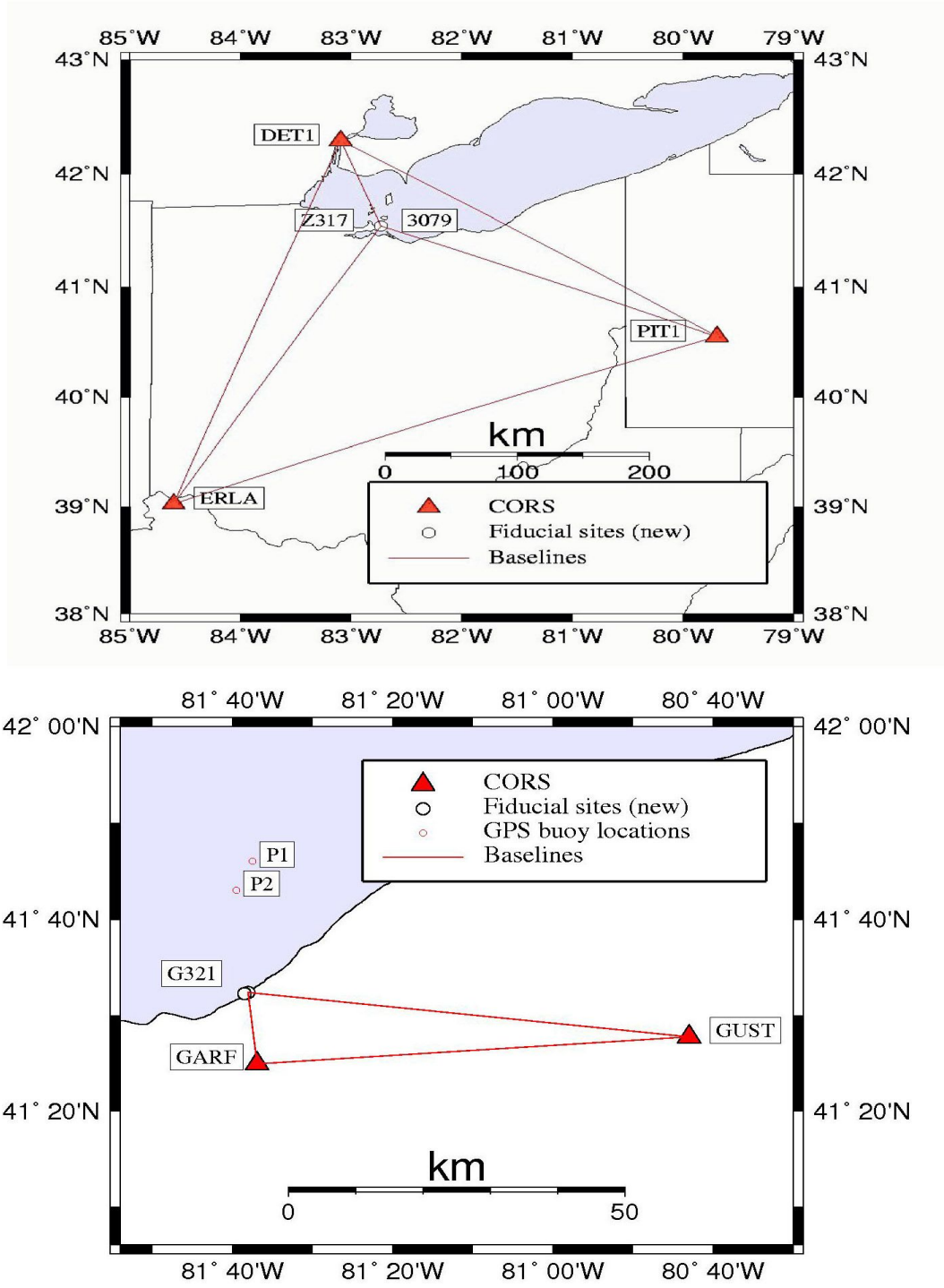

Figure 2.4. The GPS networks in the Marblehead campaign (top) and in the Cleveland campaign (bottom).

2.4 GPS buoy data processing

Since in this study a waverider buoy is used to measure the mean water surface height, the buoy data are post-processed with DGPS with respect to the onshore reference stations. The coordinates of the reference stations were determined by the weighted P-MINOLESS within the network, in which solution the NGS CORS in the vicinity served as the fiducial stations; so, both the coordinates and the associated variance of these onshore reference stations were determined. The general procedure involved:

i) solving the GPS network with high inner consistency,

ii) producing the epoch-by-epoch solution of the buoy with respect to the closest reference station using the final orbit (~ ±5 cm accuracy) from IGS, and,

iii) filtering the high-frequency waves and tidal signals out to obtain mean water surface height.

PAGE is a menu-driven software developed by NGS to process GPS static data for the applications that demand high accuracy (Blackwell and Hilla, 2000). It incorporates the three-dimensional coordinates and the velocity estimates of each CORS while accounting for the crustal motion related to plate tectonics and isostatic effects. It uses the full covariance matrix in the calculation and is, therefore, selected in this study to process each individual baseline of the network.

The Kinematic And Rapid Static (KARS) is a software program that have been developed by Mader (1986) at the NGS. It has the ability to constrain the vertical position of a floating object in the stage of ambiguity search. Thus, it is preferable in this study to

produce the epoch-by-epoch solution of the buoy. The antenna codes in both PAGE and KARS are consistent with the NGS antenna calibration result, so, the user needs to specify the antenna height from the monument to the ARP. Then both programs pick up the offsets between ARP to the L1 and L2 phase centers based on the NGS published antenna calibration specification.

This section uses the GPS buoy campaign data from Cleveland to test the solution of the GPS buoy position to see the impact from both the baseline length as well as the sampling rate. The data from the Cleveland campaign are preferred because the two CORS in the network, Garfield Height CORS (GARF) and Gustavus CORS (GUST) (see the bottom of Figure 2.4), provided the data in a 1-second interval during the campaign. As a result, the 1-Hz buoy data collected at P1 and P2 in the lake can be processed with respect to these two CORS without decimation, thus allowing the comparison of buoy solutions with different baseline lengths. The land-based GPS data collected from the stations in the network were intentionally processed using the epoch-by-epoch method. The epoch-by-epoch solutions derived from KARS are then verified with the baselines determined from PAGE in order to analyze the KARS solution with different baselines. In addition, the sampling rates of every 1-, 2-, and 5-second with the longest baseline in the network, about 83 km, is analyzed.

In this section, the tests were carried out with the data collected in the inland lake, since the water surface conditions, such as waves and currents, are less complicated than those of an ocean. However, the generic procedure may also be used for ocean applications.

2.4.1 GPS network solution

The coordinate-based least-squares solution of a GPS network leads to a rank-deficient Gauss-Markov model as there is a datum deficiency of dimension three because of the unknown translation parameters for the network. A GPS network described in this section is formed by a number of NGS CORS, which serve as the fiducial stations, and the onshore reference stations whose coordinates are to be determined. The goal of the network adjustment is to determine the coordinates of these onshore reference stations with the associated variances and covariances, from which the buoy may be positioned with DGPS later.

The network requires high inner consistency, and unlike traditional network densification, the coordinates of the CORS are here allowed to change on the basis of given criteria. Hence, the weighted P-MINOLESS described by Snow (2002) is used to solve for the network. This solution is appropriate for the application that requires highest inner consistency of the network while allowing the coordinates of the CORS to change based on the given weights. The formula can be found in Snow and Schaffrin (2004). The selection matrix selects the CORS only: $S = Diag(1, ..., 1, 0, ..., 0)$, in which the numbers of ones and zeros on the diagonal refer to the numbers of the CORS in the network and of the onshore reference stations to be freely determined, respectively.

The Cleveland GPS network (see the bottom of Figure 2.4) is composed of two CORS and two 'new' stations whose coordinates are to be determined. The two CORS are designated as GARF and GUST, both of which recorded GPS data every second. The new stations are G321 and PARK. Their locations were selected based on site stability, sky

visibility and the proximity to the GPS deployment locations. They served as the main reference stations for GPS buoy positioning since they are onshore and the baselines from their locations to those of the deployed GPS buoy in the lake are shortest among other stations in the network.

The weighted P-MINOLESS of the network is listed in Table 2.1. The *a-priori* coordinate variances of the CORS and that of the new stations are selected to be $(\pm 1\text{cm})^2$ and $(\pm 100\text{m})^2$, respectively. The initial coordinates of each station in the network are provided on the NGS-published data sheets, projected to the campaign date. The "residual" is really the coordinate increment after the adjustment. Since the objective of the network adjustment is to maintain inner consistency, the coordinates of the CORS are allowed to change.

ID		*A-priori* (m)	Adjusted (m)	Residual (m)
	X	698558.344 ± 0.010	698558.344 ± 0.0002	0.000
GARF	Y	-4739152.991 ± 0.010	-4739153.000 ± 0.0005	0.009
(CORS)	Z	4197329.703 ± 0.010	4197329.711 ± 0.0004	-0.008
	X	772251.591 ± 0.010	772251.591 ± 0.0002	0.000
GUST	Y	-4724227.253 ± 0.010	-4724227.244 ± 0.0005	-0.009
(CORS)	Z	4201259.668 ± 0.010	4201259.660 ± 0.0004	0.008
	X	695623.684 ± 100.0	695623.684 ± 0.0005	0.000
G321	Y	-4730265.461 ± 100.0	-4730265.467 ± 0.0019	0.006
	Z	4207592.002 ± 100.0	4207592.011 ± 0.0016	-0.009
	X	695007.795 ± 100.0	695007.795 ± 0.0011	0.000
PARK	Y	-4730547.702 ± 100.0	-4730547.693 ± 0.0003	-0.006
	Z	4207377.252 ± 100.0	4207377.245 ± 0.0029	0.007

Table 2.1. The weighted P-MINOLESS solution of the Cleveland GPS network. The coordinates are given in ITRF00 at the campaign date.

2.4.2 Epoch-by-epoch solution of the GPS network

Because of the impact of waves on the buoy's vertical location and the buoy's movement, the buoy's location is therefore solved on an epoch-by-epoch basis to produce a time series of the buoy's location. This section uses the land-based data collected at the GPS network in the Cleveland campaign (see the bottom of Figure 2.4) to verify the agreement between the epoch-by-epoch solution and the network solution.

The weighted P-MINOLESS solution of the PAGE-processed baseline is used as the control. The coordinate comparisons at G321 with 14-km baseline and at GUST with 75-km baseline are presented in Table 2.2. The X, Y, and Z components of the epoch-by-epoch solution agree with the GPS network solution is within 16 mm in the case of the

From GARF to G321 (14km)	X (m)	Y (m)	Z (m)	h (m)
Epoch-by-epoch solution	695623.680	-4730265.451	4207592.014	142.261
GPS network solution	695623.684	-4730265.467	4207592.011	142.271
Coordinate difference (mm)	-4	16	3	-10
From GARF to GUST (75km)				
Epoch-by-epoch solution	772251.593	-4724227.264	4201259.678	282.036
GPS network solution	772251.591	-4724227.244	4201259.660	282.009
Coordinate difference (mm)	2	20	18	27

Table 2.2. The comparison of the epoch-by-epoch solution to the GPS network at G321 and at GUST. The ellipsoidal height is calculated with GRS80 Reference Ellipsoid.

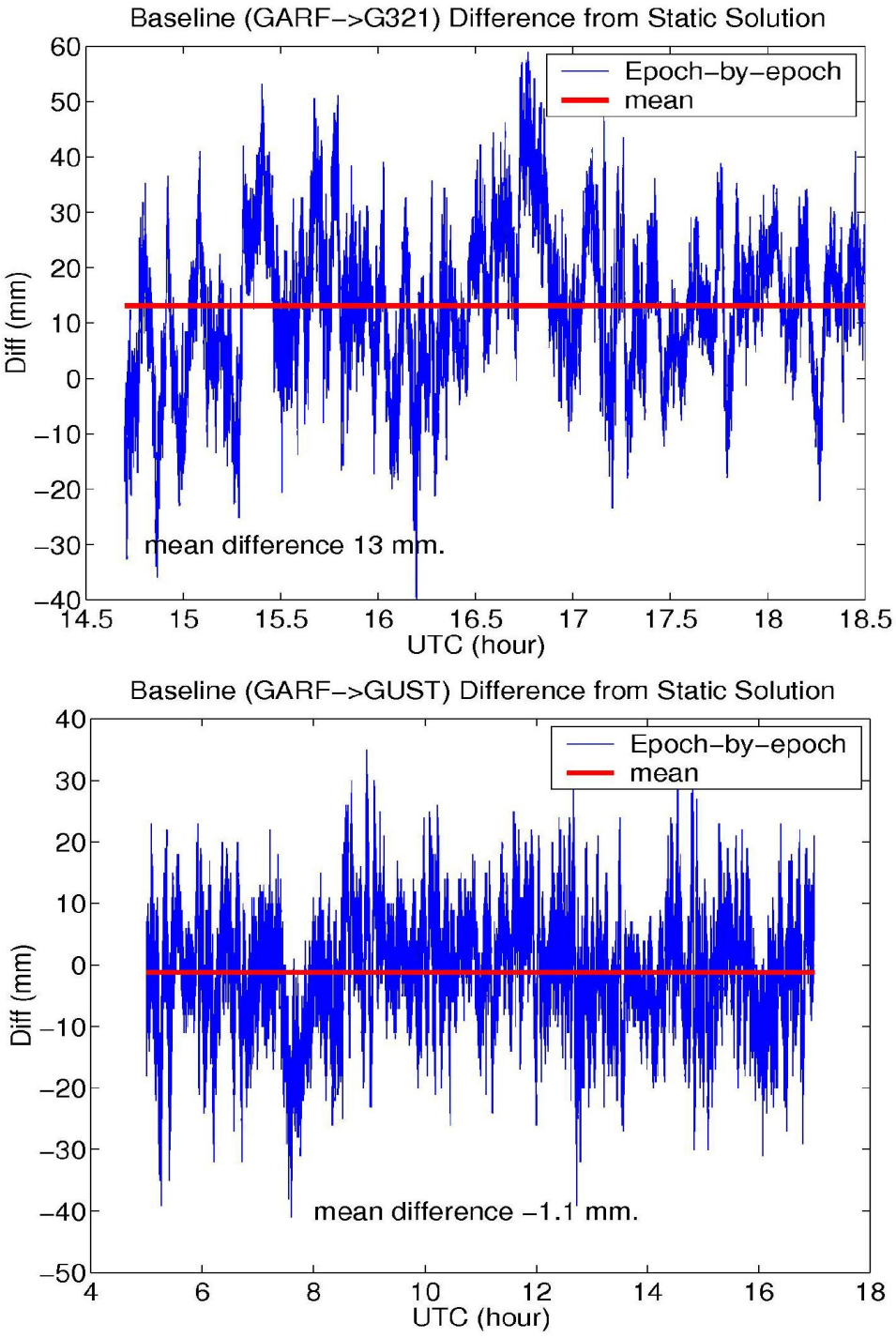

Figure 2.5. The epoch-by-epoch baseline length compared to the network baseline.

short baseline (14 km) and within 20 mm in the case of the long one (75 km). The larger differences can be seen in the Y and Z components, which are correlated with the vertical component more than the X component in this area.

On the other hand, the baseline length calculated at each epoch is compared to the GPS network and the result is presented in Figure 2.5. The mean baseline difference is about 13 mm in the case of the short baseline which is consistent with the coordinate difference. For the case of the long baseline, the calculated epoch-by-epoch baseline shows much smaller change (1 mm on average) when compared to that of the GPS network. However, the discrepancies found in the coordinates are about 27 mm. Since the fixed integers were reached in the epoch-by-epoch solution, this does indicate that not all integer ambiguities were correctly resolved in this case. In addition, the tropospheric path delay is solved for in the GPS network with PAGE, but is not in the epoch-by-epoch solution with KARS. Hence, it affects the discrepancy more in the longer baseline.

This section verified the land-based epoch-by-epoch solution with the GPS network. The epoch-by-epoch solution collected from a buoy on the water surface is analyzed in the following section.

2.4.3 Epoch-by-epoch solution of the buoy

The time series of the buoy's location contains the high-frequency terms that were caused by the buoy's movement and the waves during the data collection session. Therefore, the mean water surface height of the buoy is determined by averaging the time

series of the buoy's height solution. By averaging the entire time series, the impacts from the movement of the buoy and the waves can be reduced due to their high-frequency nature.

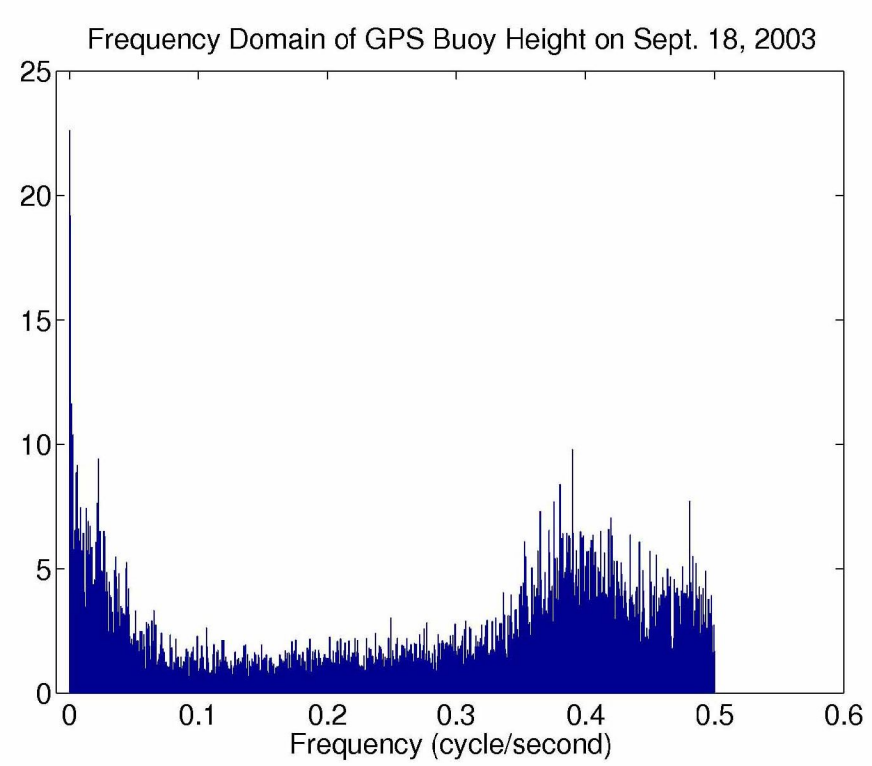

Figure 2.6. The frequency content of the GPS buoy height solution on September 18, 2003. The frequency of the waves is about 0.2 to 0.5 cycle/second based on the campaign observation.

Figure 2.6 presents the frequency content of the GPS buoy height solution, with the data collected every second for 1.7 hours. The waves, whose frequency range from 0.2 to 0.5 cycle/second based on the campaign observations, can be seen in the figure as the dominant signals in the right-hand side of the frequency domain. The frequencies of the

wind-induced waves in the oceans are typically in the range of 0.05 to 1 cycle/second (Thurman, 1991). The time span of the figure is too short to clearly identify the semi-diurnal tidal signal but some of the dominant low-frequency terms may be caused, in part, by the aliasing of the tidal signals.

The GPS buoy was deployed at P1 and P2 for two hours and the data were processed with the selected reference stations on the land. The choice of the reference station G321 is legitimate since the baseline is shorter than those of other CORS in the GPS network, and it has a better sky visibility than PARK. Therefore, it is used as the reference for other solutions to compare with. It is assumed that both the tropospheric path delay and the second-order of the ionospheric path delay, are identical throughout the GPS network area and the buoy deployment locations at P1 and P2. Since the time span of the buoy data is less than 2 hours, the following measures in KARS were employed for the comparisons:

- Use of IGS precise ephemerides (the final orbit with 5-cm accuracy).
- Use of DGPS solution with the reference station of choice determined from the weighted P-MINOLESS of the GPS network in Table 2.1.
- Forming of iono-free combinations for phases to remove the first-order ionospheric path delay.
- Rescaling the integer ambiguities with both, the wide lane solution and the difference between wide land and iono-free solution.
- Constraining of the vertical component in the ambiguity searching space.

- Forming of double-difference equations for phases to remove common systematic errors.
- Use of a 12º mask angle.
- Observation of 6 satellites
- Discarding of the solution when the DOP (Delusion of Precision) exceeds 3.
- No occurrence of a reference satellite change.

The integer ambiguities are verified with multiple reference stations according to:

$$N_{XB} = N_{XY} + N_{YB} \tag{2.1}$$

where N is a vector that contains the double-differenced ambiguities of all satellites tracked. Its subscription indicates 'from' and 'to' stations. For example, N_{PQ} is the vector of double-differenced integer ambiguities formed with the observations from *Station P* as the reference station to *Station Q* as the rover. For the notation in Eq. (2.1), subscription B indicates the buoy's location; subscription X is an arbitrary reference station, and subscription Y is the closest reference station to the buoy. For instance, Y is G321 in the Cleveland campaign. N_{XY} is provided by the PAGE-processed baseline from the network and N_{YB} results from the determination of the buoy's location from G321.

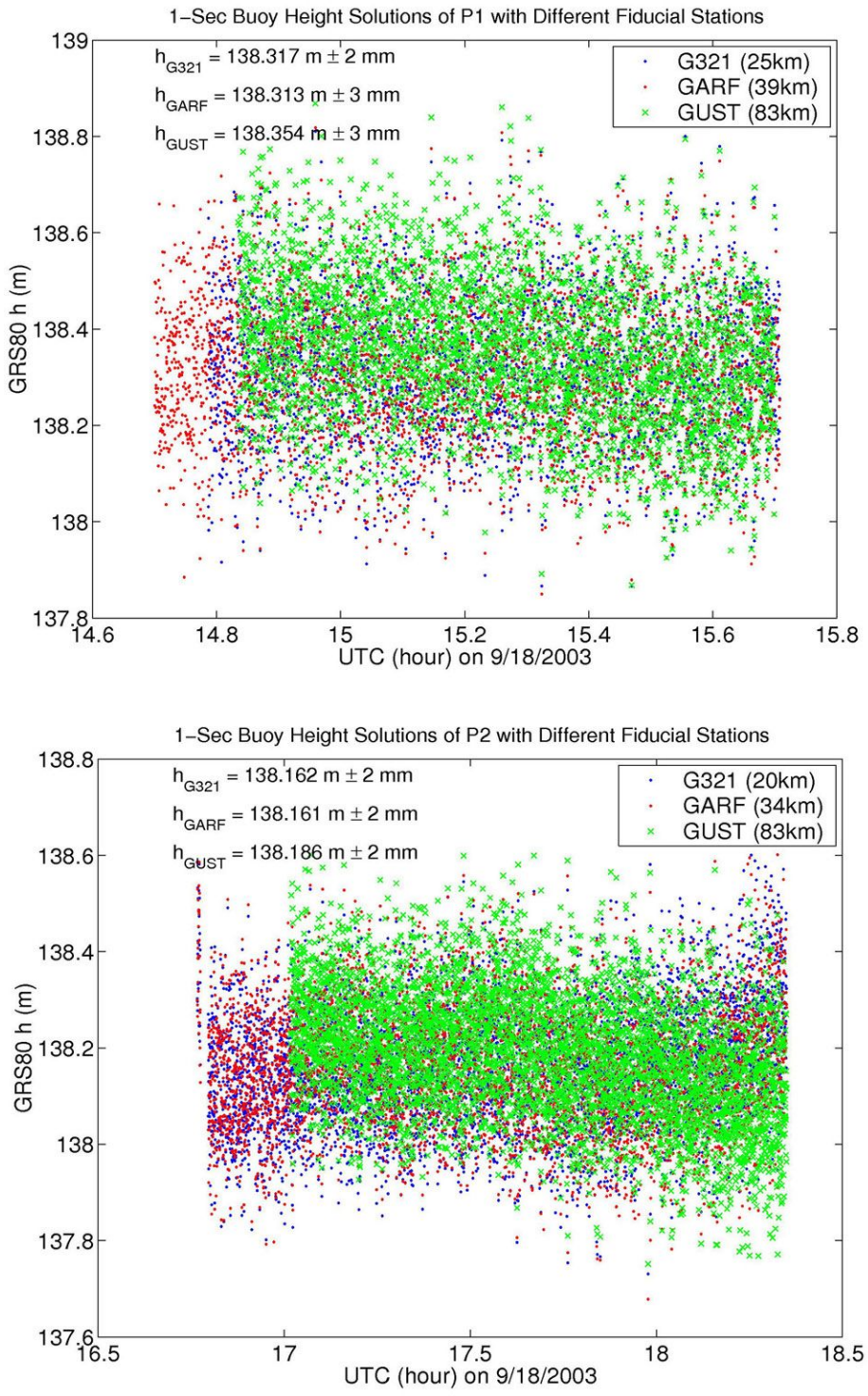

Figure 2.7. GPS buoy solutions of P1 and P2 from different reference stations.

From	To	Baseline (km)	Height solution	Discrepancy (mm)	# SV	Np
G321		25	138.317 m ± 2 mm	-	5	1
GARF	P1	39	138.313 m ± 3 mm	-4	5	3
GUST		83	138.354 m ± 3 mm	41	5	3
G321		20	138.162 m ± 2 mm	-	6	0
GARF	P2	34	138.161 m ± 2 mm	-1	6	0
GUST		83	138.186 m ± 2 mm	25	6	4

Table 2.3. The solutions of P1 and P2 from different reference stations. SV is the number of the satellite vehicle. Np is the number of integer ambiguities provided by the multiple reference station approach.

The GPS buoy solutions at P1 and P2 from different choices of the reference stations are compared and the results are listed in Figure 2.7 and Table 2.3. Some solutions need the ambiguities be provided from the multiple reference station and from the GPS network.

The buoy occupied P2 approximately one hour after the buoy had finished the 2-hour data collection session at P1. Due to different observing hours, the session at P2 had one more satellite available and, hence, the height solution at P2 derived from GARF (a 34-km baseline) does not need any *a-priori* integer ambiguities.

The discrepancies at P1 and at P2 are within 41 mm. The solutions at P1 and P2 with the mid-range baselines from GARF (a 39- and a 34-km baseline) are very close to that derived from G321. The discrepancies at P2 are smaller since the session at P2 had one more satellite available. It was assumed that the common errors, due to troposphere and other influences are similar at both ends of the baselines so that they can be canceled out by double differencing. However, the discrepancies at P1 and P2 derived from GUST

(> 80 km) are about 25 and 41 mm, respectively. This indicates that the common errors, such as troposphere, multipath and others, may not have been sufficiently identical to be canceled out by differencing in the area on the campaign day when the buoy and the reference station were about 80 km apart.

The results from the cases of long baselines presented in Table 2.3 are idea since some of the integer ambiguities have been provided from *a-priori* information that was derived from multiple reference stations. It reduces the number of unknown parameters to solve for and, thus, produces a solution that is consistent with the result derived from the shorter-baseline cases. In addition, the buoy was deployed at an inland lake, whose wave condition is less complicate to that of an open ocean. Therefore, the small discrepancies found here are, therefore, optimistic. It may serve as an upper bound of the epoch-by-epoch solution in the near idea situation. It may not be achievable in an open ocean with an 80-km baseline.

The result in this section is consistent with Leick (1994) who emphasizes that the key to the cm-level accuracy for the epoch-by-epoch solution consist of the accurate determination of the integer ambiguities. In this section, it shows that for a short-range 34-km baseline with 6 satellites, the discrepancy is 1 mm without any *a-priori* information for ambiguities. If the situation is worst than that, the *a-priori* water surface height is necessary for cm-level buoy positioning. Therefore, we conclude that a survey plan is essential since it helps us to select the optimal campaign time period with the most available satellites.

The *a-priori* water surface height for ambiguity determination can be obtained, for example, from repeated GPS buoy campaign or from other techniques such as satellite altimeter measurements or hydrodynamic models.

2.4.4 Ambiguity verification and sampling rate

Since the session at P2 observed one more satellite than that of P1, it is used here to test the impact of the sampling rate. Different sampling rates, 1-, 2-, 5-, 10- and 15-second, are tested at P2 with baselines from GUST (about 83 km) and from GARF (about 34 km). Figure 2.8 presents the height solutions and their mean heights at P2 from GARF (34-km baseline) without any ambiguity verification from multiple reference stations. The 2-second data set is not significantly different from the 1-second data set under a 95% confidence level. It can be seen that the incorrect ambiguities were apparently achieved in the 5-second data set because of the height jump and the drift. On the other hand, Figure 2.9 demonstrates the height solutions and their mean heights at P2 from GUST (about 83 km) with ambiguity verification from multiple reference stations. Under a 95% confidence level, the significant change in the height solution is not found until the sampling rate reaches 15 seconds.

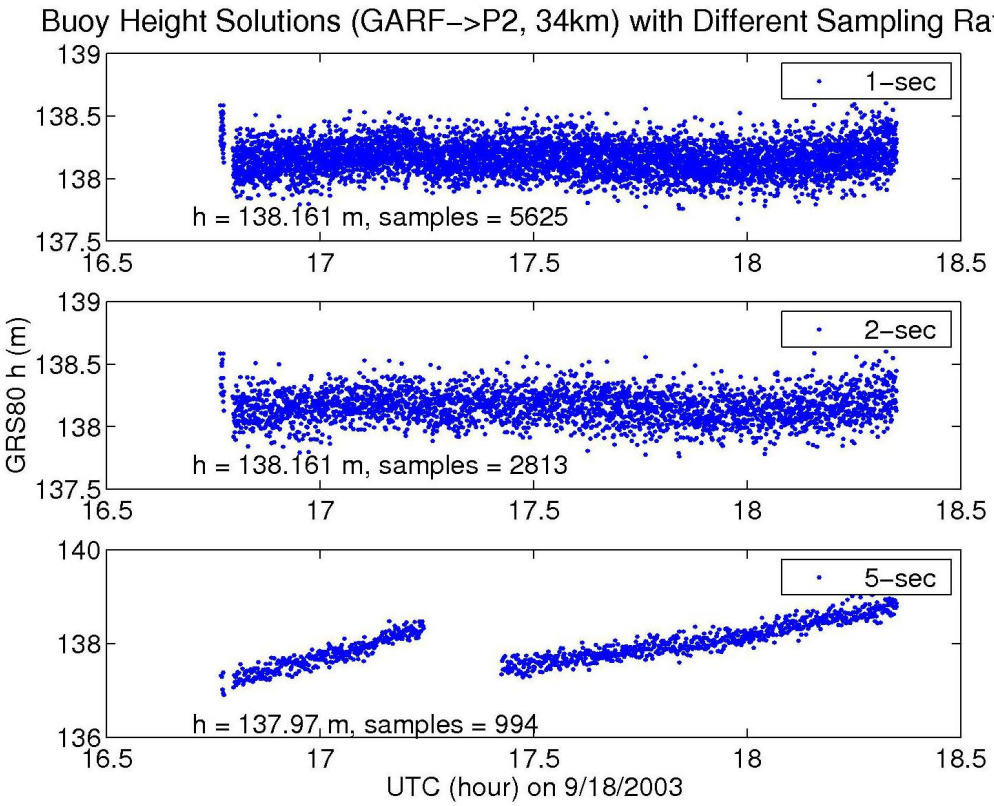

Figure 2.8. The buoy height solution and the mean height at P2 determined from GARF with different sampling rates.

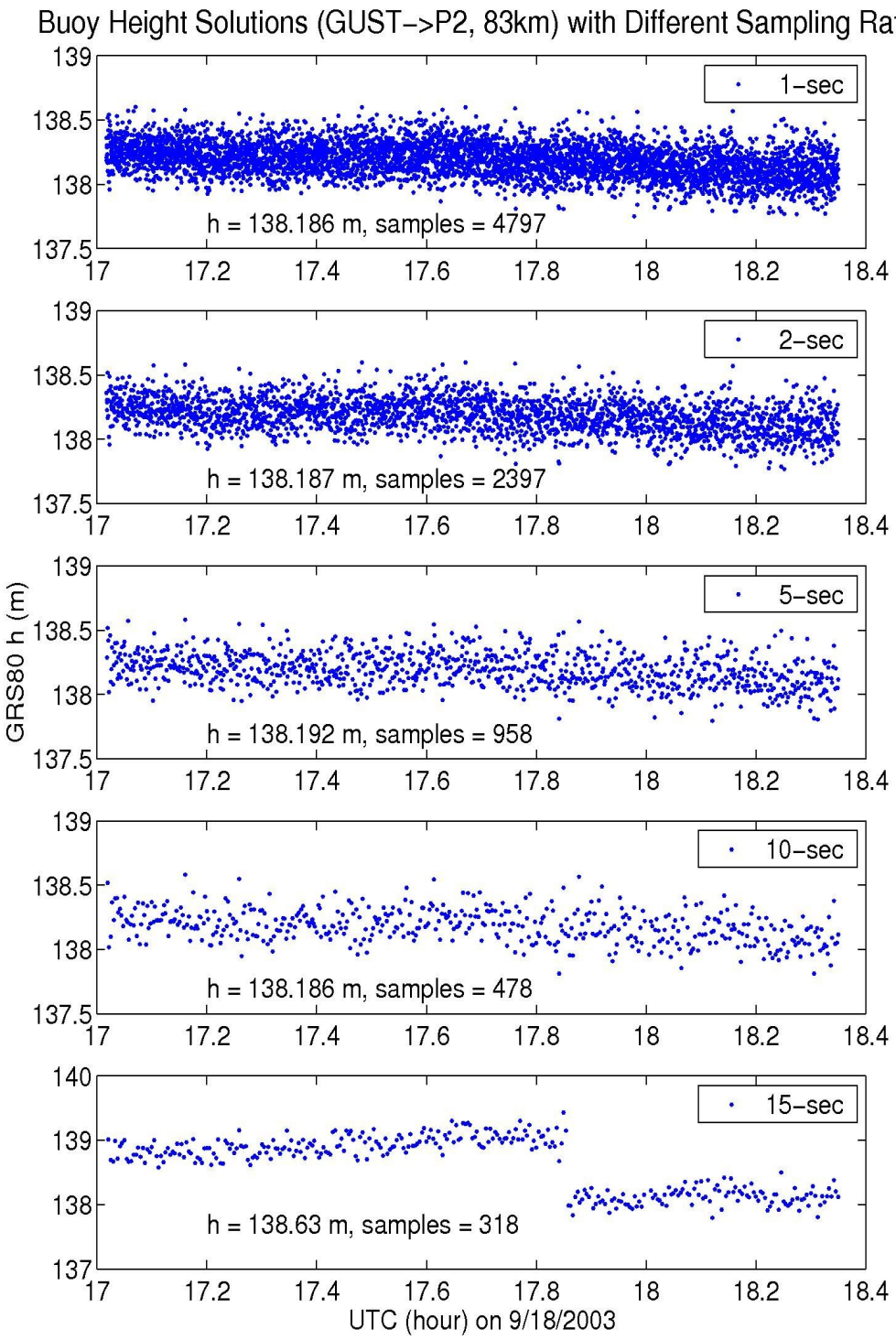

Figure 2.9. The buoy height solution and the mean height at P2 determined from GUST with different sampling rates.

The decimation of the original 1-second data set increases the chances for KARS to get the wrong integer ambiguities because it largely reduces the number of redundant data samples, although they are needed to determine the correct ambiguities. This can be seen in the 5-second data set in Figure 2.8. Interestingly, the result in Figure 2.9 clearly suggests that the ambiguity determination is more of a decisive factor than the sampling rate. With verification of the integer ambiguities using Eq. (2.1) to ensure that the correct ambiguities are achieved, even the 10-second data set produces a similar mean height to the original 1-second data set. However, the *a-priori* information is usually unavailable in the real situation, so it is recommended to collect the data in the highest possible sampling rate for baseline longer than 34 km and satellites fewer than 6.

2.5 Summary

This chapter reviewed past GPS buoy applications for the observation of oceanic phenomena such as wave heights, sea state, ssh, water depths and others. Other geodetic applications have also been mentioned. The characteristics and applications of a waverider GPS buoy have been explained, and the results of two GPS buoy campaigns in Lake Erie have been presented.

This chapter discussed the general procedures to process data in order to achieve a time series for the buoy's location. They include a weighted P-MINOLESS adjustment of the regional network, in which the NGS CORS were selected to be the fiducial stations, and the onshore reference stations for each campaign were treated as the new stations

whose coordinates were to be determined. NGS CORS were also selected by the Selection Matrix, *S*, in the network adjustment so that their coordinate changes as well as the "residuals" of baseline components are consecutively minimized during the adjustment.

The epoch-by-epoch solution was analyzed with the land-based GPS data from the network. It was compared to the static result and showed 10- and 27-mm height discrepancies in the cases of a 14-km and a 75-km baseline, respectively. The baseline discrepancy in the case of the 14-km one is consistent with the height discrepancy. In contrary, the baseline discrepancy of the latter one is not. It is likely caused, in part, by the fact that the tropospheric path delay is not solved for in the KARS epoch-by-epoch solution.

The epoch-by-epoch solutions of the buoy data, collected in the lake from different reference stations, were also tested. It showed that a 34-km baseline with 6 satellites tracked does not need any ambiguity verification and the height solution agree to 1 mm to the solution derived from the shorter baseline. The height solutions agree within 4 cm for a 83-km baseline as long as the integer ambiguities are verified with those of multiple reference stations.

For all baselines that are longer than 34 km and with fewer than 6 satellites, the *a-priori* information is needed in order to ensure that the correct ambiguities are determined. If such information is unavailable, it is recommended to record data in the highest possible sampling rate.

CHAPTER 3

LINKING WATER LEVEL GAUGE RECORDS TO ITRF IN THE GREAT LAKES

This chapter addresses the issue of linking the water level gauge datum around the Great Lakes to the geocentric ITRF in terms of the ellipsoidal height above the chosen reference ellipsoid. The objective is to tie or link water level gauge benchmarks, the time series of the gauge records or the elevation change from the lake circulation model to satellite measurements such as altimetry or GPS (buoy) because these data sources usually do not refer to a common reference frame. Although the procedures described in this chapter are applied to the Great Lakes, or more specially, Lake Erie, they are generally also applicable to areas such as the oceans.

The common situation in the coastal area is that there exists spatial information of various types, and the vertical component may refer to different reference frames. For example, Parker et al. (2003) pointed out that there are at least 28 different vertical datums that have been used in the U.S. They also noted that it is difficult to integrate vertical information from different agencies since various kinds of a vertical datum such as three-dimensional, orthometric, or tidal datum have been used. Thus, one of the goals of this chapter is to present a general procedure to incorporate various types of spatial

data in the coastal area into a common datum with the ultimate goal to form a seamlessly integrated coastal and offshore spatial database regardless of the vertical datum to which these data are originally referenced.

The water level gauge records usually refer to a local vertical datum so it is necessary to link them to a global datum when the combination of the historical water level gauge records and the satellite observations is desired. A local vertical datum, called the International Great Lakes Datum of 1985 (IGLD85), was adopted by the U.S. and Canada to be the datum for water level gauges around the Great Lakes. Its linking to the global datum can be achieved by deploying a GPS buoy next to the gauge. This method provides a direct link of the water level, which is simultaneously observed by the GPS buoy and the water level gauge, to the global datum. Alternatively, a GPS antenna may occupied a benchmark on land in the vicinity to provide the link.

As illustrated in Figure 3.1, the GPS buoy provides the ellipsoidal height of the lake level, the offset from the water level to the ellipsoidal height can be determined. Therefore, the link of the water level to the ellipsoidal height is directly provided by the GPS buoy survey. The approach is advantageous because it does not need to identify the location of the gauge's zero point (e.g., A is the relative height measured from the gauge zero point in Figure 1.2 on page 12).

Alternatively, the benchmarks can be surveyed with GPS antenna. This approach is relatively not as complicate because the GPS operation are all on land. It allows longer observing time for better result. However, the link in this case is only to the benchmarks, not to the actual water surface. It can not account for the error (or bias) that may exist in the offset between the gauge's zero point and the benchmarks.

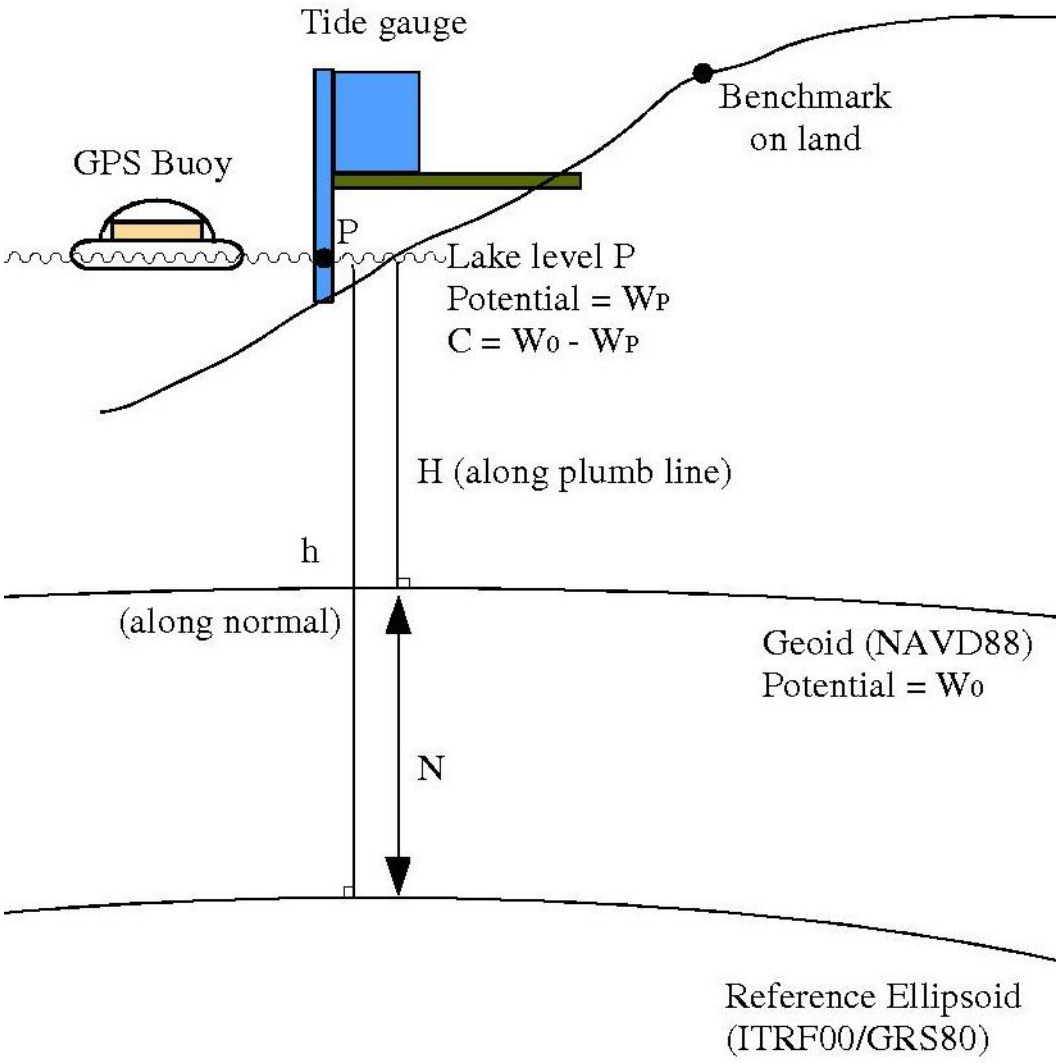

Figure 3.1. Schematic diagram of the GPS buoy collocated near a water level gauge. *H, h* and *N* are orthometric, ellipsoidal, and geoid heights at the gauge, respectively. *C* is defined as the geopotential number. W_p and W_0 are gravity potential values at the gauge and at geoid surface.

The National Geodetic Survey (NGS) of the U.S. provides a vertical datum transformation tool, called VDatum (Parker et al., 2003), which transforms spatial information among the various vertical datums, including the orthometric, tidal, and

three-dimensional datums that are commonly used in the U.S. The current version (1.06, as of January 2005) is available for 6 coastal areas in the nation and it is anticipated to be available nationwide in the near future. However, none of these areas are in the Great Lakes. As an example, this study will demonstrate the use of a GPS buoy, similarly to what has been done by Parker et al. (2003), to connect the records of two water level gauges at Marblehead and Cleveland in Lake Erie to the geocentric ITRF.

The potential applications of linking a coastal water level gauge record to a geocentric datum include the absolute calibration of satellite altimeters. Shum et al. (2003) calibrated the JASON-1 altimeter over Lake Erie, using the historical record of one coastal water level gauge. They used a GPS buoy to determine the local geoid height at the gauge and to survey the lake surface gradient between JASON-1 footprints.

The following sections discuss the underlying theory, the most common datums used in the U.S., the error budget and the effect of the vertical motion of the water level gauge benchmarks.

3.1 Theory and background

The North American Datum of 1983 (NAD83) and the North American Vertical Datum of 1988 (NAVD88) are the three-dimensional and orthometric datums commonly used in the Great Lakes and the neighboring area. In addition, water level gauges in this

area record lake level in terms of the heights that are based on the International Great Lakes Datum of 1985 (IGLD85). The definition of each datum and a brief description of it are provided in the following sections.

3.1.1 Ellipsoidal height and the North American Datum of 1983

The ellipsoidal height along the ellipsoidal normal is defined as the height above the chosen reference ellipsoid of a three-dimensional datum. The relationship between the ellipsoidal and the orthometric heights is illustrated in Figure 3.1 and in Eq. (3.1), where h, H, and N are ellipsoidal, orthometric, and geoid heights, respectively. Although the ellipsoidal height is measured along the normal and the orthometric height is measured along the curved plumb line, they are treated linearly due to the negligible deflections of vertical in this area:

$$h = H + N \tag{3.1}$$

where h and H are ellipsoidal and orthometric height, respectively, and N is called the geoid height. The geoid height can be determined if both ellipsoidal (h) and orthometric (H) height are available at the same location. In addition, different geoid models were developed by NGS such as GEOID99, GEOID03, G99SSS, USGG2003 and others. GEOID03 and USGG2003 are the recent update models of GEOID99 and G99SSS respectively. The geoid height is required when converting the orthometric height to the ellipsoidal height.

Historically, NAD83 is the third horizontal geodetic datum of the continental extent in the North America. It was implemented, based on a simultaneous adjustment involving some 1.7 million observations and 26,000 stations in the U.S., Canada, Mexico and Central America, though 95% of the stations belong to the U.S (Schwarz, 1990). It was proposed to be geocentric with the reference ellipsoid adopted by the Geodetic Reference System of 1980 (GRS80). Therefore, the ellipsoidal height of this datum is defined as the height above the GRS80 Reference Ellipsoid. However, Soler et al. (1992) revealed that the origin of NAD83 was off by about 2 m when compared to the ITRF stations. In addition, NAD83 is intentionally held fixed whereas the realizations of ITRF change with time. Hence, a coordinate transformation is needed between NAD83 and ITRF and the transformation parameters can be found in National Geodetic Survey (2004).

3.1.2 Dynamic height and the International Great Lakes Datum of 1985

The geopotential number, C, is defined in Eq. (3.2) and Figure 3.1. It is the potential difference at a given point, P, relative to the potential on the geoid (W_0). Every point on any equipotential surface has the same geopotential number and, hence, the geopotential number can be considered as the natural measure of height (Heiskanen and Moritz, 1967). The dynamic height is defined in Eq. (3.3) by the geopotential number scaled by a nominal value of normal gravity at mid-latitude (e.g., $\gamma_0 = 980.6199203$ gal;

GRS80 value, Moritz, 1992). The dynamic height does not have geometric meaning but, rather, represents the potential difference relative to the geoid expressed in the distance unit (Jekeli, 2000).

$$C = W_0 - W_P \tag{3.2}$$

$$H_{dyn} = \frac{C}{\gamma_0} \tag{3.3}$$

The International Great Lakes Datum of 1985 (IGLD85) is one of the common vertical datums adopted from the water level gauges in the Great Lakes which are maintained by CO-OPS, USA and by MEDS, Canada. IGLD85 is realized through the mean water levels at a set of master water level gauge stations in the Great Lakes. Its height is based on an adopted elevation at Point Rimouski/Father's Point (National Geodetic Survey, 2003a). Due to various observational, dynamical, and steric effects, there is a small discrepancy between IGLD85 and the dynamic height which is known as the hydraulic corrector (HC), see Figure 3.2. By definition, the dynamic height is obtained by adding the hydraulic corrector to the IGLD85 height (Coordinating Committee on Great Lakes Basic Hydraulic and Hydrologic Data, 1995). The hydraulic correctors around Lake Erie range from 2.7 to -2.6 cm and the larger ones (over 10 cm) occur on the west bank of Lake Michigan.

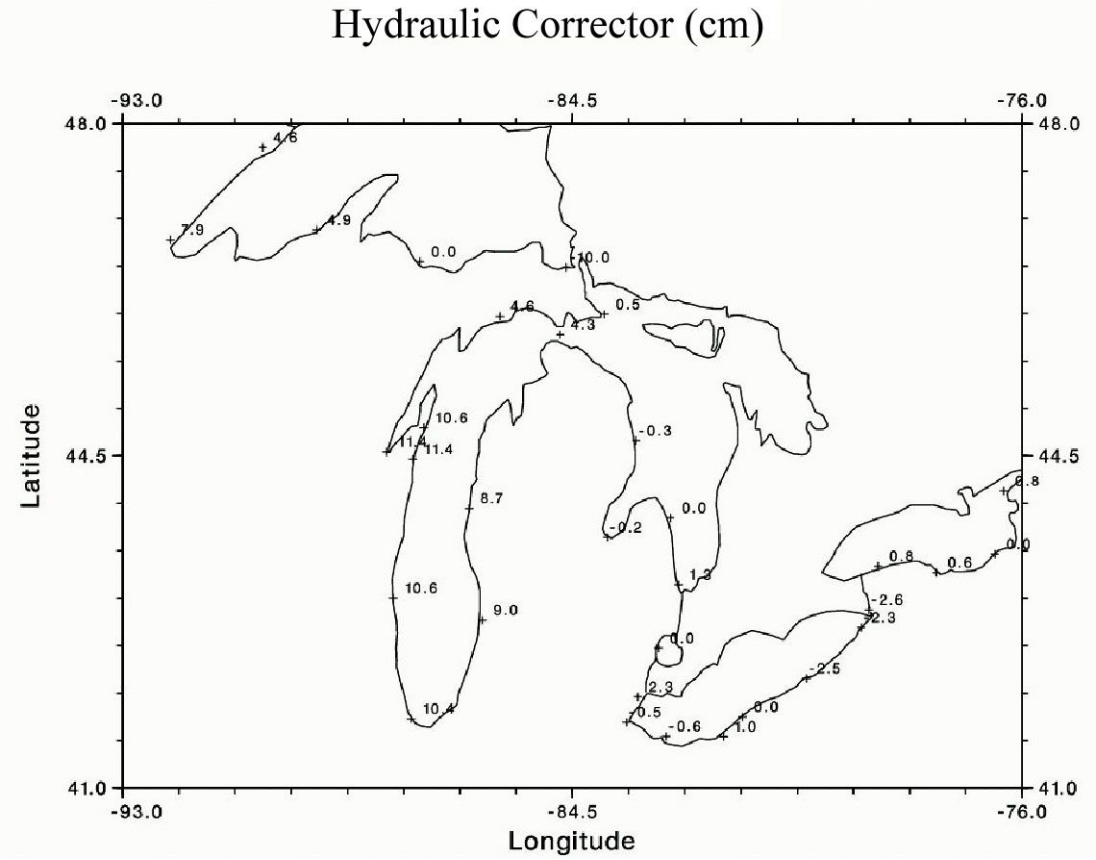

Figure 3.2. The hydraulic corrector in the Great Lakes area (Conner, 2002, personal communication).

3.1.3 Orthometric height and the North American Vertical Datum of 1988

The orthometric height is approximately given in Eq. (3.4) as the geopotential number divided by the average gravity along the plumb line from that point to the geoid. It has definite geometric meaning supposedly representing the actual distance to the point

above the local geoid along the plumb line. However, the average gravity along the plumb line is usually inaccessible and requires a hypothetic value for the mass density of the crust (Jekeli, 2000).

NAVD88 is based on Helmert's orthometric height (Zilkoski et al., 1992) with its origin at Point Rimouski/Father's Point (National Geodetic Survey, 2003a), the same as for IGLD85. It is used exclusively as the main vertical control for applications such as spirit leveling and digital elevation modeling (DEM) in the U.S.

Eq. (3.4) defines Helmert's approximation of the orthometric height, H, in which the average gravity along the plumb line, $\bar{g}$, is obtained by using the surface gravity value and its reduction according to Prey (Heiskanen and Moritz, 1967). The orthometric height in Eq. (3.4) needs to be solved iteratively since it appears on both sides of the equation. In Eq. (3.4), the geopotential number is in g.p.u. (geopotential unit = km gal), the gravity is in gal and the height is in km.

$$H = \frac{C}{\bar{g}} = \frac{C}{g + 0.0424\,H} \tag{3.4}$$

The conversion between IGDL85 and NAVD88 can be seen in Eq. (3.4) by substituting the geopotential number, C, from Eq. (3.3) into Eq. (3.4):

$$H = \frac{C}{g + 0.0424\,H} = \frac{H_{dyn}\gamma_0}{g + 0.0424\,H} = \frac{(H_{IGLD} + HC)\gamma_0}{g + 0.0424\,H} \tag{3.5}$$

where H, H_{dyn}, and H_{IGLD}, in km, are the NAVD88 height, dynamic height, and IGLD85 height respectively. HC is the hydraulic corrector.

3.2 Vertical datum conversions

The conversion includes the following steps.

3.2.1 Conversion from IGLD85 to NAVD88

Converting water level gauge records from IGLD85 to NAVD88 is shown in Eq. (3.5). By differentiating Eq. (3.5), the conversion errors from gravity, the water level gauge record and the hydraulic corrector can be analyzed as following:

$$dH = -\frac{\gamma_0 \cdot (H_{IGLD} + HC)}{(g + 0.0424\,H)^2}\,dg + \frac{\gamma_0}{g + 0.0424\,H}\,dH_{IGLD} + \frac{\gamma_0}{g + 0.0424\,H}\,dHC \qquad (3.6)$$

where *dH* in the left-hand side is the overall conversion error in NAVD88 height contributed by these factors. Without the real gravity observations involved in this study, the model gravity values provided by the NGS data sheets at seven CO-OPS water level gauges on the southern bank of Lake Erie were used, including: Toledo, Marblehead, Cleveland, Fairport, Erie, Sturgeon Point and Buffalo. The model gravity is the same interpolated value that was used in the NAVD88 general adjustment (National Geodetic Survey, 2003a). The average model gravity at these gauges is 980.270 gal and the average NAVD88 and IGLD85 heights are 174.538 and 174.466 m respectively. The conversion

error propagated from different sources in this specific area can be calculated by Eq. (3.6) with these nominal values. As a result, the conversion error, in mm, from IGLD85 height to NAVD88 height becomes:

$$dH \approx -200 \frac{mm}{gal} \cdot dg + 1.0003 \cdot dH_{IGLD} + 1.0003 \cdot dHC \tag{3.7}$$

In can be seen that there is a 2-mm conversion error contributed by every 10 mgal of the gravity error, and an about 1:1 ratio (1:1.0003 to be exact) of conversion error contributed by the water level gauge records and by the hydraulic corrector. For the static terrestrial gravity method, it can easily reach ±0.02 mgal uncertainty over 1 km. Airborne gravimetry and the satellite based methods provide uncertainty of ±6 mgal over 2-5 km, and a few mgal over 50-100 km, respectively (Garcia-Lopez, 1997). However, the overall errors of water level gauge records depend on the instruments, the error of the benchmarks, and the local dynamical and steric phenomena that affect the hydraulic corrector at each gauge.

3.2.2 Conversion from NAVD88 to geocentric ITRF00

NGS GEOID99 is a local geoid model using gravity and GPS measurements at spirit-leveled benchmarks in the continental U.S. to support the direct conversion of NAD83 ellipsoidal heights into NAVD88 Helmert's orthometric heights. On the other hand, G99SSS is the model that is based solely on the gravimetric observations (Smith and Roman, 2001). Their relationship can be seen in Figure 3.3, and a nationwide average

of 52cm bias is found between the global geopotential surface and the NAVD88 datum. GEOID03 and USGG2003 are NGS's recent update models of GEOID99 and G99SSS, respectively.

Smith and Roman (2001) compared the GEOID99 model to the GPS Benchmarks data on the land and found a rms error of ±4.6 cm in the difference. Because Lake Erie is nearly located at the boundary of GEOID99 model, however, and since the data that were used to produce the model are unavailable in the lake area, the error of GEOID99 around Lake Erie is likely to be larger (Dan Roman, personal communication). A preliminary mean lake surface height comparison, using 3 years of water level gauge records of Lake Erie, with TOPEX/Poseidon (T/P) altimetric lake surface heights showed a 18 cm discrepancy, which can in part be contributed to the geoid model error in Lake Erie (Niu et al., 2003).

Since we are seeking the geoid height between the NAVD88 orthometric height and the ellipsoidal height on the GRS80 Reference Ellipsoid, see Figure 3.3, G99BM would have been ideal for the direct application. However, it was only temporarily released by NGS for experimental versions and is unavailable around Lake Erie area. There are, at least, three alternatives: transforming the GEOID03 model from NAD83 to ITRF00, applying G99SSS with 52 cm bias, or using the GPS buoy.

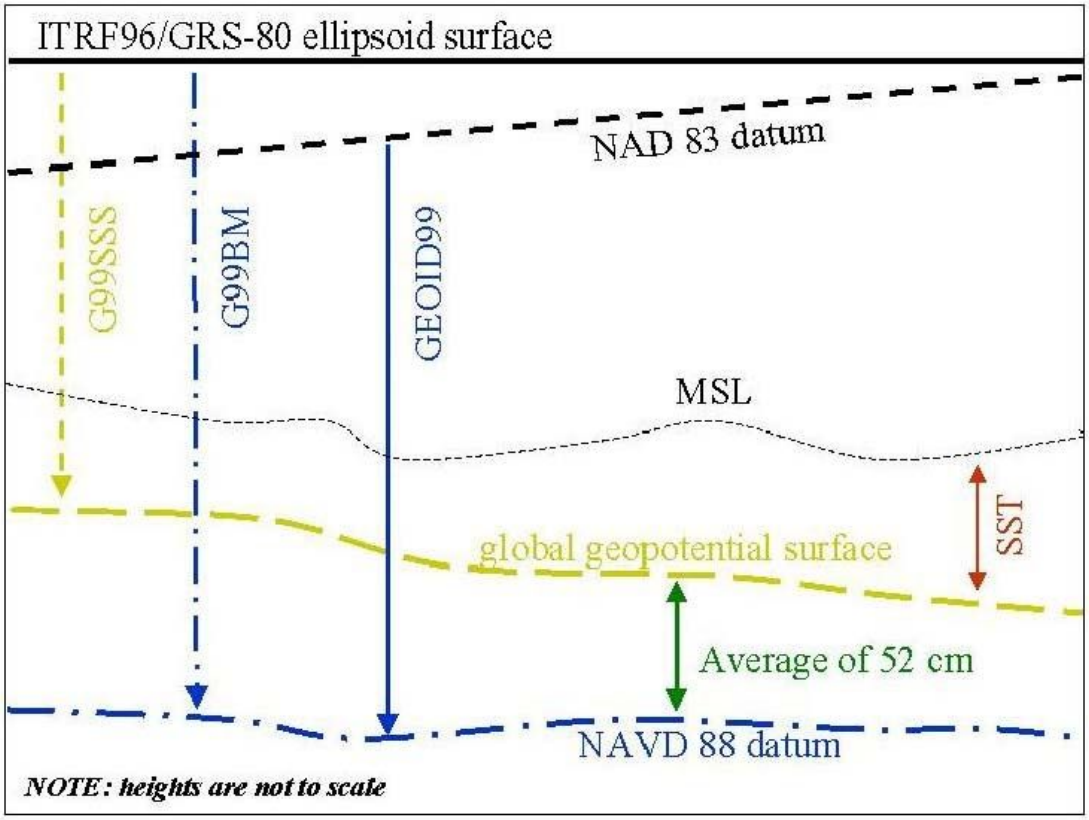

Figure 3.3. NGS geoid models and their relationship (National Geodetic Survey, 2001). G99BM is unavailable in Lake Erie. MSL and SST are mean sea level and sea surface topography, respectively.

The transformed GEOID03 model from NAD83 to ITRF00 is suggested by D. Roman (personal communication). It is the GEOID03 model value with the additional consideration of the height change due to a seven-parameter similarity transformation from the NAD83 datum to the ITRF00 at the location where the model value is acquired. The parameters and their velocity estimates can be found in National Geodetic Survey (2004). The transformation can be performed with NGS Horizontal Time-Dependent Positioning (HTDP) software. In addition to the coordinate transformation, the software

considers the crustal motion related to plate tectonics and earthquakes (Snay, 1999). The reference epoch is selected to be at the midnight UTC on January 1, 2002 (2002.0) in order to be consistent with the published coordinates of NGS CORS.

G99SSS, after the application of the 52 cm bias, is also analyzed in the same area at the same reference epoch in order to test this nationally averaged bias in the Lake Erie area.

The local geoid at the Marblehead and Cleveland water level gauges was estimated with a GPS buoy from two GPS buoy campaigns in which the GPS buoy occupied the lake near the water level gauge. The buoy's 3-dimensional Cartesian coordinates at the campaign time in ITRF00 were determined by DGPS from the onshore reference stations. The coordinates were projected to the 2002.0 reference epoch with the NGS HTDP software. It was found that the projection did not change the height by more than 1 mm at both water level gauges. As a result, the geoid height at the water level gauge can be determined by Eq. (3.1) with the orthometric height taken from the conversion of the water level gauge records from IGLD85, and the ellipsoidal height is directly provided by the GPS buoy. The datum relationship and the corresponding GPS solution at both gauges are shown in Figures 3.4 and 3.5.

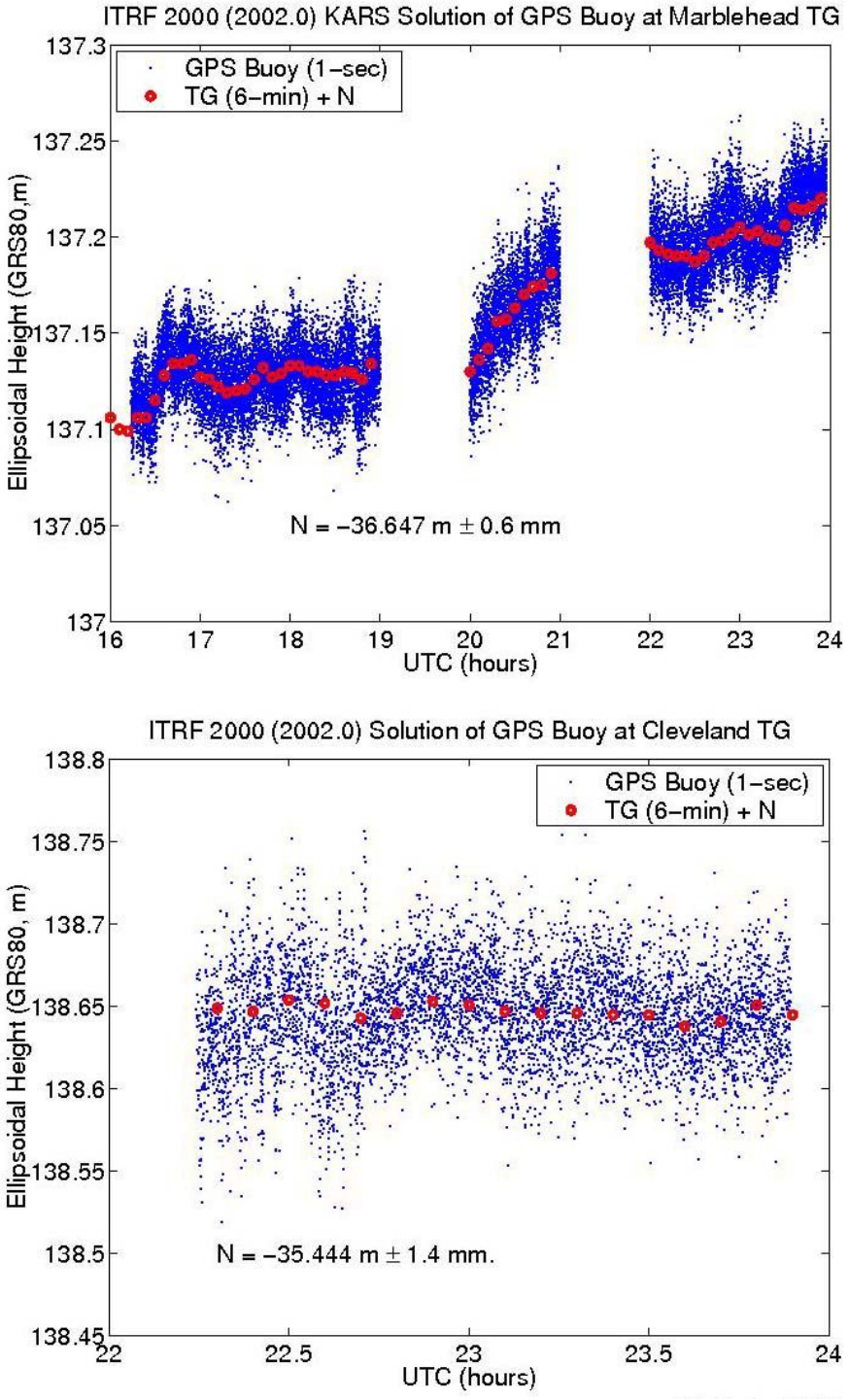

Figure 3.4. The GPS buoy solutions at Marblehead (top) and Cleveland (bottom). The estimated geoid heights are added to the gauge records in NAVD88.

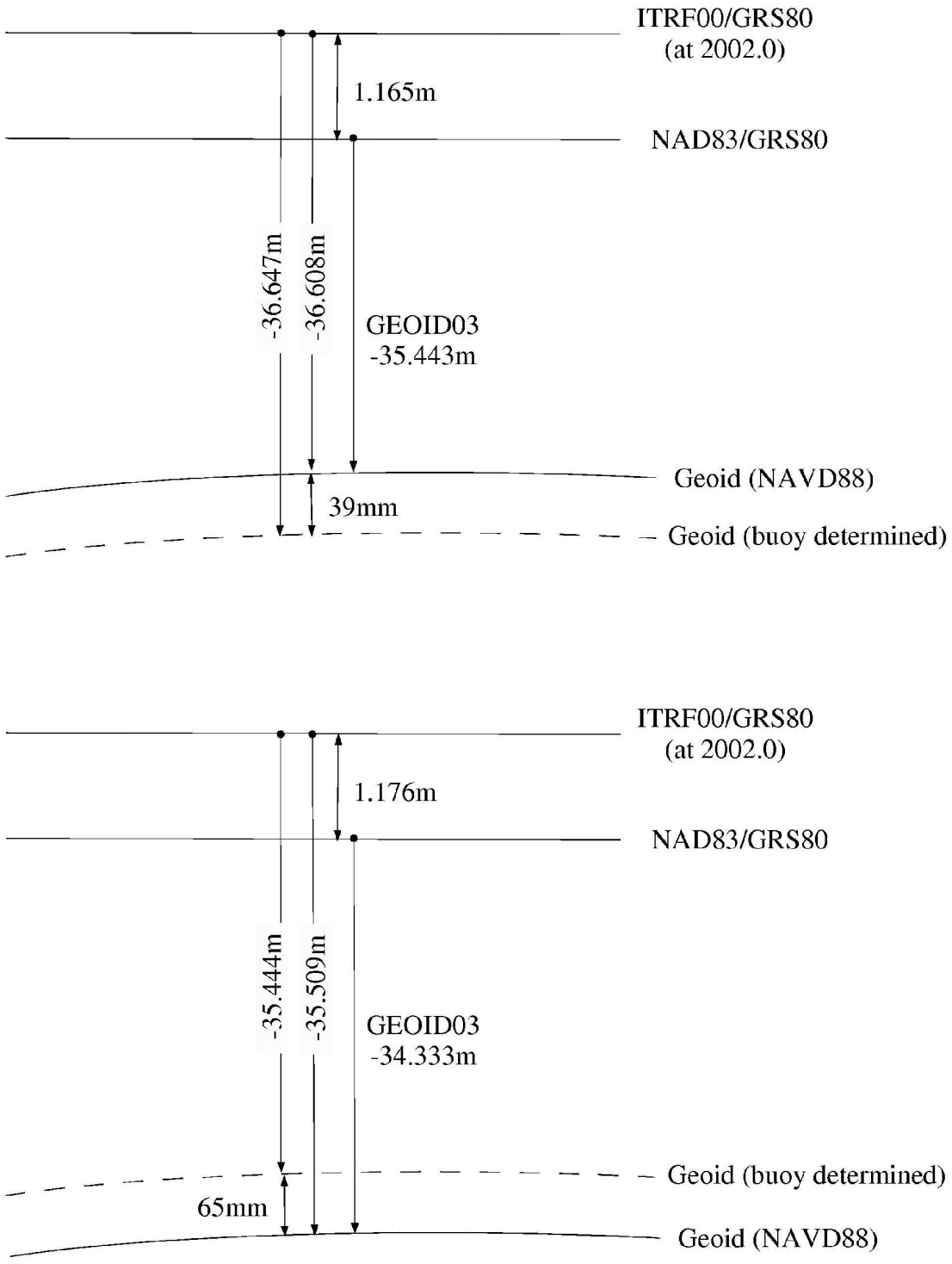

Figure 3.5. Datum relationship at Marblehead (top) and at Cleveland (bottom).

Geoid determination	Marblehead	Cleveland
Transformation GEOID03	-36.608 m	-35.509 m
G99SSS, with 52 cm discrepancy applied,	-36.637 m	-35.606 m
GPS buoy	-36.647 m	-35.444 m
Discrepancy (G99SSS-GEOID03)	-29 mm	-97 mm
Discrepancy (GPS-GEOID03)	-39 mm	65 mm

Table 3.1. The geoid comparison at both Marblehead and Cleveland gauges.

Table 3.1 presents the results from these three approaches for the determination of geoid at the water level gauges: the transformed GEOID03, G99SSS with 52 cm bias applied, and the result from a GPS buoy. It shows that the GPS buoy-determined geoid is within -39 and 65 mm to the coordinate-transformed GEOID03 at Marblehead and Cleveland water level gauges respectively. Based on the results at these two gauges, the 52 cm bias between the global geopotential surface and the NAVD88 as seen in Figure 3.3 seems to be reasonable at the Marblehead gauge. It is slightly too low at the Cleveland gauge and with an different sign. Since the bias is an average value based on the available information from the entire nation, it may not totally represent the local effect at Cleveland.

3.2.3 Vertical motions

Both water level gauge records and GPS buoy measurements are relative observations. The measurements either refer to the onshore benchmarks or the reference stations. Therefore both are not sensible to the local crustal motions including local subsidence, tectonic uplift and the post-glacial rebound (PGR). The PGR, also known as glacial isostatic adjustment (GIA), is a physical phenomenon that describes how the solid earth returns to an isostatic equilibrium since the deglaciation of the ancient ice sheets (i.e., the Laurentide Ice Sheet) that were accumulated during the Last Ice Age. The GIA effect occurs primarily in the mantle which is much thicker than the crust.

Satellite altimetry provides the lake surface height independently of the local crustal motion and can, hence, be used along with water level gauge records to determine lake-wide vertical motion. For example, Kuo et al. (2004a, b) determine the vertical motion around the Great Lakes, using daily records from 50 water level gauges around the Great Lakes and T/P altimeter lake surface height measurements from cycles 4–300. In particular, Kuo et al. (2004a), as illustrated in Figure 3.6, estimate the lake-wide vertical motion based on the data from 50 water level gauges and T/P cycles 3–330 in the Great Lakes compared with estimates using relative water level change from Great Lakes gauges (Manville and Craymer, 2005) and with GPS determined vertical velocities by USGS. The background of the figure is the vertical motion predicted by a GIA, ICE-4GVM2 (Peltier, 2002). In general, the local vertical motion in the southern bank of Lake

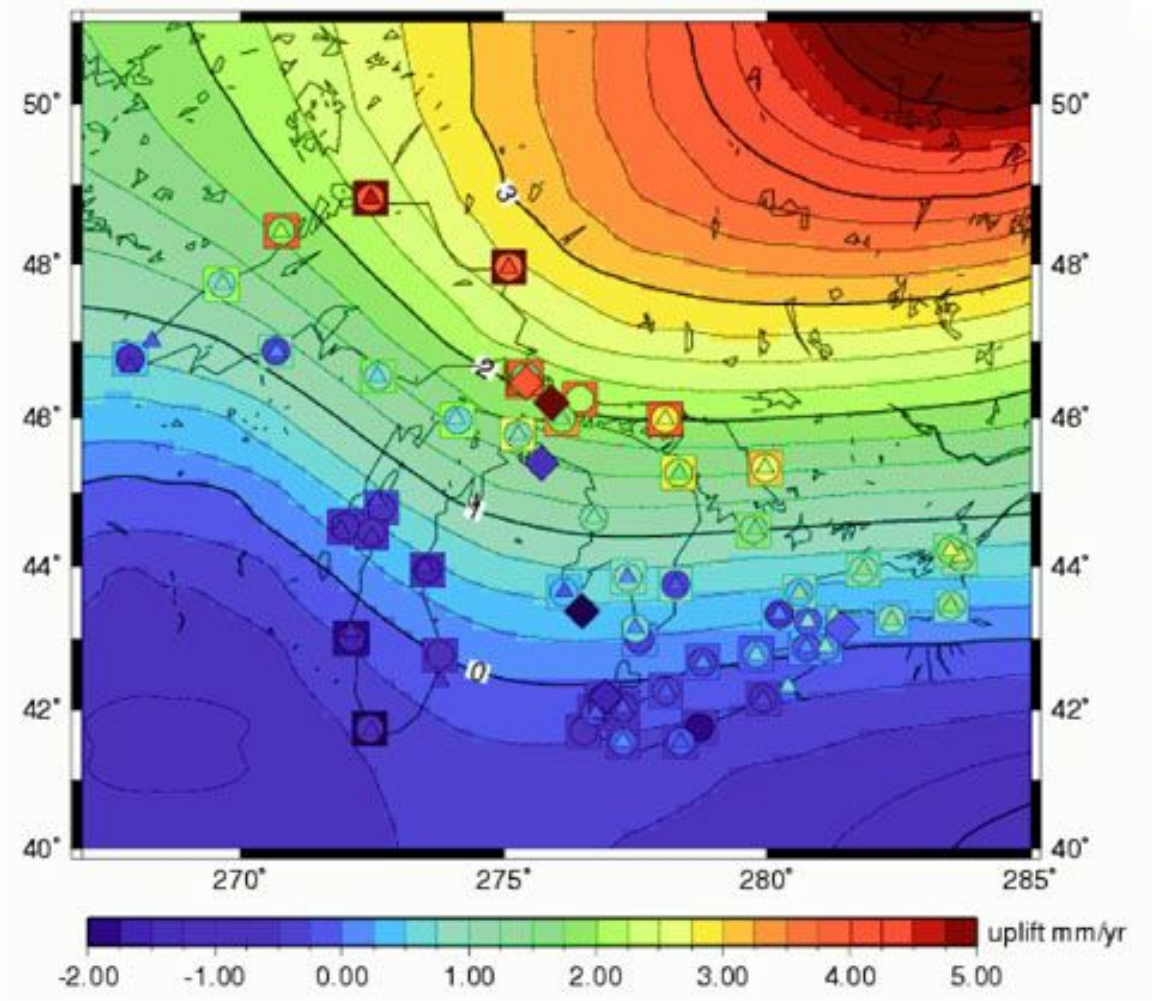

Figure 3.6. Vertical motion based on 50 tide gauges and TOPEX cycles 3–330 in the Great Lakes. Background shows predicted vertical motion of the ICE-4G VM2 model (Peltier, 2002). Triangles represent estimates of a tide gauge only analysis by Mainville and Craymer (2003). Squares indicate GIA model predictions of Mitrovica (Lithospheric thickness = 120 km, Upper mantle viscosity = $1x10^{21}$ Pas, lower mantle viscosity = $3x10^{21}$ Pas). Diamonds are USGS GPS velocity estimates (Figure adapted from Kuo et al., 2004a).

Erie is is estimated to be 0.2 mm/year (subsidence) and appears to be negligible for this study. However, other part of the Great Lakes have higher motion and this effect accumulates with time and should thus be modeled.

Alternatively, the vertical land motion can also be detected by the long-term GPS data (e.g., the USGS Great Lakes solution in Figure 3.6) obtained from continuous GPS networks in the regional or global scale. A regional CORS network implemented by the NGS and a regional Great Lake CGPS network in this region can be seen in Figure 2.2a, b on page 27, respectively.

3.3 Error budget

The error sources of converting a water level gauge record from IGLD85 to geocentric height above the GRS80 Reference Ellipsoid is presented in Table 3.2. The error budget coming from gravity and the hydraulic corrector uncertainties are based on Eq. (3.7) with the average height, normal gravity and model gravity in Lake Erie. The hydraulic corrector depends on the instrument and the steric phenomena. It affects the conversion in almost 1 to 1 ratio as seen in Eq. (3.7). The dominant term among the error sources stems from the geoid model. Three approaches for geoid determination have been tested in the previous section. GEOID99 presents a rms error of ±46 mm in the national average. However, due to the lack of gravimetric data around the lakes, the actual error in the Lake Erie area is expected to be larger. GEOID03 is the updated version of GEOID99, and its accuracy in this region still remains to be assessed.

	Error sources	Error budget
IGLD85 to NAVD88	Hydraulic corrector (HC)	1:1 ratio
	Model gravity	±(2 mm / 10 mgal)
NAVD88 to ellipsoidal	geoid model	±46 mm* (at least)
	GPS buoy and gauge	±1 mm (SD)
Vertical motions	Post-glacial rebound	< 1 mm / year

* RMS difference between GEOID99 and GPS benchmark (Smith and Roman, 2001).

Table 3.2. Error budget after converting the water level gauge IGLD85 record to ellipsoidal heights in the Lake Erie area.

The use of a GPS buoy collocated at water level gauge to estimate the geoid, has mm-level precision and shows discrepancies of -39 and 65 mm at Marblehead and Cleveland, respectively. The choice of geoid determination depends on the particular applications. The use of any NGS geoid model is sufficient for applications demanding decimeter accuracy. However, for the applications that need higher accuracy, such as altimeter calibration, it can be recommended to survey the geoid with GPS buoys (e.g., Shum et al. 2003).

3.4 Summary

In order to accomplish a seamless digital database in the coastal area to support safe navigation, regional decision-making, and coastline monitoring, the water level gauge records need to be incorporated into other forms of spatial information such as DEM, remote sensing images, and the lake level heights provided by GPS buoys and by satellite altimeters. It requires that these various data sets to be converted to one common geodetic reference frame.

The combination of the water level gauge records with the satellite data is beneficial. Spatially, the gauge records are collected by the lakeshore whereas the altimeter data and the lake surface heights measured by a GPS buoy are taken further away from the shoreline and toward the interior of the lake. Although the quality of the height determined by the buoy is limited by the baseline length, satellite altimeters are able to observe the lake-wide surface, mostly in the middle of the lake. Temporally, the buoys used in this study only provide a few lake surface height observations, while the total data span of satellite altimetry at present is only slightly longer than a decade or so. Both present a problem when a long-term trend of the lake surface change is needed. However, longevity of the water level gauge record is very helpful, in this case, for a reliable estimation of the trend.

The linking of both water level gauge and shoreline datum around Lake Erie to the ITRF is presented in this chapter, along with a detailed description of the common datums used in the Great Lakes area. The conversion formulas and an error budget table

are reported. For the conversion between IGLD85 to NAVD88, every 10 mgal error in the model gravity contributes about 2 mm error on the conversion. The error in the water level gauge record as well as the hydraulic corrector contribute nearly in an 1:1 ratio to the conversion. The hydraulic corrector tried to correct the observational, dynamical, and steric effects at each gauge. Unfortunately there is no quantifiable error information available about these error sources at present.

Generally, the combination of data from satellite observations and the gauge record requires the knowledge of geoid height since the gauge records usually refer to, or can be converted to, the orthometric height above the geoid. Three approaches for geoid determination were compared: i) the use of a GPS buoy at the Cleveland and Marblehead water level gauges, ii) the use of the GEOID03 model with followed by a 7-parameter similarity transformation, and iii) the use of G99SSS together with the application of the 52-cm nationwide averaged bias. The result of these three approaches at Marblehead and Cleveland agree to several cm. It is found that this bias is reasonable near the Marblehaed gauge and is slightly low near the Cleveland gauge.

Both water level gauge and GPS buoy provide relative observations with respect to the benchmarks and the onshore reference stations, respectively. Their observations are therefore not sensitive to the vertical ground movement. Hence, the impact of the vertical motion of the land is expected to be 0.2 mm/year (subsidence) in the southern bank of Lake Erie. It should be considered, especially in dealing with long-term water level gauge records. It is worth noting that the described procedure, applicable to Lake Erie or the rest of the Great Lakes area, can be generalized to other coastal ocean applications.

CHAPTER 4

ABSOLUTE CALIBRATION OF SATELLITE ALTIMETERS

This chapter discusses the principle of satellite altimetry and the basic idea of absolute calibration of satellite altimeters with *in-situ* water level data. Section 4.1 will discuss the fundamental principle of satellite altimetry, some of the current operational satellite altimeters, and their corrections.

The current operational radar satellite altimeter missions include TOPEX/Poseidon (T/P), JASON-1, European Remote Sensing satellite (ERS-2), ENVIronment SATellite (ENVISAT), and GEOSAT Follow-On (GFO). Both T/P and JASON-1 are joint missions between the National Aeronautics and Space Administration (NASA) of the U.S. and the Centre National d'Etudes Spatiales (CNES) of France. ERS-2 and ENVISAT are missions launched by the European Space Agency (ESA). The GFO is operated by the U.S. Navy and the Ice, Cloud and land Elevation Satellite (ICESat) of NASA is a spaceborne laser altimeter currently also operational. The mission description of T/P, JASON-1, ERS-2, ENVISAT, and GFO will be included in Section 4.1. The altimeter principle and waveform processing are discussed in Section 4.2. The related corrections are provided in Section 4.3.

The absolute calibration based on the rigorous adjustment model will be discussed in Section 4.4. Additional numerical comparison of results for the so-called "closure equation", using various adjustment models, will be presented in Chapter 6.

The different types of *in-situ* water levels provided by the GPS buoy, the GPS-equipped vessel, the coastal water level gauges, and the BPG will also be addressed. Two calibration sites: Lake Erie and the South Pacific Calibration Sites as well as their calibration results, are discussed in Sections 4.5 and 4.6. The establishment of both calibration sites involves the use of the GPS buoy, or the GPS-equipped vessel, respectively, to collocate at the water level gauges, or at the site of the bottom pressure gauge, in order to link their records to a geocentric reference frame for calibration. Section 4.7 summarizes the chapter.

4.1 Satellite altimetry

One of the first discussions of using satellites to observe sea surface height happened at the 1969 Williamstown Conference of Solid Earth and Ocean Physics (Kaula, 1969). Four year later in the Skylab orbiting platform, the first space-borne altimeter measurements of the oceans were made by the on-board S-193 radar altimeter with about 1-m precision (Gopalapillai et al., 1975). Since then, a number of altimeter missions have been implemented with more precise instruments. Table 4.1 presents a list of past and future altimeter missions, including their orbital parameters. Some of the new

Mission	Active Dates (month/year)	Altitude (km)	Inclination (degrees)	Repeat Period (days)	Agency
GEOS-3	4/75-12/78	840	115	Non-repeat	NASA
SEASAT	7/78-10/78	790	108	17, 3	NASA
GEOSAT GM	3/85-11/86	780	108	Non-repeat	US Navy
GEOSAT ERM	11/86-12/89			17	
ERS-1 A	7/91-11/91	785	98.5	3	ESA
ERS-1 B	11/91-3/92			3	
ERS-1 C	4/92-12/93			35	
ERS-1 D	12/93-4/94			3	
ERS-1 E	4/94-9/94			168	
ERS-1 F	9/94-3/95			168	
ERS-1 G	4/95-6/96			35	
TOPEX/POSEIDON	8/92-present	1354	66	10	NASA CNES
ERS-2	4/95-present	785	98.5	35	ESA
GFO-1	5/98-present	800	108	17	US Navy
ENVISAT	06/2001	785	98.5	35	ESA
JASON-1	2001	1354	66	10	NASA CNES
ICESat	2003	600	94	8, 91	NASA
CryoSat	2005	720	92	369, 30	ESA
JASON-2	2008	1336	66	10	NASA CNES
NPOESS*	2006-2018	800-1300	66-98.5	10-35	Int'l

* planned

Table 4.1. Satellite altimeter missions.

missions are designed as the follow-on missions. For example, JASON-1 and ENVISAT are the follow-on missions for T/P and ERS-2, respectively.

Since the first experiment on the Skylab, satellite altimetry has evolved into an operational observing system for synoptic measurements of the global sea surface height (ssh) above the reference ellipsoid with respect to a well-defined ITRF with rms error better than ±3 cm, temporal resolution of 1-2 weeks, and cross-track spatial resolution of up to 50 km (Chelton et al., 2001). In addition to about a decade long global ocean observations by the previously operational altimetric missions, the currently operational satellite altimeters include T/P, JASON-1, ERS-2, ENVISAT, GFO, and ICESat. This unprecedented opportunity of several concurrent operating satellite altimeters will improve the temporal and spatial resolution of ocean observations which will benefit various scientific aspects such as better understanding of the ocean circulations (Wunsch, 2001), global sea surface topography, gravity modeling, the study of the climate pattern, global sea level change, and others.

Some of the new missions such as JASON-1 and ENVISAT offer the data nearly in real-time. For example, JASON-1 is near real-time ssh anomaly (Product #148) has a 3-hour latency containing ssh anomaly, significant wave height, altimeter wind speed, and various corrections. ENVISAT has the Fast Delivery Geophysical Data Record (FD) with about the same latency for weather forecasting, sea state, and real-time ocean circulation applications (Resti et al., 1999). This advancement in the near real-time data delivery plays a key role in the short-range ocean prediction. It makes it possible to monitor the mesoscale signals near real-time, and to adjust the model more regularly (Menard et al., 2003).

The principle of satellite radar altimetry is quite straightforward. The altimeter emits a radar pulse and measures its travel time when the radar pulse is bounced back from the instantaneous sea surface. The instantaneous range between the satellite and the surface is inferred from half of the travel time. However, the actual observable is a time series of the received power distribution of the reflected pulses, which are called waveforms. Details will be discussed in Section 4.2.

There are three fundamental measurements of a satellite radar altimeter from the waveform processing: the instantaneous range, which is usually expressed as the instantaneous ssh above the reference ellipsoid, the wave height, and the wind speed. In addition, there are instrumental, media, and geophysical corrections that are needed for the raw altimeter measurements.

Radar altimetry is exclusively designed for the oceans and large inland lakes because of the favorable reflectivity of the radar signals on the large water surfaces. In addition to radar, laser has recently been implemented in the ICESat mission. Although its operation time is hampered by the hardware heating problem, one can still see its potential of being used to provide elevation measurements on nearly all types of surfaces, including ocean, land, ice and cloud. It even provides the canopy height and vegetation height as a byproduct (Braun et al., 2004).

4.1.1 TOPEX/Poseidon mission

Figure 4.1. Artist's concept of TOPEX/Poseidon (Courtesy of the Jet Propulsion Laboratory).

TOPEX/Poseidon is a joint satellite radar altimeter mission by NASA (USA) and CNES (France). It was launched on August 10, 1992, with an approximate 10-day repeat, nearly circular orbit, 66° inclination, and an altitude of 1354 km. It was the first radar altimeter mission specifically designed for studying general ocean circulations (Fu et al., 1994) and, therefore, highest accuracy was required. Many innovations were incorporated in the mission design to meet these requirements such as the first dual frequency (C- and Ku-band) altimeter for the first-order ionospheric delay corrections, a three-channel microwave radiometer for measuring integrated water vapor contents, and three satellite tracking systems including Satellite Laser Ranging (SLR), Doppler Orbitography by Radiopositioning Integrated on Satellite (DORIS), and GPS for precise orbit

determination. T/P measures the sea surface height with a ±1.7-cm precision and an overall accuracy of ±4.7 cm. This accuracy is almost twice better than the original mission requirement of ±13.4 cm (Fu et al., 1994).

The TOPEX altimeter has redundant Sides A and B hardware. The signals from Side A altimeter began to show performance degradation in 1999. Therefore, after 6-year of exclusive Side A operation, the TOPEX Science Working Team and the Jet Propulsion Laboratory engineers decided to switch to Side B at 15:04 UTC on February 10, 1999 (Hayne and Hancock, 2000). The success of the T/P mission has ensured the place of satellite oceanography as both a prominent and bountiful area of scientific study (Urban, 2000). In December 2001, T/P and JASON-1 were placed in the same orbit forming a so-called tandem phase where JASON-1 led T/P by about 70 seconds. The tandem phase lasted about 7 months and T/P has been moved since August 2002 to the orbit with the ground tracks in between its old ones. JASON-1 took over the T/P old orbit. The detail of the tandem phase is discussed in the next section.

4.1.2 JASON-1 mission

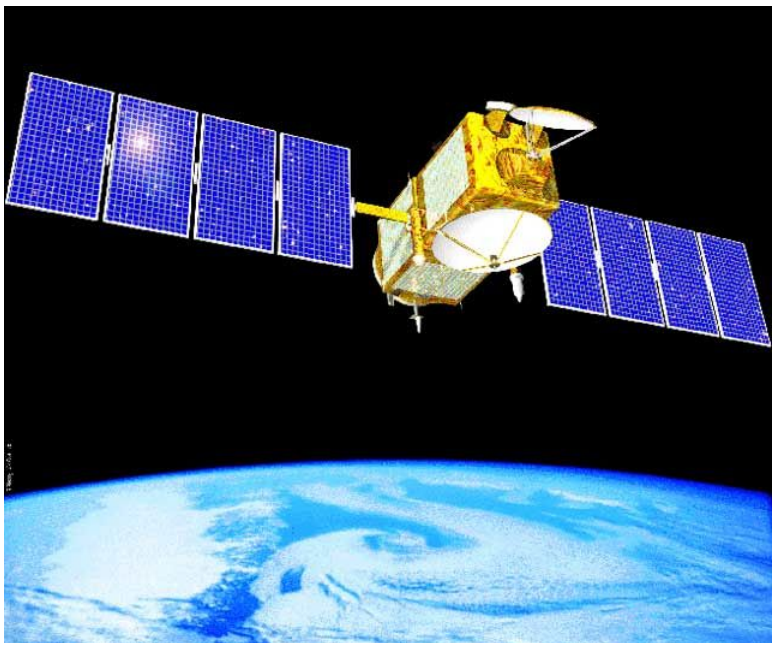

Figure 4.2. Artist's concept of JASON-1 (Courtesy of the Jet Propulsion Laboratory).

The JASON-1 satellite is also a joint mission between NASA (USA) and CNES (France) and intended to be the follow-on mission to T/P. It was designed to measure the sea level along the T/P reference ground tracks with equivalent or better accuracy than T/P (Menard et al., 2000). It has orbital parameters and a payload similar to those of T/P. The on-board Poseidon-2 altimeter is derived from the Poseidon-1 altimeter, but works at C- and Ku-bands for ionospheric delay correction. The DORIS device, a GPS receiver and a Laser Retroreflector Array (LRA) are also on-board for the precise orbit determination. A three-frequency JASON-1 microwave radiometer (JMR) is used to measure the water vapor contents along the nadir for the calculation of tropospheric delay

correction. The prelaunch error budget found in the JASON-1 Geophysical Data Record (GDR) for the global ssh is about ±4.2 cm (1σ) over the T/P ground tracks (Menard et al., 2003).

Its primary goals include i) the measurement of the sea surface topography to continue observations of T/P in order to determine the general oceanic circulation for a better understanding of its role in global climate change, ii) the measurement of global mean sea level to improve the understanding of its relationship to oceanic heat and water exchange with the atmosphere, the solid Earth, and the ice sheets, iii) the contribution to observations of the mesoscale ocean variability such as the eddies, iv) the improvement in the tide modeling, and v) the support of other types of investigations in marine meteorology (Menard et al., 2003).

JASON-1 was launched into the T/P old orbit in December 2001. For a period of about seven months, it led T/P by about 70 seconds, with both running on the T/P orbit. It is called the tandem phase. The common model error in both missions can be canceled by differencing. It also allows the direct comparison of the corrections for both missions. These cross-verifications provide better understanding for the long-term system stability (Bonneford et al., 2003). The tandem phase lasted for 7 months; then T/P was moved to its new orbit, with the ground tracks halfway in between its old ones. Along with other operational altimeters, the move of T/P increases the spatial and temporal resolution globally.

4.1.3 ERS-1/-2 missions

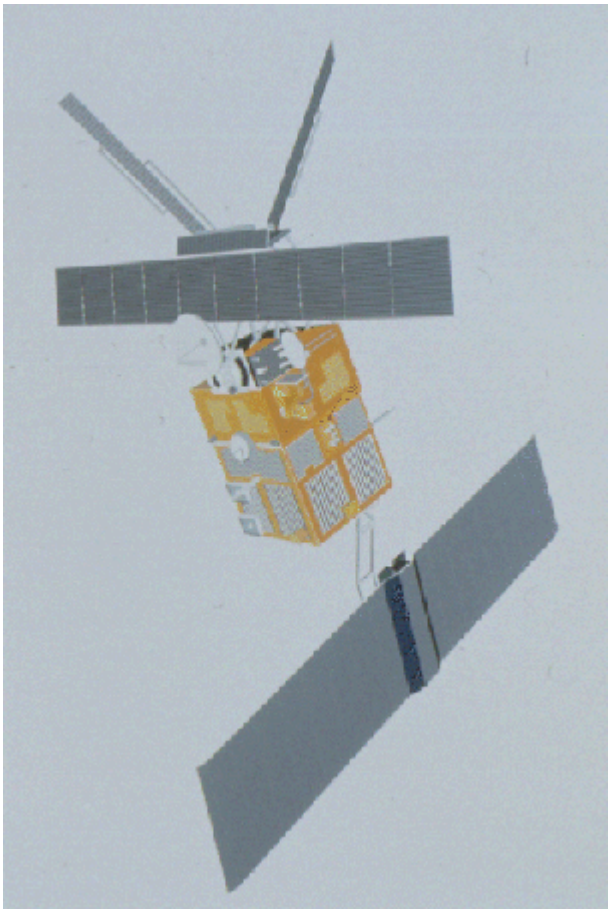

Figure 4.3. Artist's concept of ERS-2 (Courtesy of ESA).

ERS-1 was implemented by ESA and was launched on July 17, 1991. Its mission objective was to observe the Earth's atmospheric and surface properties using radar techniques. ERS-1 contains seven phases (Phases A to G) with three orbit designs (see

Table 4.1) for different purposes. For example, there were a 3-day repeat orbit for calibration and ice-sea observation, a 35-day repeat orbit for multi-disciplinary ocean observations, and a 168-day repeat orbit for geodetic applications.

ERS-2 is the follow-on mission to the ERS-1 mission. It was launched on April 21, 1995. The goal of the ERS-2 mission is to continue the ERS-1 mission, with improved and additional tasks to observe the Earth, in particular the atmosphere and the oceans. In contrast to the different orbits and phases of ERS-1, ERS-2 operates on a polar sun-synchronous 35-day orbit, similar to one of the ERS-1 orbits. During the period from August 1995 to June 1996, it formed a tandem operation with ERS-1 in the same orbit, where ERS-2 passes the same location 24 hours after ERS-1 does (European Space Agency, 1997). Shortly after the launch of ERS-1, however, the Precise Range And Range-rate Equipment (PRARE) failed due to the high radiation environment (Schäfer and Schumann, 1995). As a result, its orbit accuracy was ±5 to ±7 cm rms error with the SLR tracking (Bordi, 1999).

The radar altimeter (RA) on the ERS satellites is a Ku-band (13.8GHz) nadir-pointing active sensor to measure the returned echoes from the ocean and ice surfaces. It has two modes: ocean and ice and is able to provide ssh, wave height, wind speed and other parameters over sea ice, and ice sheets. The ionospheric path delay was acquired from the Bent model (Llewellyn and Bent, 1973), and the wet tropospheric path delay was measured by the on-board microwave radiometer (MWR). In addition to the RA, both satellites carry Synthetic Aperture Radar (SAR) and other remote sensing instruments.

4.1.4 ENVISAT mission

Figure 4.4. Artist's impression of ENVISAT after the completion of the primary deployment of the solar arrays. (Courtesy of ESA).

ENVISAT was implemented by ESA as the follow-on mission to ERS-1/-2. It follows the same ground tracks of ERS-1/-2 and attempts to provide a continuous time series of local sea height variation, which will span more than 15 years. It will allow a more reliable trend estimate to support studies of global and regional sea level rise, dynamic ocean circulation, significant wave height climatology, and ice-sheet elevation.

ENVISAT was launched on March 1, 2002, in the sun-synchronized 35-day repeat orbit with an inclination of 98.5º, the same as that of ERS-1/-2. This inclination makes it possible to reach ±81.5º latitude, which covers more of the polar regions than in the case of T/P and JASON-1. Its Radar Altimeter 2 (RA-2), the microwave radiometers, and the positioning instruments, including DORIS and laser retroreflector, were switched on 12 days after the successful launch (Benveniste et al., 2002). Its RA-2 system is based on dual-frequency (at 13.575 GHz in the Ku-band and at 3.2 GHz in the S-band). The dual-frequency design helps to correct for the first order of the ionospheric delay. The radiometer measures the water contents along the nadir to provide the tropospheric delay correction. In addition to the altimeter unit, it has other instruments on board such as the Advanced Synthetic Aperture Radar (ASAR) and other sensors for remote sensing.

Resti et al. (1999) mentioned that the post-processing mode in the RA-2 on ENVISAT is separated from the on-board processing. It is used when the power of the reflected radar pulse is over the limit for the on-board processing and, thus, requires the extraction of geophysical quantities. The separation enhances the RA-2 ability, within the pulse-limited technique, to be used on the non-ocean surfaces. It was argued that it is able to track the sea ice freeboard height with the accuracy of about ±0.5 m; it was also pointed out that it might be used to determine non-ocean surfaces such as land elevation in the near future.

4.1.5 GFO mission

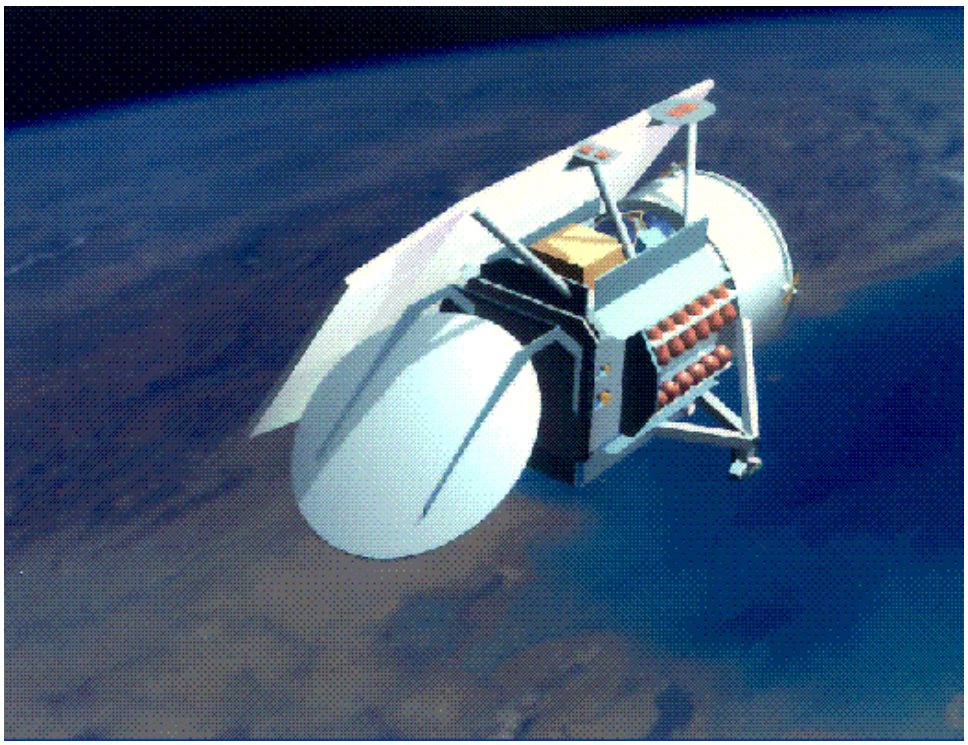

Figure 4 5. Artist's impression of GFO mission (Courtesy of the U.S. Navy)

The GEOSAT Follow-On (GFO) mission was launched by the U.S. Navy on 10 February 1998 and the space vehicle was placed into a 17-day repeat orbit, corresponding to a similar orbit used by GFO's precursor mission, GEOSAT, the so-called Exact Repeat Mission (ERM). The primary objective of GFO mission is to develop an operational series of radar altimeter satellite to maintain continuous ocean observation for accurate global measurements of both mesoscale and basin-scale oceanography (Zhao, et al., 2003).

Its payloads contain a single frequency (Ku-band) radar altimeter system with 3-cm height precision, a dual-frequency water vapor radiometer, a Turbo-star 16-channel GPS receiver, and Doppler beacons which allows operational orbit be determined within precision of 1.8 cm in radial. An extensive calibration and validation process has been undertaken from June 1999 to October 2000. Since 29 November 2000, the altimeter system became operational (U.S. Navy, 2005). However, shortly after launch, the onboard GPS receiver failed to track more than one satellite. The GPS receiver was intended to be one of techniques for the precise orbit determination and for providing time tags to the measurements. As a result, the satellite laser ranging (SLR) technique was used as the primary approach for its orbit determination. For example, Zhao et al. (2003) determined an orbit with data from the SLR data and altimeter measurements at crossover locations, and the TEG3 gravity model (Tapley et al., 1997) with a rms error of 5–6 cm radially. The precise orbit for GFO is being routinely computed by NASA/GSFC (Goddard Space Flight Center) Space Geodynamics group of using SLR, and the civilian use of GFO satellite altimetry data product is coordinated by the Laboratory of Satellite Altimetry at NOAA.

Since 1 September 2005, the ground processing system of the GFO data has been stopped momentarily due to the catastrophic damage caused by the Hurricane Katrina in the area from Louisiana to Alabama in the U.S. The satellite is functioning normally and the data is being archived in the hope that the data processing will resume when the ground processing system at Bay St. Louis, Mississippi returns to normal operations (U.S. Navy, 2005).

4.2 Waveform processing

As mentioned earlier, the actual observations in satellite radar altimetry are collected as time series of the received radar power distribution of the reflected pulses, also known as the altimeter waveforms. Figure 4.6 presents an ideal average altimeter waveform for water surface and its associated surface illumination pattern. Due to favorable water reflectivity, radar altimetry is primarily designed for the oceans and large inland lakes although measurements over reflecting surfaces, such as ice sheets and lands, have contributed to scientific studies.

As illustrated in Figure 4.6, AGC (Automatic Gain Control) is the maximum returned energy of an altimeter waveform. It is often used to normalize the altimeter waveform when sensing different surfaces such as land, ocean and ice. t_R represents the time at the half power point, which is determined at half of the maximum received radar power. By multiplying the half of the total travel time with the speed of light, the range between the satellite radar antenna to the instantaneous sea surface can be determined. The wave height on the sea surface affects the waveform slope in the leading edge, which is also known as the significant wave height (SWH). In addition, the wind changes the waveform slope in the trailing edge. It is called back-scattering cross-section (σ_0) at nadir, represented by the slope of the trailing edge of the waveform.

Therefore, the altimeter range, SWH, and σ_0 are three fundamental altimeter measurements derived from the altimeter waveform. The non-directional wind speed can be derived from σ_0 with a model function. Also with the satellite altitude known above the chosen reference ellipsoid, the ssh can be derived from the altimeter range and the altitude. The next section will present the formulas of ssh with the necessary corrections.

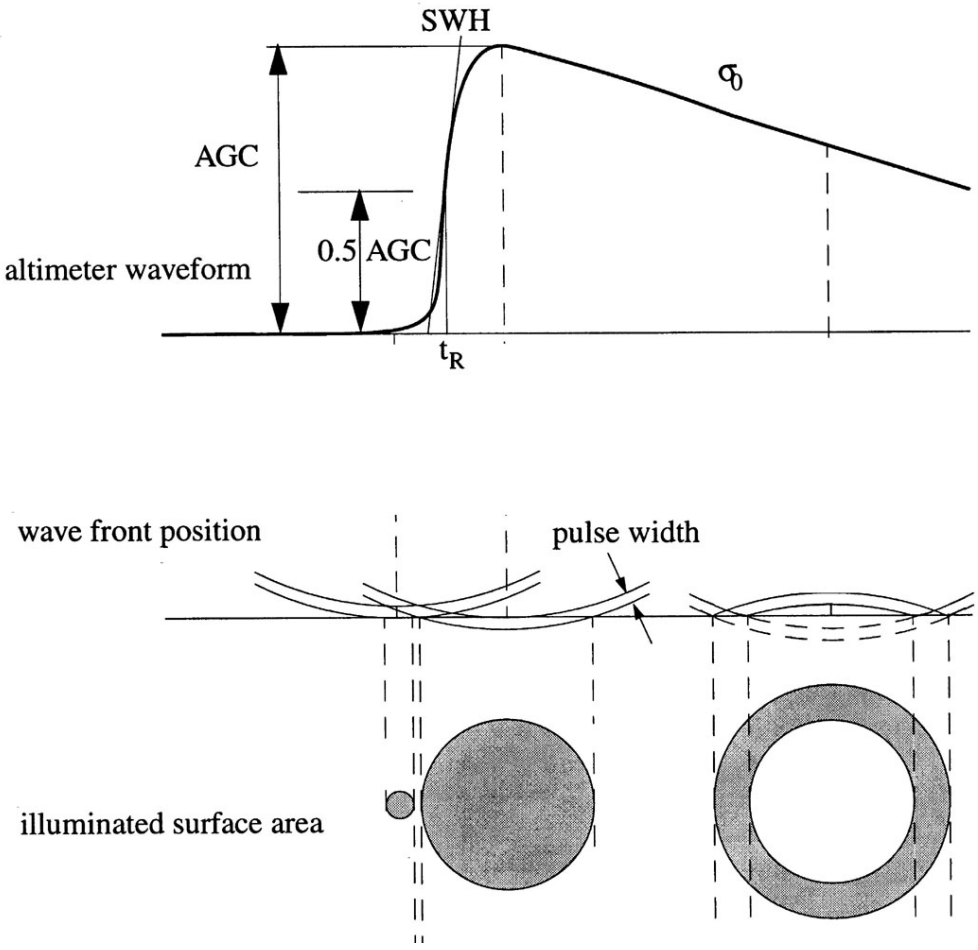

Figure 4.6. The ideal average altimeter waveform for the water and its illumination pattern (Kruizinga, 1997).

4.3 Sea surface height and corrections

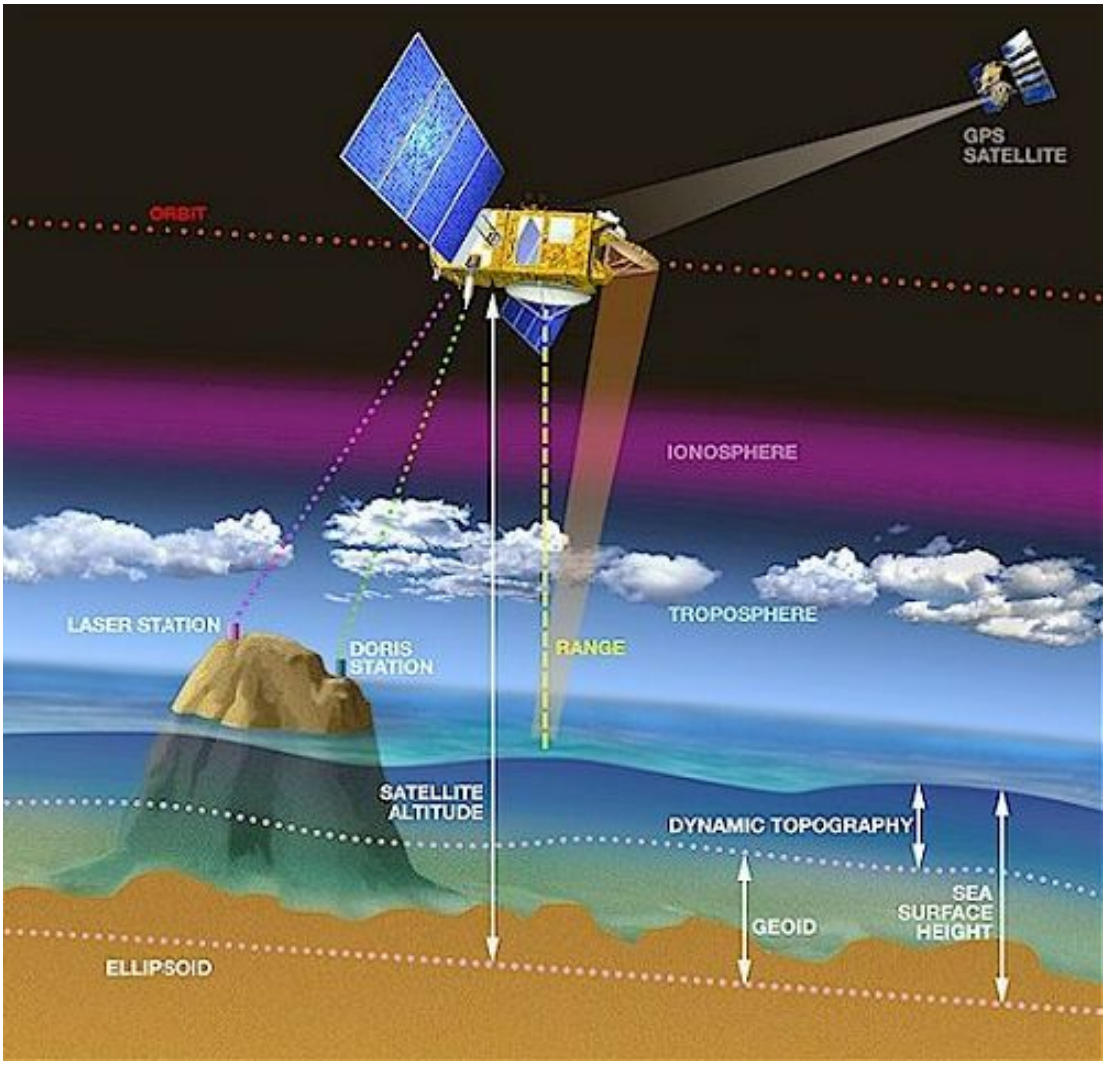

Figure 4.7. The geometry of satellite altimetry (Courtesy of AVISO).

Figure 4.7 presents the geometry of satellite altimetry in an ideal case. Assuming that all quantities are normal to the reference ellipsoid, the instantaneous ssh, which is defined as distance above the selected reference ellipsoid, can be formulated through Eq. (4.1).

$$h_{ssh} = h_{orbit} - h_{altcor} \tag{4.1}$$

where h_{ssh} is the instantaneous sea surface height, h_{orbit} is the altitude of the satellite in its computed orbit and h_{altcor} is the actual altimeter range.

The satellite altitude (h_{orbit}) is computed by precise orbit determination, using different satellite tracking techniques such as SLR, DORIS, and GPS. Its error sources involve the error in the terrestrial gravity field and others dynamical models used in orbit determination, errors in the ground tracking stations, ITRF and earth orientation, measurement errors, the imperfection of the orbit computation procedure, and others.

The dynamic topography can be split into the mean dynamic topography and the time-varying dynamic topography, which is caused in part by tides, currents, and atmospheric loading, etc. The total effect of the mean and the time-varying dynamic topography is also called sea surface topography (sst), whose magnitude is about 1-2 meters. Further descriptions about the sea surface topography can be found, for example, in Calman (1987).

Usually the mean sea level, which is called the stationary sea surface by Lisitzin (1974), is understood to be the sea surface that is free from all time-dependent variations such as tides, currents, and atmospheric pressure. However, the sea surface moves and it

may deviates from the geoid by the quantity of the sea surface topography in the order of 1-2 m. Hence, the often used approximation of the geoid by the mean sea surface is not generally valid, if a resolution is required that is better than 2 m.

The altimeter range observation, which is derived from the multiplication of half the total travel time with the speed of light, does not really represent the actual range between the instantaneous sea surface and the satellite because the measured time epochs are affected not only by random noise, but also by the instruments, the atmosphere that the radar pulse penetrates, and other geophysical factors. Therefore, altimeter range corrections are necessary whose quality directly affects the accuracy of the corrected altimeter range and, hence, the ssh measurements. There are basically three categories of systematic altimeter range corrections: instrumental, media, and geophysical. They need to be applied to the altimeter range measurement so that the corrected range measurement can better represent the intended observable. However, all the corrections are either taken from measurements (e.g., ionosphere and wet troposphere), or are derived from physical or empirical models. Therefore, individual corrections in the form of constant biases and the drifts could manifest themselves as part of the total altimetric bias, including the drift.

With all corrections applied, the corrected altimeter range in Eq.(4.1) can be defined as following.

$$h_{altcor} = (h_{alt} + h_{instru} + h_{ssb} + h_{dry} + h_{wet} + h_{iono} + h_{tides} + h_{ib}) - \beta - e \qquad (4.2)$$

where

h_{altcor} is the actual altimeter range,

h_{alt} is the raw altimeter range observation, derived from the multiplication of half of travel time with the speed of light,

h_{instru} is the total of the instrument corrections,

h_{ssb} is the sea state bias correction,

h_{dry} is the dry tropospheric path delay,

h_{wet} is the wet tropospheric path delay,

h_{iono} is the ionospheric path delay,

h_{tides} are the tide corrections, including solid earth tides, ocean tides, and pole tides,

h_{ib} is the inverted barometer correction,

β is the constant altimeter range bias, and

e is the random noise.

Replacing h_{altcot} in Eq. (4.1) by Eq. (4.2), the mean sea surface height is defined as:

$$h_{ssh} = (h_{orbit} - h_{alt} - h_{instru} - h_{ssb} - h_{dry} - h_{wet} - h_{iono} - h_{tides} - h_{ib}) + \beta + e \tag{4.3}$$

Even with all the corrections, derived either from the observations or from the physical models, applied in Eq. (4.3), there still exists an altimeter bias, β, between the altimeter-measured mean ssh and the real one. This is the reason why the calibration is required in order to determine this bias and, thus, better account for it. It is of importance for acquiring the accurate ssh measurements, especially in linking multiple satellite radar altimeter missions. In fact, every correction may contribute to this bias since there are errors in the observations and imperfections in the physical models at the time when they

were derived. Each individual altimeter has its own constant bias, and it is found that the bias of each mission drifts in different ways. Therefore, there are several dedicated calibration sites in the world to calibrate them. They provide accurate *in-situ* water level information directly along the altimeter ground track for absolute calibration. The calibration principle and two calibration sites at Lake Erie and in the Southwest Pacific Ocean will be discussed in Sections 4.5 to 4.6.

The systematic corrections of the raw altimeter data include the following:

(1) Instrumental corrections

The instrumental corrections are necessary due to the variations in spacecraft hardware, resulting from the nature of the return signal, satellite motion and pointing errors, satellite temperature variations, and other hardware properties. They include, among others, Doppler corrections, center-of-mass offsets, mispointing tracking adjustments, and internal calibrations.

The Doppler correction corrects the range measurements to account for the Doppler shift due to the velocity of the satellite. The center-of-mass corrections correct the phase center of the radar altimeter antenna to the center of mass of the spacecraft, for which the orbit is computed. The internal calibration, for example on T/P, is a measured range drift due to the changes in the internal electronic path delay that are primarily caused by thermal effects. This internal instrument drift, or the Wallops Correction, has been derived and reported by the NASA GSFC/Wallops Flight Facility (Hayne, 1999).

Also, the sea state bias (ssb) includes the effects of the electromagnetic bias, skewness bias, and tracker bias (Gaspar et al., 1994). It is also required because the troughs of the waves reflect the microwave pulses better than the crests. This causes the altimeter range measurement to be biased (advanced) towards the troughs.

(2) Media corrections

The media corrections include ionospheric path delay, dry tropospheric path delay, and wet tropospheric path delay.

Ionospheric path delay is frequency-dependent; for example, the ionospheric path delay in 14 GHz (Ku-band) is about 5 cm to 20 cm, depending on the level of ionization (Lorell et al., 1982). However, it can be corrected with a certain linear combination of the range measurement in different frequencies. Most of the recent altimeter missions are equipped with a dual-frequency altimeter, and they use the returned signal from both frequencies to calculate and correct the first order ionospheric path delay correction.

The tropospheric path delay is radar-frequency independent, and it contains a dry and a wet component. Dry tropospheric path delay is caused by the dry-air components in the atmosphere, which cannot be directly measured by sensors on the altimeter satellites. Hence, the operational atmospheric global circulation models (AGCM) such as the European Center for Medium-Range Weather Forecasting (ECMWF) model. This type of models provides global atmospheric pressure at sea level, are required to interpolate dry-air components to the space-time coordinates of each range measurement and to compute the delay using a physical model. The average dry tropospheric delay is about 2.3 m (Tapley et al., 1982).

The wet tropospheric delay is caused by the water vapor contents in the atmosphere, which can be modeled by ECMWF or can be directly measured by an on-board microwave radiometer. All present and proposed radar altimeter satellites include on-board active microwave radiometer to measure the water vapor along the nadir. However, the water vapor contents measured by a radiometer could be corrupted by the liquid water (e.g., cloud or rain) along the nadir path. Also, current microwave radiometers have much larger footprints than that of the altimeter and consequently, the non-ocean surfaces (e.g., coastal lands and ice) within the footprint will prevent the radiometer from getting accurate water vapor contents measured. Therefore, radiometer-measured tropospheric path delays near the coast may be problematic. This is one of the reasons why altimeter ssh measurements are less accurate near the coasts. ECMWF model-computed delays or the delays measured by a land-based radiometer could, in this case, be used in place of the satellite radiometer-measured delays.

(3) Geophysical corrections

The geophysical corrections include tides (solid earth, ocean, and pole tides), the inverted barometer (IB) correction, and mean surface gradients.

The inverted barometer effect reflects the ocean surface deformations due to atmospheric loading, assuming that the seawater is a barotropic, incompressible fluid (Ponte, 1993). In general, the sea level is reduced by 1 cm with an approximately 1-mbar increase of atmospheric pressure. However, since the *in-situ* water level measurement usually contains effects from tides and atmospheric pressure, the ocean tide and inverted

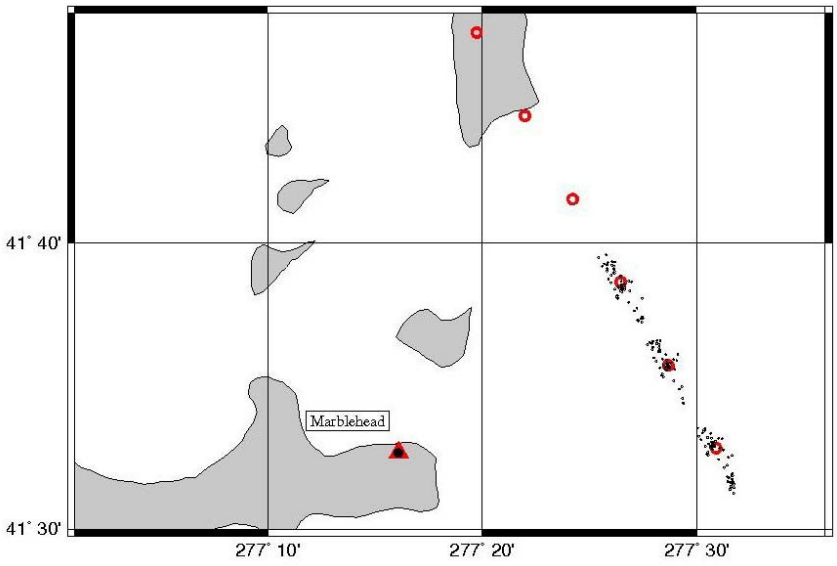

Figure 4.8. The actual scattered 1Hz footprints (dots) of JASON-1 cycles 1–106 near Marblehead in Lake Erie. The red circles are the nominal bin centers.

barometer (IB) corrections are intentionally not applied in the absolute altimeter calibration case. In contrast, the solid earth tide correction is applied since it is not sensible to the *in-situ* water level measurements.

Despite the repeat orbit design of the altimeter satellite, the actual track of each repeated satellite visit deviates from the nominal ground track. For example, the footprints of all repeated T/P satellite visits near Marblehead in Lake Erie scatter within an approximate 6-km along-track and 2-km cross-track area (Figure 4.8). This area is defined as a *bin* in the stackfile database system that was originally designed and developed by the Center for Space Research, University of Texas at Austin. Further information about the stackfile database system can be found in Urban (2000) and Guman (1997).

Within a bin, the mean ssh for this bin as well as the along- and cross-track mean ssh gradients are estimated, using all valid ssh measurements in the bin with a planar approximation after the removal of the annual and semi-annual signals (Guman, 1997). The mean ssh gradient is sometimes called the geoid gradient in the literature. These gradients, estimated within a bin, do not work outside the bin without proper extrapolation.

Unless specially installed on an altimeter satellite ground track, most coastal water level gauges for calibration are not located within an altimeter bin. Therefore, good knowledge about the local geoid and the sst for gradient determination outside the bin is required before one can use such a water level gauge to perform absolute altimeter calibration. Alternatively, the GPS buoy or the GPS-equipped vessel can be used to survey the area to improve the gradient determination at it can be seen, for example, in Shum et al. (2003). Calmant et al. (2004) referenced the high rate altimeter data to the nominal latitudinal parallel, instead of the bin center, to prevent the need of the along-track gradient in the Southwest Pacific region. The details will be discussed in Section 4.6.

4.4 Absolute calibration with *in-situ* water levels

Eq. (4.3) defines the constant altimeter bias, β, between the noise-free altimeter ssh measurement and the actual mean sea surface height at the location where the ssh measurement was made. It is important to resolve the altimeter bias for applications that

demand high accuracy in the ssh measurements. For example, the studies of the global sea level rise are trying to identify a signal with approximate magnitude of ~1 mm/year. Therefore, a stringent observation requires the knowledge of the constant altimeter bias and its drift to at least better than 1 cm and 1 mm/year, respectively. Moreover, in order to get consistent decadal global ssh measurements from different missions, the knowledge of the relative altimeter biases and their drifts between the missions is also essential.

For these reasons, several dedicated calibration sites were established to provide the long-term calibration records. They include the Harvest Platform (Haines et al., 2002b; Christensen et al., 1994), Bass Strait (Watson et al., 2003; White et al., 1994), and the British Channel (Murphy et al., 1996). Moreover, several calibration sites for multiple missions have also been established such as the North Sea (Schöne et al., 2002), Baltic Sea (Liebsch et al., 2002), Catalonian Coast and the Balearic Island (Cardellach et al., 2000), Catalunya, Spain (Martinez-Benjamin et al., 2000), Mediterranean Sea (Schueler et al., 2003), Lake Erie (Shum et al., 2003), Southwest Pacific Ocean (Calmant et al., 2004) and others. Figure 4.9 presents the locations of these calibration sites.

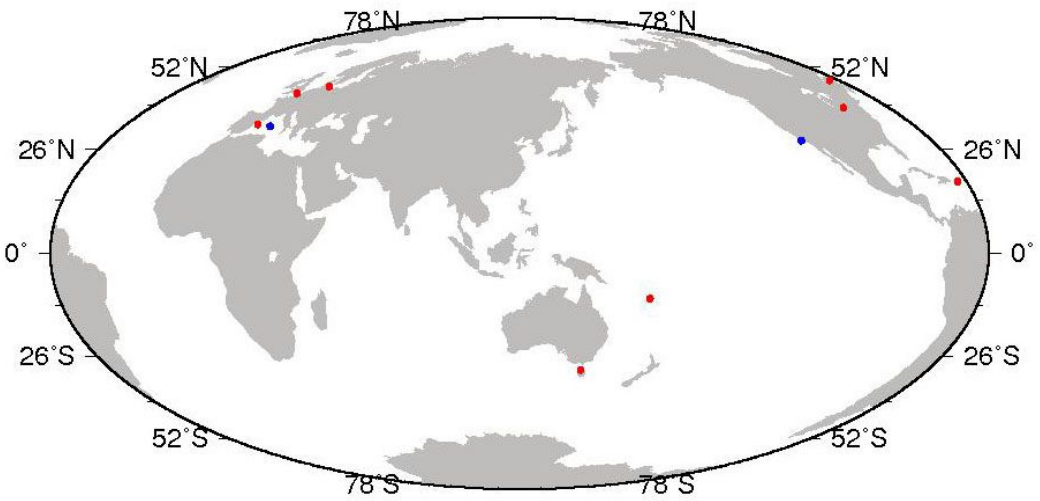

Figure 4.9. Calibration sites in the world. The blue dots are the dedication sites at Harvest and Corsica. The red dots are other sites.

The absolute calibration is to determine the constant bias between two independent data sets, namely: altimeter ssh measurement at the site, and the *in-situ* water level control. Therefore, a rigorous model can be formulated with the use the Gauss-Markov models for both data sets individually, such as:

$$\begin{aligned} h_1 &= A_1\xi_1 + e_1, \qquad e_1 \sim (0, \sigma_1^2 P_1^{-1}), \\ h_2 &= A_2\xi_2 + e_2, \qquad e_2 \sim (0, \sigma_2^2 P_2^{-1}), \qquad Cov\{e_1, e_2\} = 0, \end{aligned} \tag{4.4}$$

where the subscripts 1 and 2 represent the data sets of altimeter ssh and the *in-situ* control, respectively. The matrix A is so-call design matrix, h is the observation vector, e is the random noise vector, and ξ is the unknown vector to be determined. The dispersion matrix for the observation h is described by the multiplication of the variance component σ^2 and the weight matrix P. The dispersion matrix of the observation can be composed of, for example, the instrumental precision report or the rms error of the measurements.

In this section, each observation equation of the Gauss-Markov model at any given time epoch t for each data sets is in the following format:

$$h(t)=\beta+\delta t+C\cos(\omega t)+S\sin(\omega t)+e(t), \tag{4.5}$$

where the harmonic coefficients C and S are intended to account for the dominant annual signal found in the data set. The mean ssh β and the drift δ, along with the harmonic coefficients for each data set are to be determined with the least-squares technique. Consequently, the constant altimeter bias can be estimated by the difference between the mean estimates of both data sets and its dispersion matrix is determined by the law of error propagation. That is

$$\begin{aligned} &\hat{\beta}_1-\hat{\beta}_2 \\ &D\{\hat{\beta}_2-\hat{\beta}_1\}=D\{\hat{\beta}_1\}+D\{\hat{\beta}_2\}, \end{aligned} \tag{4.6}$$

since both data sets are independent.

However a simplified model that forms observation from the difference of two independent data sets is sometimes seen. Therefore, its comparison to the use of the rigorous model, as presented above, will be addressed fully, including the analytical formula as well as comparison of numerical result in Chapter 6.

The *in-situ* control data used in the chapter are a coastal water level gauge at the Lake Erie Calibration Site, and a bottom pressure gauge at the South Pacific Calibration Site. The GPS water level measurements from a buoy in the Lake Erie Site were utilized to convert the gauge record to the ellipsoidal height and to account for the surface gradients (height change due to different locations). In addition, a GPS-equipped vessel was used in the South Pacific Site and its data were used to link the record of a bottom pressure gauge to the ellipsoidal height for calibration. The details will be discussed in the following two sections.

4.5 Lake Erie Calibration Site

The Marblehead water level gauge, which is one of the CO-OPS gauges at the Lake Erie, was selected for altimeter calibration. This site is arguably among the first site to use an onshore water level gauge as the primary *in-situ* control for absolute calibration for altimeters. The gauge is off the nominal altimeter ground track by about 20 km. The gradient is surveyed by a GPS buoy campaign (shown in Figure 2.3 on page 28) conducted by OSU's Laboratory for Space Geodesy and Remote Sensing in 2001. The advantage of using such approach is cost-effective. It does not require to build the site

specifically underneath an altimeter ground track that is usually offshore for tens of km. Watson et al. (2003) is a calibration site in the south hemisphere that used a similar approach in about the same time.

The evaluation of altimeter systems over lakes has a number of advantages including minimal tides and a smaller dynamic variability as compared to the ocean (Shum et al., 2003). Moreover, long-term water level or water level gauge records usually exist in lakes (Morris and Gill, 1994; Schwab et al., 1996). The Great Lakes water level gauges are operated by the NOAA's CO-OPS of the U.S. and by MEDS of Canada. The insert of Figure 2.3 (on page 28) shows the locations of the 48 operational NOAA and MEDS gauges around the Great Lakes.

4.5.1 Linking of the Marblehead water level gauge record to ITRF

To prepare for absolute altimeter calibrations, a GPS buoy campaign (Figure 4.10) was conducted on 20-21 October 2001 at Lake Erie near Marblehead, Ohio. The primary objective of the GPS buoy campaign is to map the lake surface gradient in the vicinity of the Marblehead site, where a Marblehead water level gauge (Figure 4.11) routinely provides water level measurements every six minutes. The measured lake surface gradient was used to account for height difference the water level gauge measurements to predetermined footprints of the T/P and JASON-1 altimeters which are about 20 km east of the Marblehead gauge. The GPS buoy data and data from the corresponding GPS occupation at the Marblehead water level gauge are also intended to provide a datum conversion for the water level gauge records, which was originally collected in IGLD85, to a global reference frame such as the ITRF.

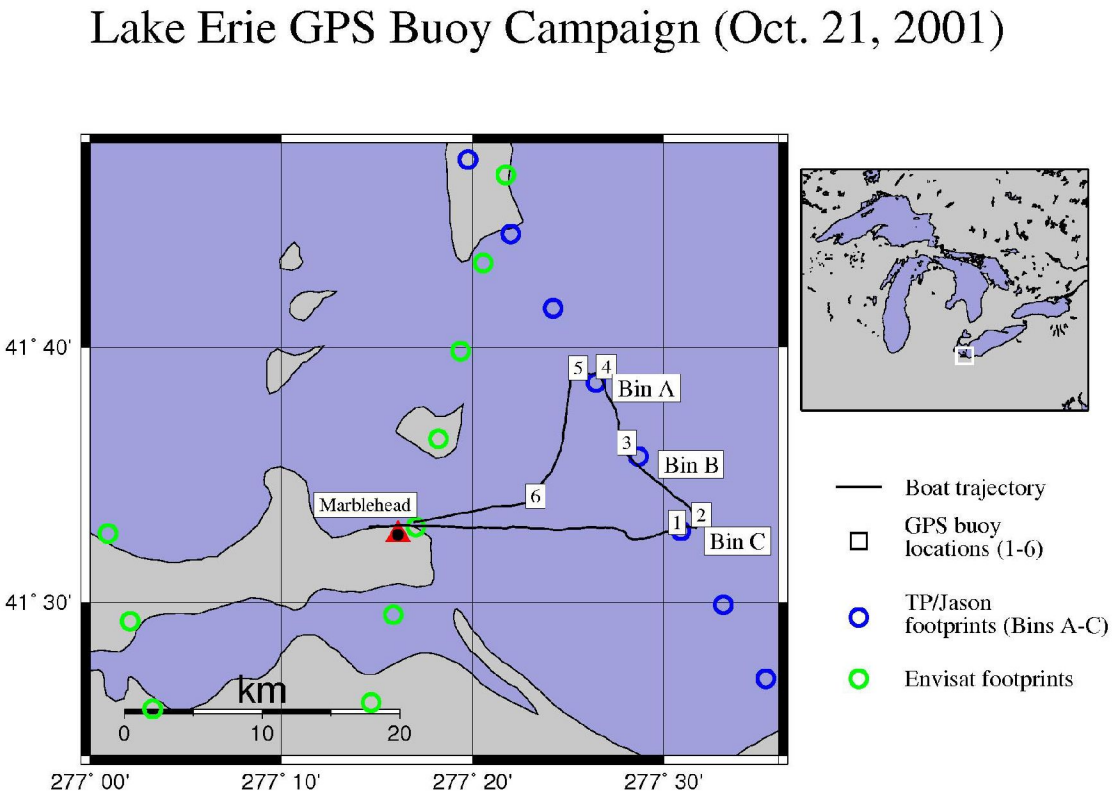

Figure 4.10. GPS buoy campaign at Marblehead.

Figure 4.11. The Marblehead water level gauge located in the Marblehead Coast Guard Base. The white box to the left of the boat is the gauge house built by CO-OPS.

	Coordinates	Standard deviation
X	604849.546 m	±4 mm
Y	-4742507.212 m	±42 mm
Z	4207835.815 m	±32 mm
Ellipsoidal latitude	41.542936º	±1.2 msec.
Ellipsoidal longitude	-82.731853º	±0.3 msec.
Ellipsoidal Height	141.371 m	±37 mm

Table 4.2. The ITRF 97 coordinates of Z317 at the campaign date. Its geodetic coordinates are calculated based on the Topex Reference Ellipsoid.

A GPS network, as illustrated in Figure 2.4 (on page 30), was established with two NGS ground control points: Z317 and 3079, and a NGS CORS in the vicinity. Z317 was chosen as the main reference station to position the buoy in the lake due to better sky visibility. These two sites were selected because they are by the lakeshore and, hence, reduce the baseline lengths in the kinematic DGPS processing. The MINOLESS solution at Z317 is presented in Table 4.2. The coordinates were later transferred to ITRF 2000 at the campaign time. The campaign information such as the station observation logs, visibility plots, and the NGS data sheets are documented in Cheng (2004).

The water level gauge at Marblehead was already linked to the ITRF in Chapter 3. In addition, the geoid determined by the GPS buoy (see Figure 3.4, page 63) has also been compared to the NGS geoid models: GEOID03 and G99SSS in Chapter 3, and showed the cm-level agreement (see Figures 3.4 and 3.5, as well as Table 3.1).

4.5.2 Gradient corrections

There are two types of gradient corrections are needed in order for the gauge record to be consistent with altimeter lake level height measurements: i) the gradients within the bin; and ii) the gradient from the water level gauge to the nominal bin center. The formal one is caused by the nature of altimeter system and the latter is caused by the fact that the gauge is not exactly located underneath the altimeter ground track.

The along- and cross-track at Bins A, B, and C were determined using JASON-1 mean lake surface height measurements from Cycles 1-106 with an algorithm similar to Guman (1997).

The gradients from the Marblehead water level gauge to the three nominal bin centers were determined by comparing the GPS buoy solution at the three bins to the corresponding Marblehead gauge record. The GPS buoy solutions on these bins were processed with two software packages (see Figure 4.12): KARS (developed by Mader, 1986) and Trimble Geomatic Office (TGO). The corresponding water level gauge records are also plotted in Figure 4.12. Table 4.3 presents the along- and cross-track gradients within the bin, as well as the height changes from the Marblehead water level gauge to the three nominal bin centers. The former two gradients correct the scattered altimeter footprints to the bin center, whereas the last gradient accounts for the location difference between the water level gauge to the bin centers. As a result, a direct comparison of the water level gauge records, which have already been converted to the ITRF00 in terms of the ellipsoidal height above the Topex Reference Ellipsoid, with the altimeter lake surface heights is established.

	Along-track (mm/km)	Cross-track (mm/km)	From Marblehead gauge (mm)
Bin A	3 ± 14	-38 ± 66	165 ± 6.4
Bin B	2 ± 17	2 ± 69	191 ± 2.8
Bin C	-17 ± 9	85 ± 43	315 ± 2.3

Table 4.3. The along- and cross-track gradient estimates within the bin, and the height change from the Marblehead water level gauge to the nominal bin centers.

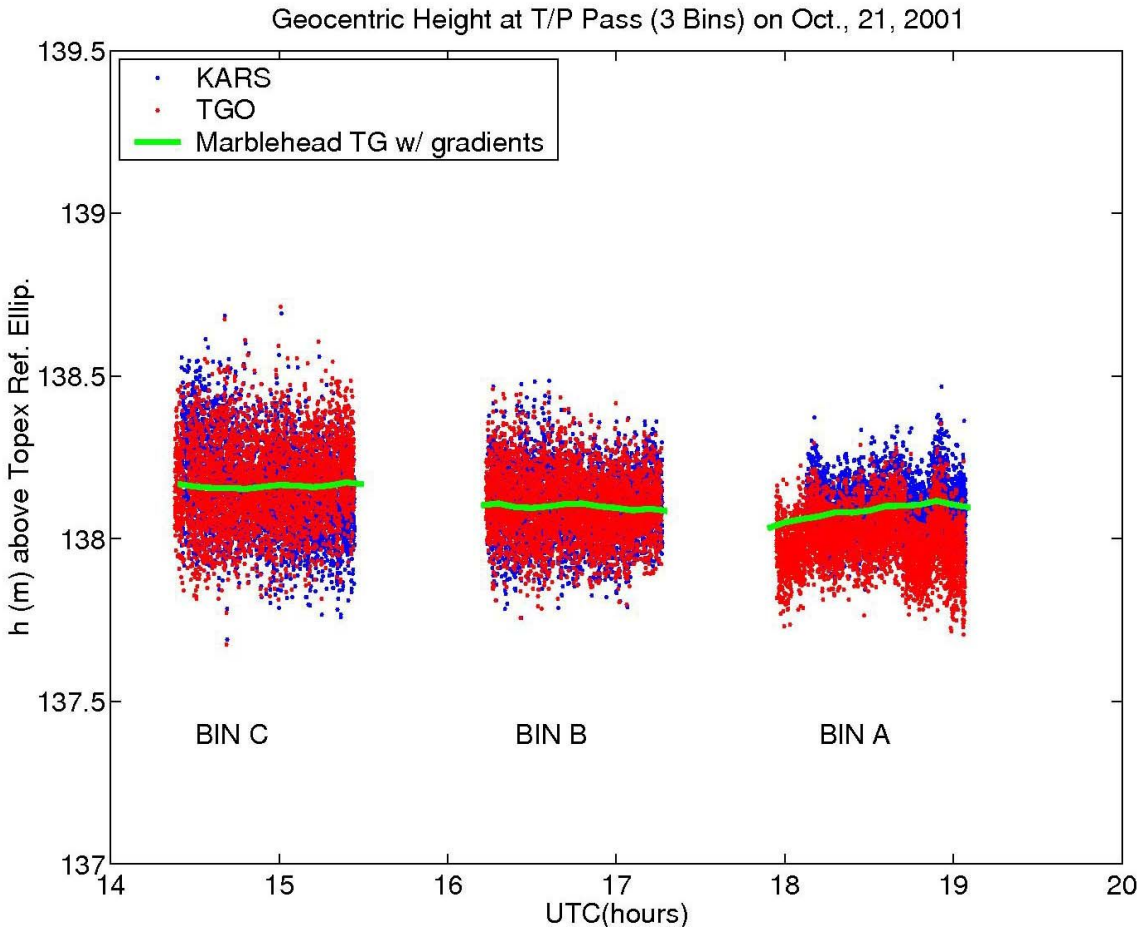

Figure 4.12. The GPS buoy solutions at three bins.

4.5.3 Calibration results

T/P and JASON-1 have been calibrated at the Marblehead Site. The T/P data used in this study are available as the stackfile (OSU version) form September 2000 to August 2002, which period corresponds to cycles 294 to 364 of the Side B altimeter of T/P. From cycles 365 to 369, its space vehicle has undergone an orbit maneuver and was moved to its new orbit that occupies the ground tracks halfway in between its old ones. Consequently, no more valid T/P data are available near the Marblehead site after cycle 365.

The JASON-1 data used in this study were prepared in GDR form from February 2002 to November 2004, which period corresponds to cycles 1-106. The data processing criteria in this chapter are similar to those of Shum et al. (2003), but with the time series being extended to 2004. Also, the Interim GDR (IGDR) used in Shum et al. (2003) were replaced with standard GDR which has a better orbit accuracy (~ ±2–3 cm) and better corrections such as those of Gaspar et al. (2002) for the ssb correction.

The mean and drift for the altimeter ssh (with corrections and gradients applied) and for the water level gauge are estimated with least-squares using the model in Eq. (4.4). The precision of each water level gauge is published by the CO-OPS and is used in the dispersion matrix for gauge records. On the other hand, the rms error of each altimeter lake surface height obtained from the GDR is used for the dispersion matrix of altimeter height measurements.

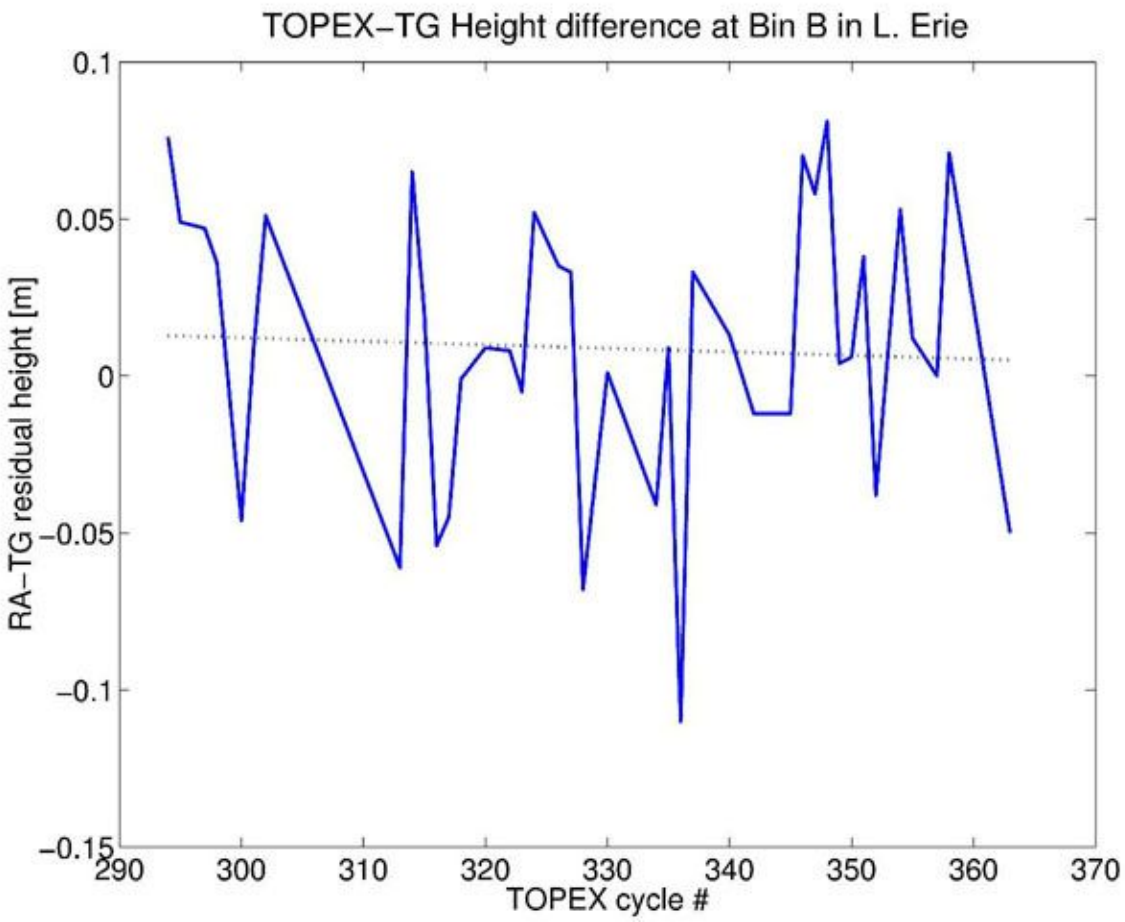

Figure 4.13. The calibration results of T/P Side B (Shum et al., 2003).

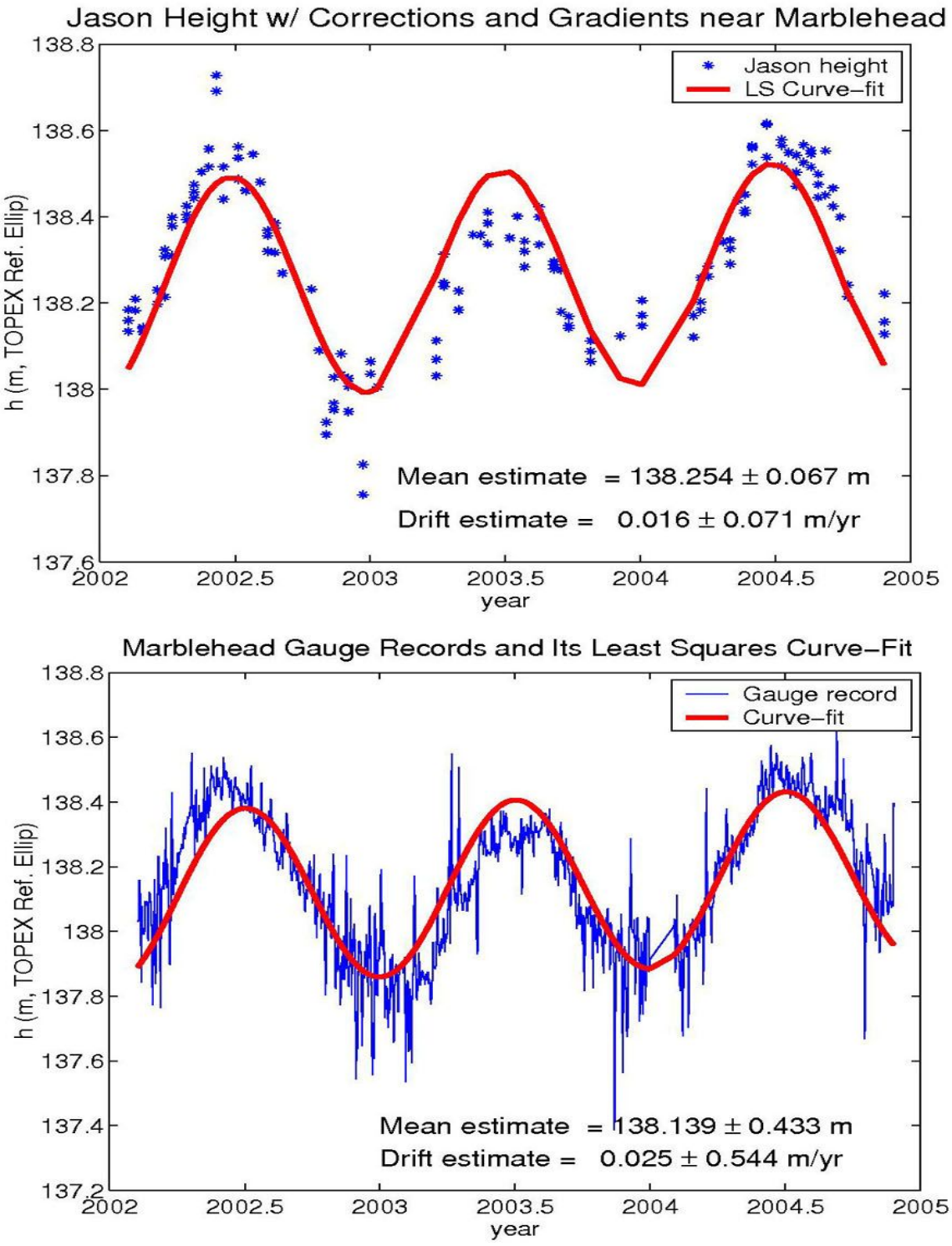

Figure 4.14. The calibration results for JASON-1.

Altimeters	Sites	Bias (mm)	Drift (mm)	Cycles	Time span (mo/year)
T/P	Marblehead	9 ± 44	-4.2	294–365	09/2000–08/2002
	Harvest	4 ± 4	N/A	236–365	08/1999–08/2002
	Corsica	6 ± 3	N/A	236–365	08/1999–08/2002
JASON-1	Marblehead	115 ± 9	-9 ± 10	1–106	02/2002–11/2004
	Harvest	126 ± 6	-16	1–63	02/2002–10/2003
	Corsica	103 ± 6	-13	1–63	02/2002–10/2003

Table 4.4. Constant altimeter bias and drift estimates at the Marblehead Site. Results of Harvest and Corsica sites are provided by Bonnefond et al. (2004), Haines et al. (2002a) and JASON-1 and the CALVAL activities web site.

The result for T/P is shown in Figure 4.13 (Shum et al., 2003) and the time series of height measurements and the least-squared fit for JASON-1 are shown in Figure 4.14, respectively. The mean water level height is resolved simultaneously with the annual signal. After removing the annual signal from the height measurements, the constant altimeter bias are estimated using Eq. (4.6) and Table 4.4 lists the bias and drift estimates compared to results from the Harvest platform and Corsica (Bonnefond et al., 2004; Haines et al., 2002a). The results for T/P Side B at Marblehead is also listed according to Shum et al. (2003). The result from JASON-1 and CALVAL activities was retrieved from the web site at on September 2, 2005 at

http://calval.jason.oceanobs.com/html/calval_plan/impl_insitu.html.

The constant bias estimate for JASON-1 is comparable to the result from Harvest and Corsica despite the longer data span (Cycles 1–106; 02/2002–11/2004). JASON-1 bias drift is relatively smaller but shows the same sign. The T/P bias estimate is slightly larger than others.

4.6 South Pacific Calibration Sites

The MOTEVAS project (Mouvements Océaniques et TEctoniques Verticaux par Altimétrie Spatiale, or: Oceanic and TEctonic Vertical Movements by Space Altimetry, in English), is primarily dedicated to measure crustal motion in the oceanic domain, using bottom pressure gauges and altimetry. Its objectives include the monitoring of the seafloor motion and absolute altimeter calibration. It is near the west coast of Santo Island, Vanuatu, South West Pacific, where the Australia plate subducts beneath the Vanuatu archipelago along the New Hebrides trench (Figure 4.15). Because the Australia plate bears the d'Entrecasteaux aseismic ridge that resists subduction, this site is located in a region of active tectonics (Calmant et al., 2003). In the frame of this project, two

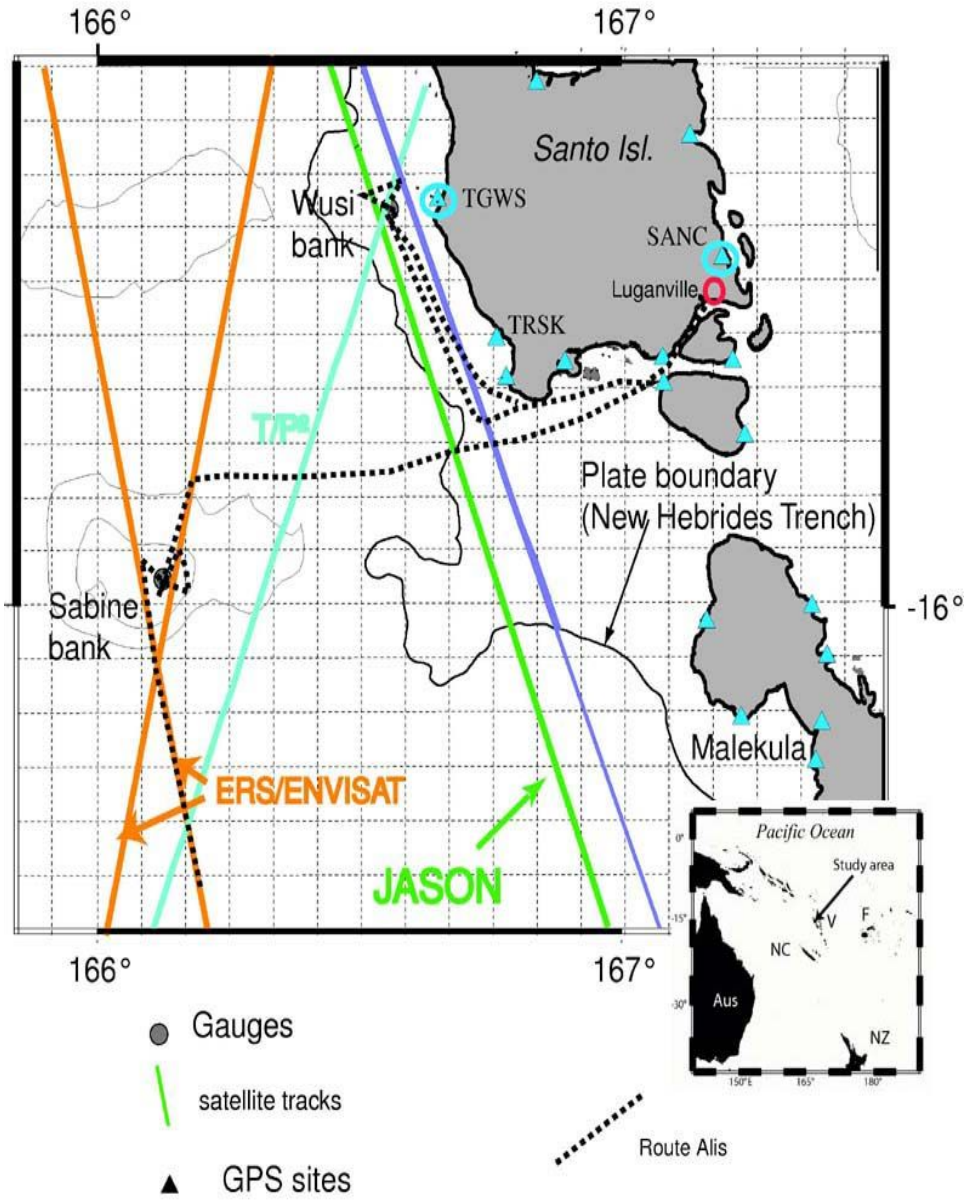

Figure 4.15. Map of the MOTEVAS project area in the South Pacific. The ground tracks of the new T/P orbit (designated as T/P^2), JASON-1, and ENVISAT are shown with 1-km width. Route Alis is the ship track of the 2003 GPS campaign. Locations in the inset: Aus: Australia; NC: New Caledonia; V: Vanuatu and F: Fiji.

BPG–Seabird 26 wave and tide recorders are currently operating at the Wusi and Sabine banks since November 1999. Those BPG devices were deployed at each side of the New Hebrides trench to record the tectonic activity. However, since both BPG's are located on the ground tracks of multiple satellite altimeters, their records are used for altimeter absolute calibration in this section.

The Wusi gauge is immerged on the JASON-1 descending track No. 238, and is about 10 km away from the west coast of Santo Island. Gauge depth is about 12 m. The Sabine gauge is immerged on Sabine Bank, the shallow top of one of the seamounts making the d'Entrecasteaux Ridge. Its depth is about 15 m. Both gauges are mounted in steel frames, anchored into coral flats. The gauge data are retrieved by divers once a yea rand the gauges are removed every other year for instrumental calibration. In addition to the pressure, seawater temperature and salinity are also recorded at both gauges.

The sea level variation with respect to the time-averaged mean sea surface can be inferred from the bottom pressure, which is directly measured by the BPG, corrected with the help of auxiliary measurements such as water temperature and salinity and surface atmospheric pressure. The bottom pressure is not sensitive to steric effects caused by the volume expansion of the water due to changes of temperature and salinity. The contribution of the thermo-haline steric effects in this section is accounted for with the equation of state, which provides a functional relationship between the seawater density, temperature and salinity. The high order thermo-haline effects that are not fully quantified in the equation of state (will be discussed in Section 4.6.2) are ignored.

4.6.1 GPS campaign

The bottom pressure gauge generates a time series of the depth variation that indicates the variation of the sea surface at its location assuming no vertical motion at the sea bottom site. In order to calibrate the altimeter ssh with the BPG, this time series needs to be referenced to the global reference frame by the occupation of the site with the GPS-equipped vessel. Therefore, a GPS campaign with a ship named Alis (Figure 4.16) equipped with two GPS antennae was conducted by CNES in March 14-20, 2003. The objective of the campaign was to survey the sea surface, and also to occupy the gauge location for the purpose of referencing the ssh variation, provided by both gauges in the

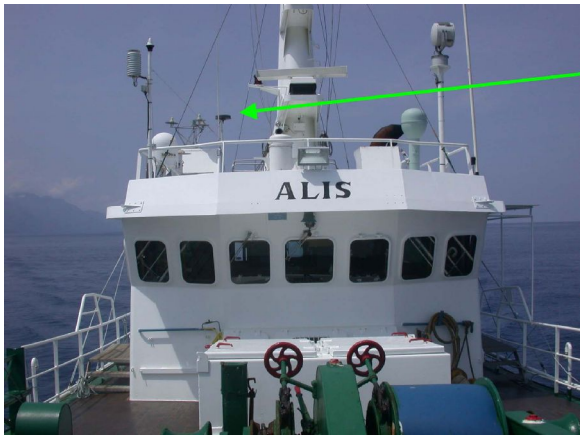

Figure 4.16. The main GPS antenna on the roof of the vessel ALIS (Courtesy of V. Ballu).

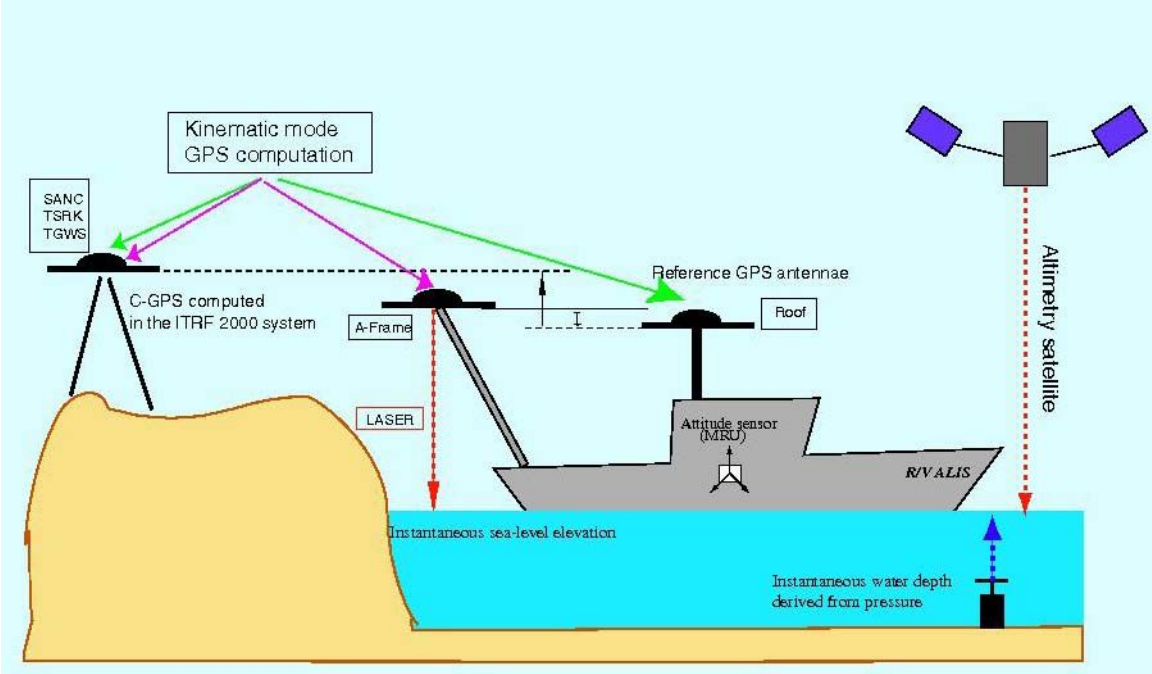

Figure 4.17. The schematic diagram for the GPS ship campaign in 2003 (Courtesy of V. Ballu).

global reference frame. A similar campaign in 2004 was also conducted. The 2004 campaign records the GPS sample in 1 Hz rate, whereas the 2003 campaign does it every 5 seconds.

The ship track is shown in Figure 4.15. The ship departed from Kouaoua, New Caledonia, and surveyed the Sabine BPG on March 16-17. It stayed in the harbor in Luganville, Santo Island, on March 17-18 and left for the Wusi BPG on March 19. After the survey of Wusi BPG, it returned to Luganville on March 20.

The schematic diagram is illustrated in Figure 4.17. The main antenna was installed on the roof of Alis which was in operation during the cruise all time. Another auxiliary antenna was installed on a retractable arm (A-Frame in the figure), on which a laser beamer was also installed to measure the instantaneous water line of the ship. It is found that there was a 35 mm offset in the vertical between the laser beamer and the ARP of the auxiliary GPS antenna.

However, due to the safety precaution, the A-Frame can only be put out when the ship sits in the harbor. When the ship is over the study area, the auxiliary GPS antenna and the laser beamer are unavailable. Therefore, it is necessary to determine the height of the main antenna on the roof. In order to do that, two GPS sessions (Sessions 2 and 3) were conducted in the harbor on March 17-18 and March 20. Two GPS antennae (one on the roof of the vessel and the other on the retractable arm in the back) were tracking at the same time, and the antenna height offset is determined by Eq. (4.7):

$$\begin{aligned} h_1(t) &= B_1 + C\cdot\cos(\omega\cdot t) + S\cdot\sin(\omega\cdot t) + e_1(t) \\ h_2(t) &= B_2 + C\cdot\cos(\omega\cdot t) + S\cdot\sin(\omega\cdot t) + e_2(t) \end{aligned} \tag{4.7}$$

where t is a given time epoch, h_1 and h_2 are the height observations from the roof and from the A-Frame, respectively. B_1 and B_2 are the mean heights, and C and S are the harmonic coefficients associated with the semi-diurnal tidal signal with period $\omega = 12.42$ hours. e_1 and e_2 are the random errors. B_1, B_2, C and S are unknowns to be determined

with the time series of heights by using the least squares technique. The antenna height offset can be determined by $\hat{B}_2 - \hat{B}_1$ through least-squares adjustment and the results are shown in Figure 4.18.

One can see that the tidal signal is the dominant one in the time series. Bouin et al. (2003) have found that the tidal signal determined by the GPS (about 70 cm amplitude) agrees with that of the FES2002 tidal model (LeProvost et al., 2002). The antenna height offsets determined in both sessions are not identical because the A-Frame was not put out into exactly the same location each time.

The averages of the laser beamer measurements are 8.480 and 8.414 m on Sessions 2 and 3, respectively. After subtracting the antenna offsets from the laser beamer (see Figure 4.17), the heights of the main antenna on the roof are estimated to be 7.990 m on Session 2 (March 17–18) and 8.044 m in Session 3 (March 20), respectively. The increased height (~5 cm) on March 20 is likely caused, in part, by the fuel consumption on the voyage of March 19 to the Wusi BPG.

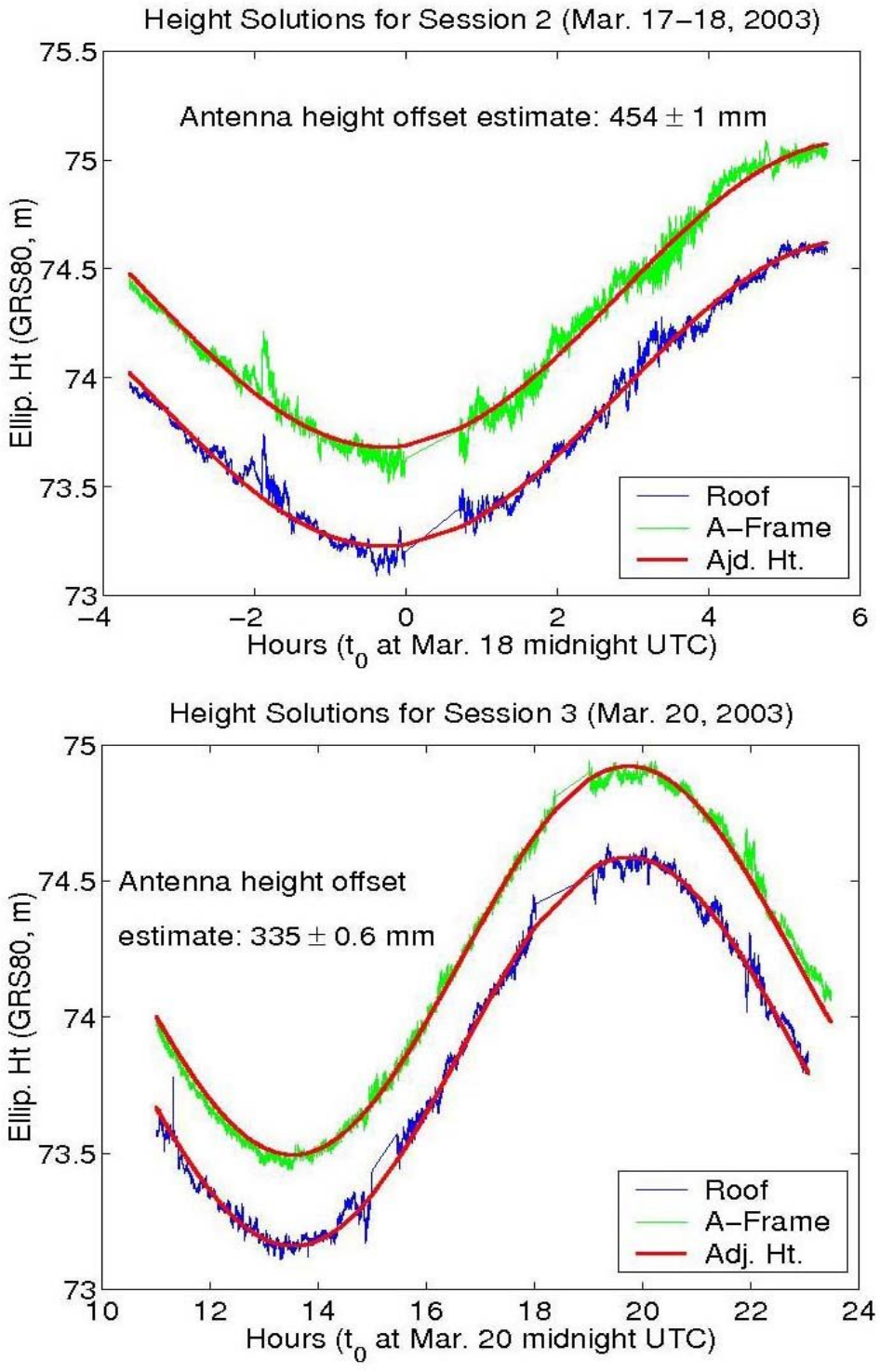

Figure 4.18. The antenna height offset estimated in Sessions 2 and 3.

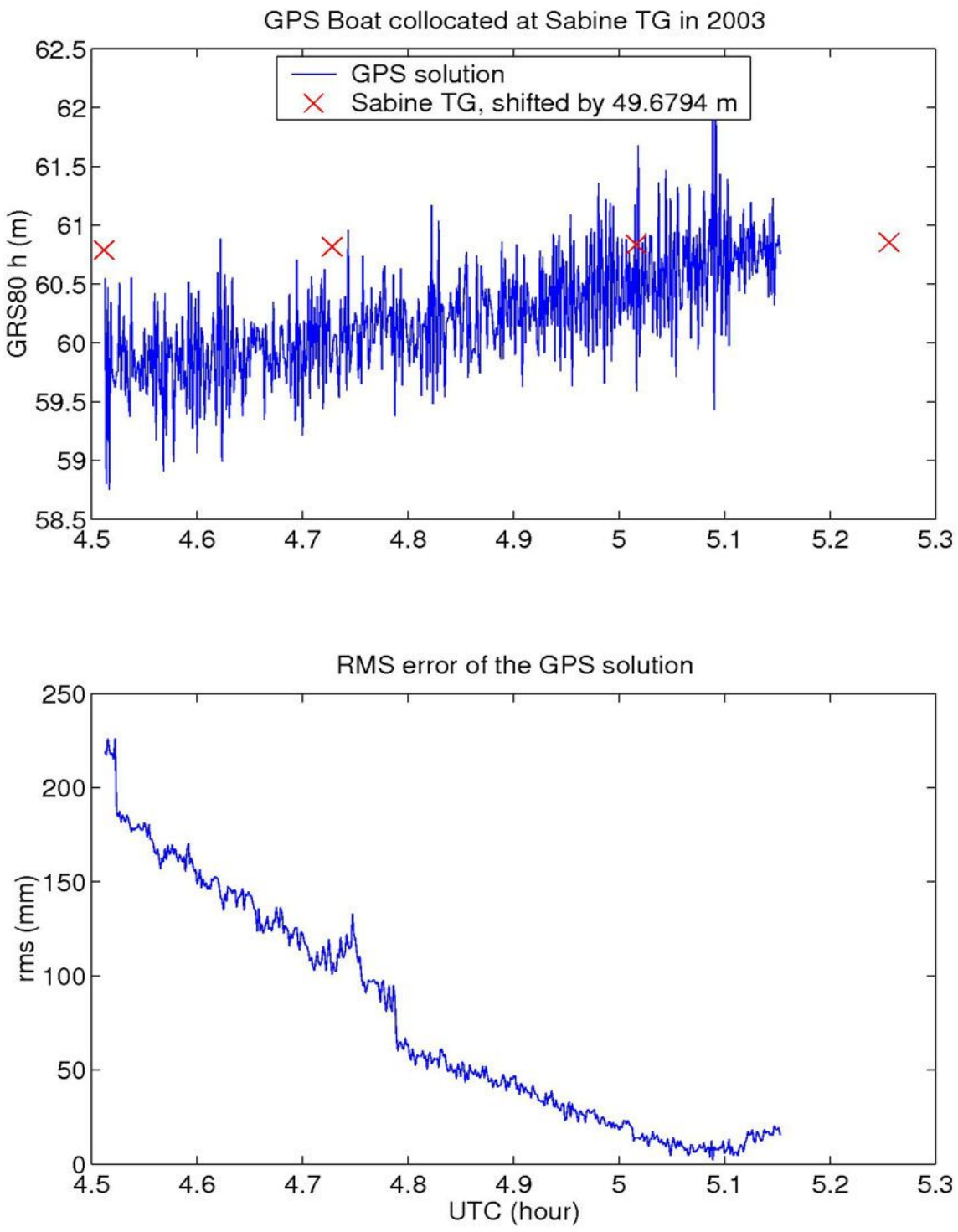

Figure 4.19. The GPS height solution (5-sec sampling rate) of the GPS boat and its associated rms error when it occupied the Sabine BPG site.

The GPS solution, when the ship occupied the Sabine BPG site, is presented in Figure 4.19. The GPS data were collected at a 5-second sampling rate with an approximately 80 km baseline from the onshore reference station TSRK. Unfortunately, the Sabine BPG did not record bottom pressure until the very end of the GPS occupation. As a result, only less than one hour of overlap was found from both data sets, despite of that, half of GPS the height solutions presented a rms error larger than ±10 cm. Although the correspondence between these two time series were established (~50 min), it is not very reliable due to the short time overlap and the data quality.

4.6.2 Sea level inferred from the bottom pressure gauge

The ocean bottom pressure measured by the BPG is caused by the water column above the gauge and the surface atmospheric pressure. The hydrostatic relation (Park and Saint-Guily, 1992) is used to connect pressure, density, and seawater column above the BPG:

$$P_b - P_a = g \int_{-h}^{0} \rho(z)\, dz \tag{4.8}$$

where P_b is the bottom pressure measured by the gauge, P_a is the atmospheric pressure at the sea surface, g is gravity, ρ is seawater density, and z is the vertical axis pointing upwards with 0 and -h indicating the time-averaged mean sea surface and gauge depth respectively. The depth of the water column, h, derived from the bottom pressure using

Eq. (4.8), does not include the steric component of the sea level because the steric effect causes volume expansion without changing the pressure, unless thermo-haline contributions are also considered in the density variations. Hence, the steric (thermal and salinity) effect is considered by using the following equation of state, and any high order effects that the equation of state does not account for are neglected. The equation of state (Leendertse and Liu, 1978) is formulated in Eq. (4.9):

$$\rho(z)=\rho(T,S)\simeq 10^3\frac{P_0}{A_1+0.689\,P_0} \tag{4.9}$$

$$P_0=5890+38\,T-0.375\,T^2+3\,S$$

$$A_1=1179.5+11.25\,T-0.0745\,T^2-S(3.8+0.01\,T)$$

where the temperature T is in °C and the salinity S is in practical salinity units (psu), both required as functions of the water depth z.

Since temperature and salinity measurements were collected at the depth of the gauge only, it is assumed that the sea temperature and salinity are constant in the seawater column above the gauge, and that density is a constant in the seawater column and its variations are only related to the time variations of the temperature and salinity, based on the equation of state. Although the gauges are located in shallow water (12-15m deep), this assumption may introduce a small error in the computation of the height of the water column above the BPG. The height of the total water column above the gauge (including the steric effect) is obtained by rearranging Eq. (4.8) as follows:

$$h = \frac{P_b - P_a}{g \cdot \rho(T, S)} \tag{4.10}$$

where the water density $\rho(T,S)$, assumed to be a constant, derived from Eq. (4.9) with the given temperature and salinity measurements. The sea level variations can be obtained by removing the mean depth from the time series of the depth derived from Eq. (4.10).

The steric effect sensed by the equation of state is validated with 35 psu (the global average seawater salinity), temperature change from 4º to 30º C (a rare case in the area), the average of the bottom pressure read by the BPG, and the average of the surface atmospheric pressure in the vicinity. It is found that the steric effect contributed for about 8 cm to sea level change. This is in good agreement with the ssh variation caused by the thermal effect (6 cm), estimated by using the World Ocean Atlas 2001 (WOA01) at 15.5º S and 165.5º E (National Oceanographic Data Center, 2003).

The bottom pressure was recorded from November 1999 to March 2003 at the Wusi gauge and at the Sabine gauge. Temperature and salinity were also recoded at the gauge level. The atmospheric pressure was recorded by the sensor on the land near the gauges. It was found that the time series of the atmospheric pressure exhibits gaps. Thus, the records from the National Tidal Facility at Port-Vila, about 200 km south of Wusi, were used to fill the gaps. Calmant et al. (2004) analyzed both datasets for overlapping sequences and found a discrepancy of 3.2 mbar. They also found that the measurements at Port-Vila provided a satisfying proxy for those at Wusi. However, some high frequency phenomena at Wusi are not fully recovered by the records at Port-Vila. Bouin et al.

(2003) have already provided the mean-removed comparison of JASON-1 with the Wusi BPG. Hence, the calibration results of ERS-2 and ENVISAT with the Sabine BPG are reported in the following sections.

4.6.3 Gradient Correction

Since the regular 1 Hz altimeter ssh measurement is the average of the valid high rate raw data (e.g., 20 Hz for JASON-1), it is possible to collect the 1-second high rate data, centered at the nominal parallel in order to form the new 1-Hz ssh measurements. The objective of this recollection is to form a time series of altimeter ssh that were taken at the same parallel for absolute calibration without the need to apply the along-track gradient. It is reasonable for the recollected 1-Hz ssh to use the corrections that come with the original 1-Hz product since there is usually no significant change on the corrections within one second. This idea was first implemented by Calmant et al. (2004). Figure 4.20 illustrates the idea of the recollection of the high rate data. As the result, the footprints of the recollected 1-Hz ssh samples are alone the nominal parallels.

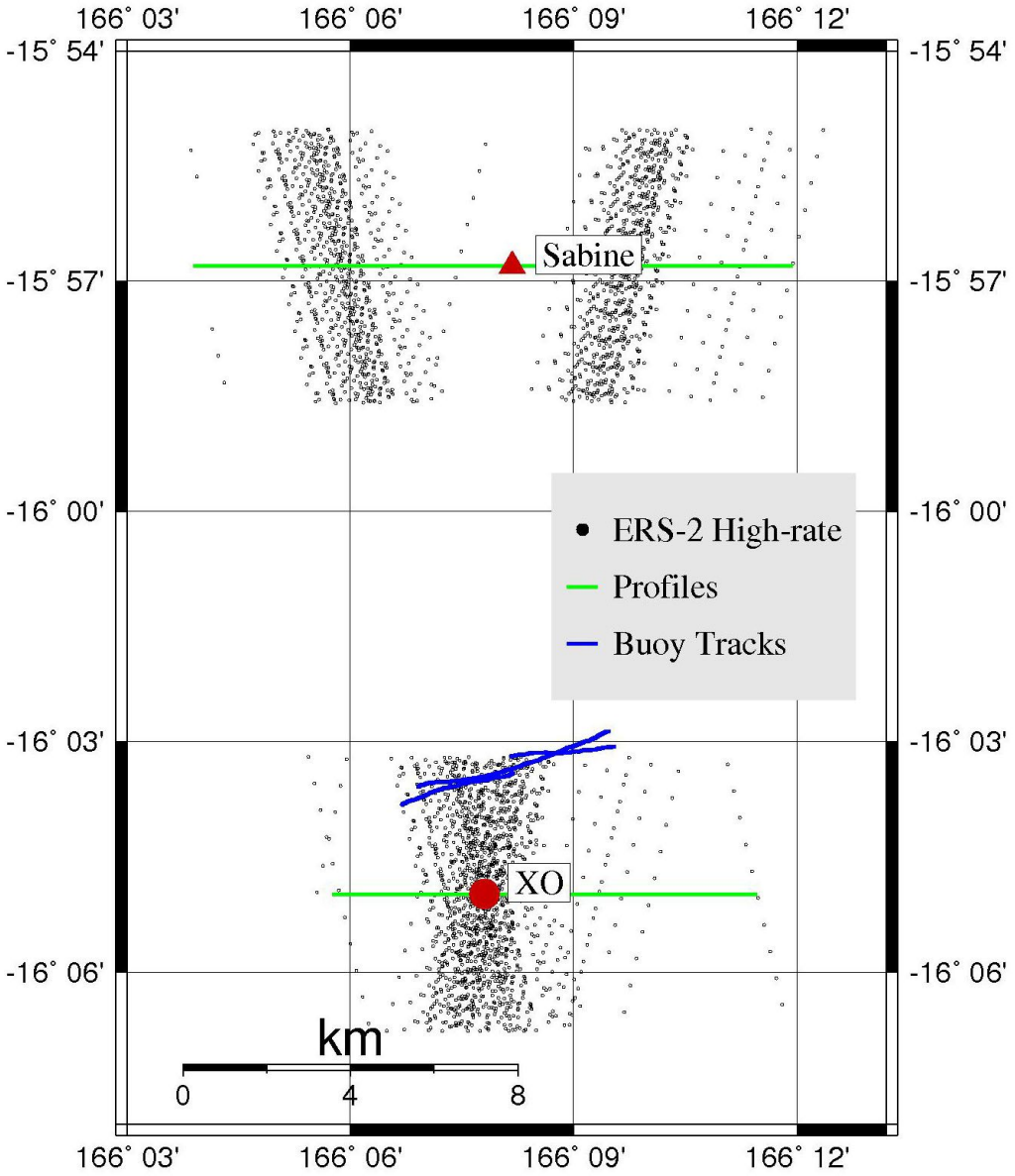

Figure 4.20. The high rate ERS-2 footprints near the Sabine BPG. The buoy tracks were from the 2004 campaign. The nominal parallels are at the Sabine BPG (at 15º56'48"S) and at the crossover (XO) point (at 16º04'59"S).

The along-track gradient determination in this area is based on the same idea of recollection. The cross-track gradient is then determined with the GPS buoy from the 2004 campaign as well as the mean ssh measurements from altimeters in the vicinity. Two profiles were chosen at the Sabine BPG (at 15º56'48”S) and at the ERS-2 crossover (XO) points (at 16º04'59”S). The gradient along these two profiles was determined with the mean ssh of ERS-2 (Cycles 1-86; 1995/05/26-2003/06/15) from the stackfile (OSU version). The gradient on the profile was fitted with a second degree polynomial. Higher order polynomials were also tested but they did not show significant fitting improvement. In addition, the gradient along the GPS buoy track (March 3, 2003) between these two profiles was also analyzed. The results are shown in Figures 4.21 and 4.22.

The gradient estimates from the Sabine and XO profiles and from the GPS buoy track agree reasonably well considering the local bathymetry (see contour lines in Figure 4.15). The Sabine BPG is deployed on the top of the sea mountain and the location of the crossover point is relatively flat. The gradients determined here will be corrected in the closure equation for calibration.

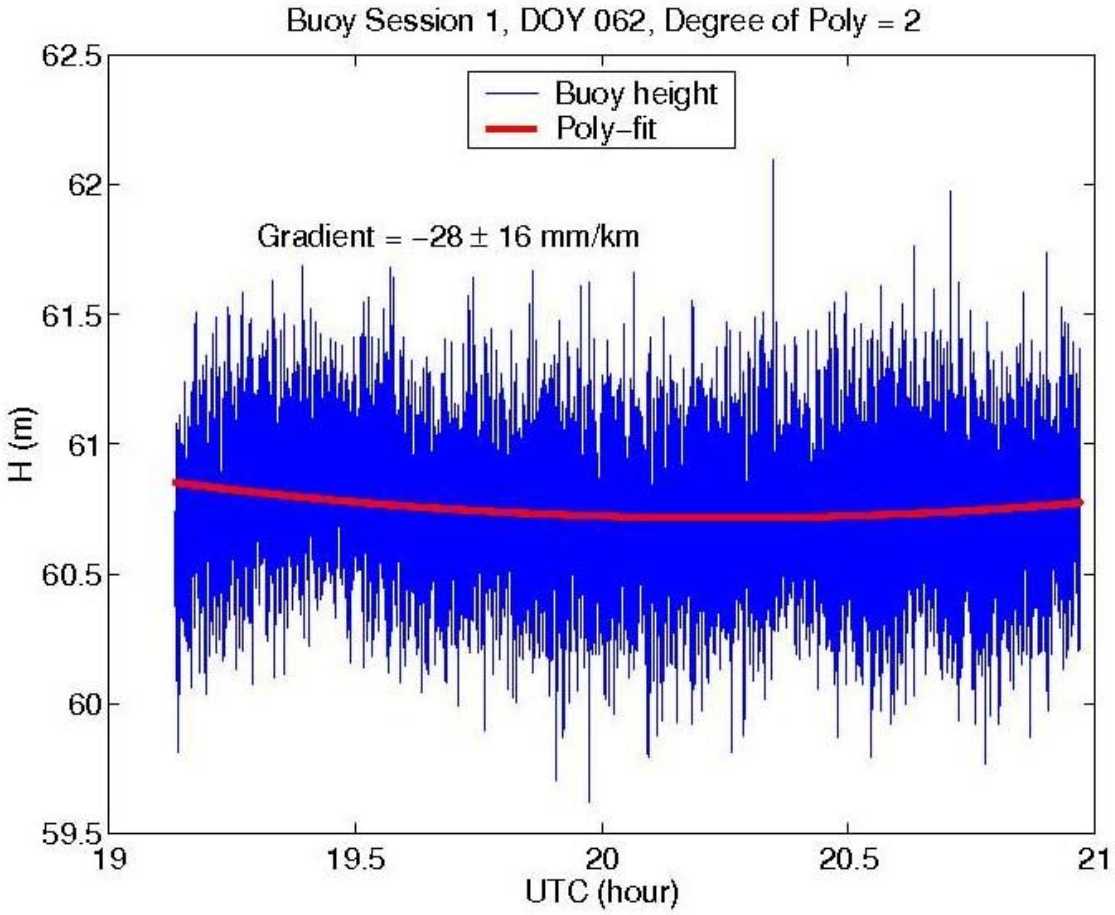

Figure 4.21. The gradient at the GPS buoy profile, fitted with a second degree polynomial with data from March 3, 2004 (DOY, Days Of a Year, 62).

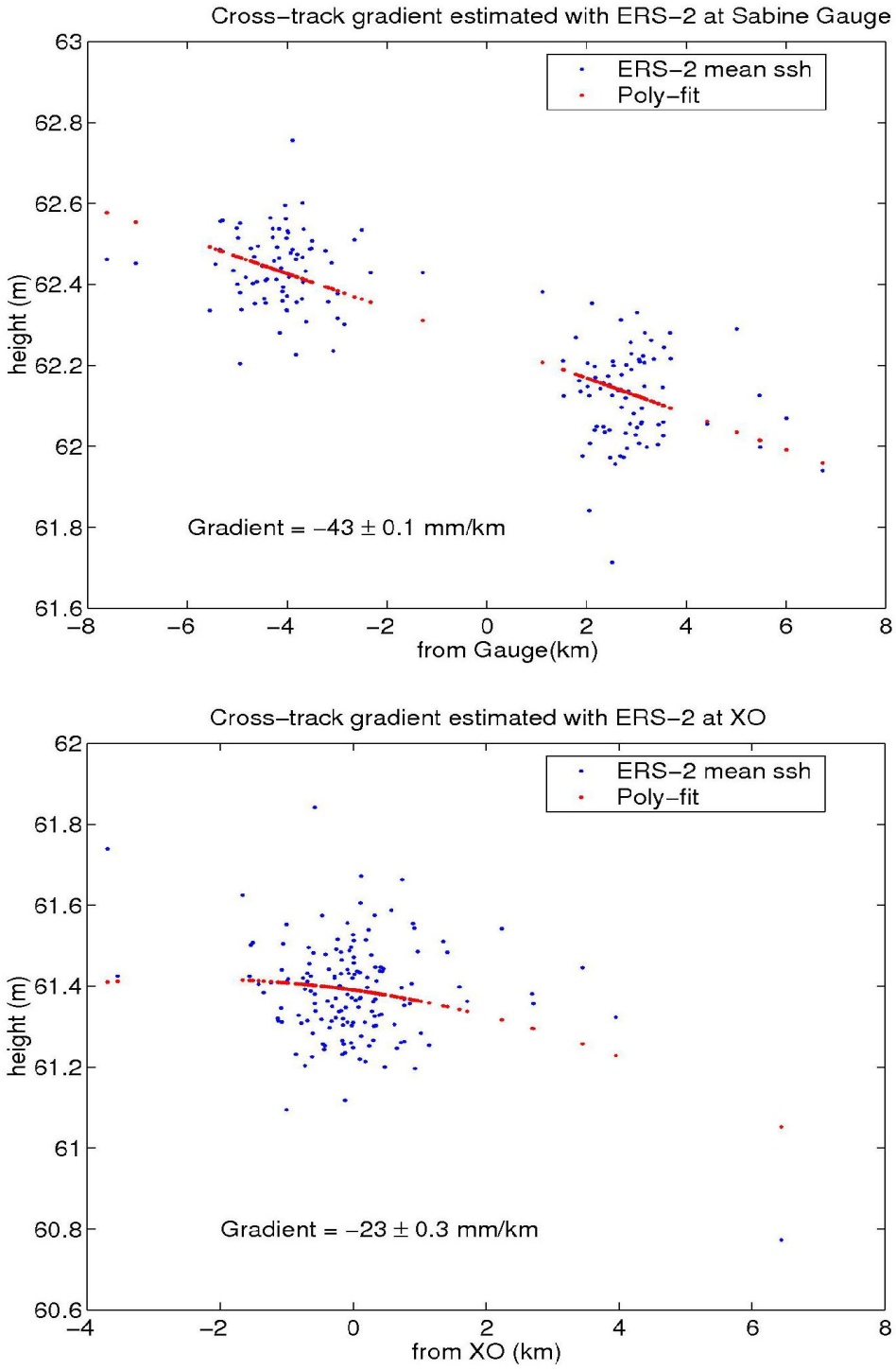

Figure 4.22. The gradient estimation at the Sabine BPG (top) and at the crossover (XO) point (bottom).

4.6.4 Calibration results

This section only considers the calibration of ERS-2 and ENVISAT with the Sabine BPG. The ERS-2 data used in this section are from the stackfile (OSU version) cycles 1–86 (May 1995 to June 2003). The ENVISAT data is from GRD released by AVISO, from cycles 10–25 (October 2002 to March 2004). The high rate ssh data were retrieved from the both data sets, and the 1-Hz ssh samples were reconstructed at the latitudinal parallels of the BPG and of the crossover (XO) point.

A simplified model using the difference between the altimeter ssh and the BPG measurements is used in this section. That is:

$$h_1 - h_2 = \tau\beta + t\,\delta + e_1 - e_2, \qquad \begin{aligned} e_1 &\sim (0, \sigma_1^2 P_1^{-1}) \\ e_2 &\sim (0, \sigma_2^2 P_2^{-1}) \\ cov\{e_1, e_2\} &= 0, \end{aligned} \tag{4.11}$$

where the subscriptions 1 and 2 represent the two data sets: altimeter ssh and the BPG ssh measurements, respectively. h_1 and h_2 are the observation vectors containing the height measurements. An nx1 vector τ consists of ones and t is the vector for elapsed time. The δ is the drift to be determined. The constant offset between these two data sets β is not of interest in this section because of the very short (about 50 min) data correspondence time. The dispersion matrix of h_1 consists of the rms errors of the altimeter ssh measurements provided by the stackfile. On the other hand, the rms error of the least-squared fit for 4 consecutive BPG readings (correspond to one hour), when the satellite passes the site, is used in the dispersion matrix for h_2.

	Drift (mm/year)	Samples	RMS error (mm)
ERS-2 at BPG	-7 ± 64	59	±152
ERS-2 at XO	-3 ± 75	54	±155
ENVISAT at BPG	23 ± 258	6	±45
ENVISAT at XO	538 ± 318	6	±68

Table 4.5. The drift estimates at the Sabine BPG and at the XO sites.

Table 4.5 and Figures 4. 23 and 24 show the drift estimates for ERS-2 and ENVISAT at the BPG and the XO sites. Note that the ENVISAT time span is too short for any reliable drift estimate. However, the drift estimates may contain the effect caused by the use of a simplified model. Hence, the further works of the South Pacific Site include the improvement in the GPS ship sampling rate, longer data correspondence time, as well as the investigation of the effect by using a rigorous adjustment model described in Eq. (4.6).

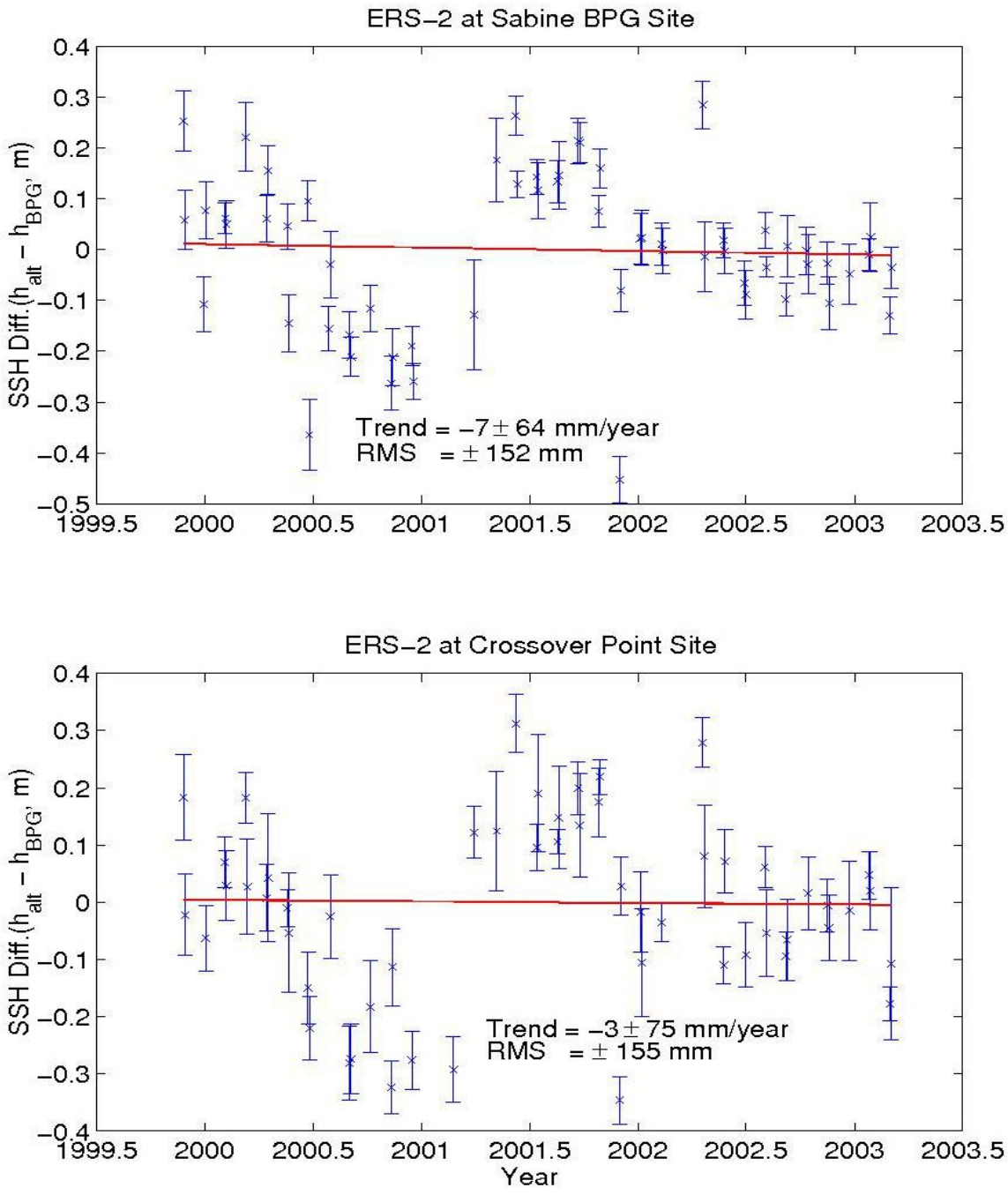

Figure 4.23. Relative comparisons of the ERS-2 ssh with the sea level inferred from the Sabine BPG.

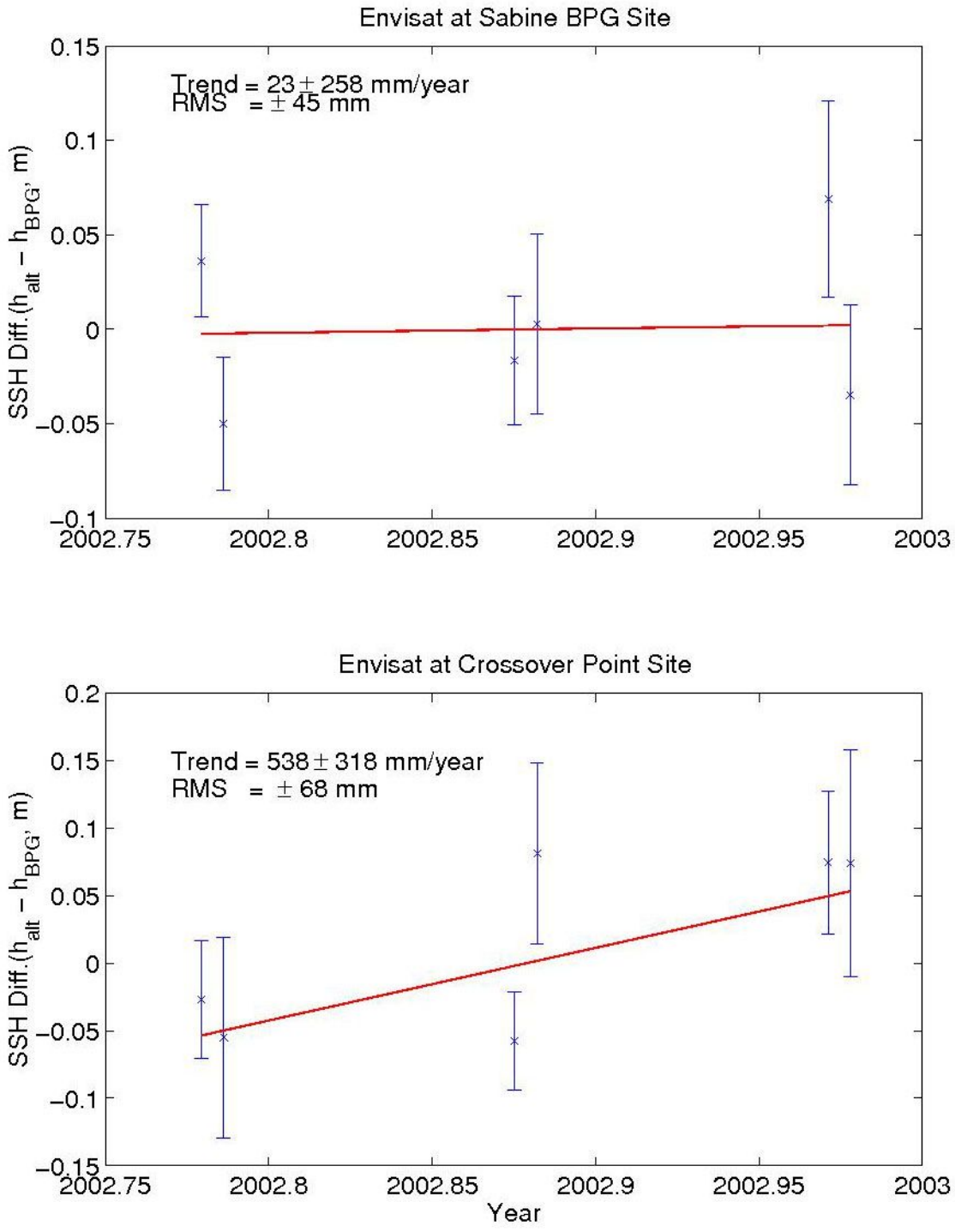

Figure 4.24. Relative comparisons of the ENVISAT ssh with the sea level inferred from the Sabine BPG.

4.7 Summary

This chapter presented the absolute calibration of various satellite altimeters as one application of the GPS water level measurements. It discusses the principle of satellite altimeters and the three fundamental observations derived from the waveform processing of the altimeters. The instrumental, media and geophysical corrections, that are necessary to correct the observed altimeter range, are also described. The idea of absolute calibration by comparing the altimeter ssh to *in-situ* observations, which is usually provided by coastal water level gauges, or bottom pressure gauges, in combination with a GPS buoy (or GPS-equipped vessel), is presented. The constant altimeter bias and drift are hence solved for by least-squares adjustment with the collection of the samples over a period of time. The approach presented in this chapter is cost-effective since it produces a similar result for JASON-1 at the Marblehead site to those of the dedicated calibration sites, which are specifically built near or underneath the satellite ground track. However, this approach of using water level gauge records as the *in-situ* data for calibration needs the extra effort to determine the local mean sea surface gradients. If the gauge records refer to a local vertical benchmark, it is necessary to accurately link the gauge records to a global reference frame in order that the gauge can be used for altimeter calibration.

Two calibrations sites: the Lake Erie Site and the South Pacific Site, are discussed in detail. One common feature at both sites is that the local mean sea surface was surveyed with either a GPS buoy or a GPS-equipped vessel. In addition, the gauges at

both sites (a coastal gauge at the Lake Erie Site and a BPG at the South Pacific Site) require GPS occupation in order to link their respect records to the ITRF00 in terms of the ellipsoidal height above the reference ellipsoid. The calibration result of JASON-1 at the Lake Erie Site, using the rigorous adjustment model, is comparable to the results from the Harvest and Corsica Sites despite longer data spans.

The calibration results at the Sabine Site suffer from very short (less than one hour) data correspondence time between the BPG and the GPS occupation. Moreover, the GPS vertical solution in the 2003 campaign used a 5-sec sampling rate, which is problematic since the baseline length is about 80 km. As mentioned in Chapter 2, a 1-2 m height jump may happen if the ambiguities are not accurately determined, due to the lack of samples in the case of a 34-km baseline in Lake Erie. Nevertheless, the calibration results of ERS-2 and ENVISAT at the Sabine site are reported despite using a simplified adjustment model. The future work at this site will be the improvement of GPS sampling rate, longer data correspondence time, and the use of the rigorous adjustment model.

CHAPTER 5

GPS HYDROLOGY

Brakenridge et al. (2005) stated that the major difficulties of making use of hydrological data such as river stage height in the Amazon River Basin, which crosses several countries in South America, include: inadequate inland data collection, poor access due to political problems, and a lack of an unified reference datum across countries to incorporate the data. However the use of satellite-based technologies such as satellite altimetry (e.g., Calmant et al., 2005; Frappart et al., 2005; Birkett et al., 2002) and radar interferometry (e.g., Alsdorf et al., 2001; 2000) have shown a great potential to mitigate such difficulties since they are able to collect river stage information beyond the political barrier. On the other hand, a GPS-equipped ship can be deployed to collect the needed river stage height in the areas where no valid observations can be made by the satellite instruments due to limitations regarding temporal and spatial sampling. Moreover, the river stage heights collected by a GPS-equipped ship can serve as the *in-situ* data to verify the height information provided by other means. Each inland river gauge can be occupied

for a while with a GPS-equipped ship, or a buoy, to link the stage record to an unified, global reference frame to facilitate data sharing and integration with satellite-based techniques.

This chapter presents a hydrological application, using the river stage heights measured by GPS and satellite altimetry, to support a study of Amazon river sedimentation and its transport behavior. A GPS campaign was conducted by the Instiut de Recherche pour le Développement (IRD, or the Institute of Research for Development) of France in the Branco River, a tributary of the Amazon, in November 2003. The campaign data are used in this chapter to demonstrate the suitability of GPS water level technique for hydrology.

5.1 GPS water level measurements for hydrology

In this section, results from the analysis of a GPS campaign in the Amazon Basin are described to introduce GPS hydrology. The campaign, illustrated in Figure 5.1, was conducted by the IRD with a GPS-equipped ship and a GPS buoy (Figure 5.2) along the course of the Branco River, Brazil, a tributary of the Amazon, from November 3-23, 2003. The main goal of the campaign was to improve the knowledge of the sedimentation and its transport behavior that is affected by the climate variability and the land movements in the Amazon Basin. Such knowledge is essential in order to quantify the sedimentation capacity, the space-time determination of the flood zone, and their relationships to both the geomorphology and current tectonics (Insitude de Recherche

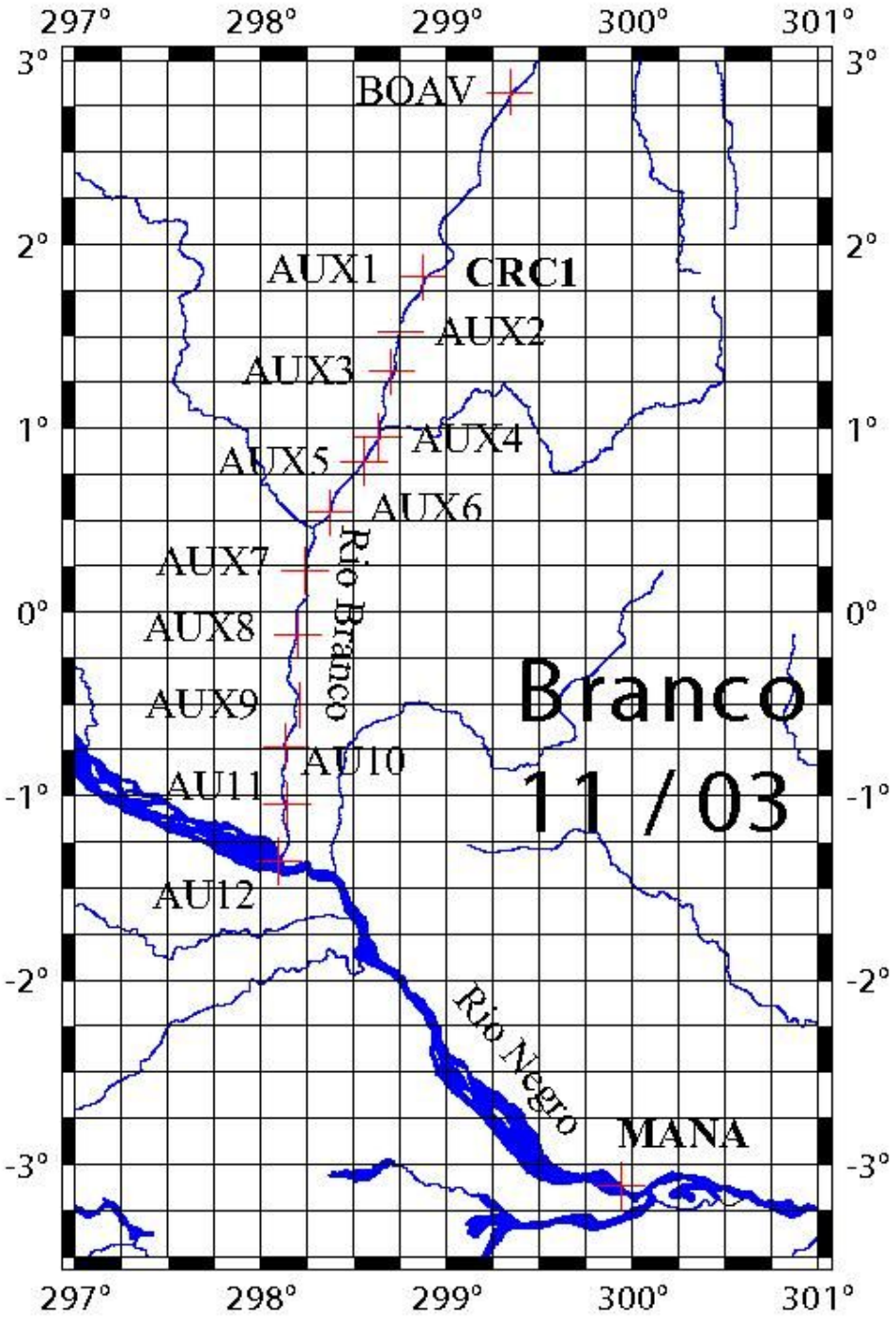

Figure 5.1. The GPS campaign in the Branco River. The fiducial and auxiliary sites are represented as crosses in the figure. (Courtesy of S. Calmant, IRD).

Figure 5.2. The GPS ship (top left), the GPS buoy (top right), and the on-board GPS antenna (bottom), used in the campaign (Insitude de Recherche pour le Développement, 2003).

pour le Développement, 2003). This is a pilot mission that utilizes a variety of data sources, including a river gauge, satellite-based techniques such as GPS surveying and satellite altimetry.

Two fiducial stations were established in the campaign area: Manaus (MANA) and Caracarai (CRC1), which operated during the entire campaign with the sampling rate of 30 seconds. Their coordinates were determined by using the Scripps Coordinate Update Tool (SCOUT), provided online by the Scripps Orbit and Permanent Array Center (SOPAC). It selects three closest sites listed in the GAMIT global GPS network, and determines the coordinates of MANA and CRC1 relative to the selected global sites. The resulting coordinates of MANA and CRC1 were expressed in terms of ITRF00 and projected to the campaign dates. Other auxiliary sites, designated AUX1 to AUX9 and AU10 to AU12, are processed with the NGS PAGE software package (Blackwell and Hilla, 2000) with respect to MANA and CRC1. The fiducial and auxiliary sites are shown in Figure 5.1. The auxiliary sites collected GPS data every second and were selected to cover the entire river branch uniformly. They are specifically selected such that the baseline length from one of them to the ship is less than 20 km. Subsequently the GPS data, collected from the ship and the buoy along the Branco River, were related to the nearest fiducial or auxiliary sites with the NGS KARS software package (Mader, 1986).

As illustrated in Figure 5.2, a Trimble Zephyr antenna was installed on the ship, and a Thales and Ashtech Geodetic IV antenna was installed on the buoy. The buoy was mainly used for calibrating the on-board antenna height and in a few selected areas that were inaccessible by the ship. Five calibration sessions were conducted during the 10-day voyage when the ship was stationary. During a calibration session, the buoy was deployed in the water to collect GPS data simultaneously with the on-board GPS antenna. By comparing the height solution derived from the ship with that from the buoy, the ARP of the on-board antenna above the waterline in each session can be obtained, provided that

Session	Aux. site	Date	Start (UTC)	End (UTC)	Duration (min)	Height offset (m)	SD (mm)	Solution type
CAL1	CRC1	11/09	20:28	21:32	64	3.510	±3	Phase (30s)
CAL2	AUX2	11/11	18:08	18:21	13	3.583	±23	Pseudorange
CAL3	AUX4	11/12	15:31	15:41	10	3.511	± 9	Pseudorange
CAL4	-	-	-	-	-	-	-	No solution
CAL5	AU12	11/17	10:08	10:22	14	3.412	±3	Phase
				Weighted average:		3.462	±29	

Table 5.1. Summary of GPS antenna height calibration.

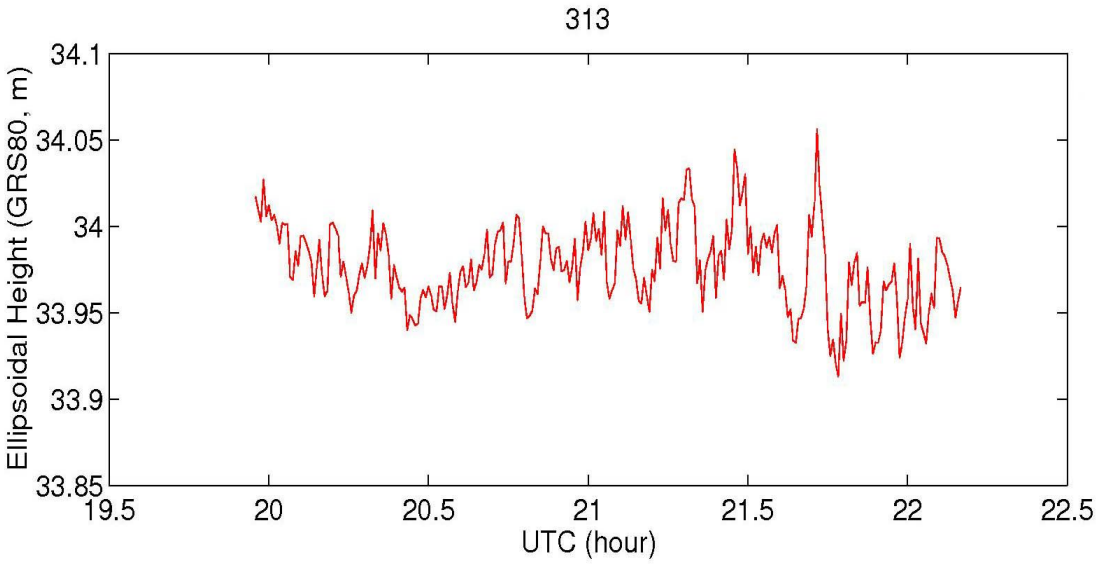

Figure 5.3. The height solution on November 9 (DOY 313), derived from the GPS ship near the Caracarai river gauge site.

the buoy's antenna height above the water was also observed in each session. The calibration results are listed in Table 5.1. The observing time for some of the sessions was relative short, and no phase solution for such sessions could be obtained. No buoy solution was successfully found in Session 4. Session 1 used data from CRC1, a fiducial station that collected data every 30 seconds, thus, longer data samples are needed for a solution.

The daily record of an existing river gauge at Caracarai (located near the Caracarai fiducial station shown in Figure 5.1) was also obtained. Unfortunately, there is no information about the data precision at present. The river stage record was collected relative to a local benchmark. Before departing for the trip, the GPS ship collected data for two hour (see Figure 5.3) near the river gauge site on November 9 (DOY, Days of a Year, 313), which are used to link the gauge record to the global reference frame. As a result, the zero level of the gauge record is estimated to be about 26.872 m ± 3 mm above the GRS80 Reference Ellipsoid defined with ITRF00. The standard deviation is formal and is associated with the GPS solution only. Note, though, that there is only one gauge record used in this linking since the gauge only produces daily records, thus, this estimation is preliminary and clearly requires further investigation. This value nevertheless links the river stage record at the gauge site to the global reference frame, in which satellite altimeter and GPS data are referenced.

5.2 River surface gradient estimates

The knowledge of river gradient is one of the key factors when considering sediment transportation, channel behavior and flood wave propagation (Birkett et al., 2002). An estimate of a few centimeters per kilometer down-stream have been reported in recent studies using estimated barometric elevation and river gauge stage records in the Amazon Basin (e.g., Meade et al., 1991). In addition, Birkett et al. (2002) used water surface height observations from T/P and geoid models to estimate the gradient to be 1.5 to 4.0 cm/km in the same area. Although this campaign only covers the Branco River, a tributary of the Amazon in Brazil, the river surface gradient along the Branco River for each day of the campaign is also calculated and reported in Table 5.2. The river stage gradient is estimated in each day by taking the 10-min average location at the beginning and the end of each day. The estimated gradients 4.8–8.4 cm/km down-stream with a standard deviation (SD) less than ±0.4 cm/km (Table 5.2). The gradient estimates are larger than 1.5–4.0 cm/km with a SD of ±0.15 cm/km estimated using T/P measurements (Birkett et al., 2002).

Figure 5.4 presents the height profile of the two particular days. The gradient, determined from the GPS ship data in this campaign, is between 4.8 to 8.4 cm/km down-stream, which is comparable to the values given by Meade et al. (1991) and is higher than that of Birkett et al. (2002). The difference may be caused, in part, by the local terrain in the Branco River watershed, which is only a small portion of the entire Amazon Basin.

Date	DOY	Surface gradient and its associated SD (cm/km down stream)
11/11	315	5.3 ± 0.4
11/12	316	5.6 ± 0.1
11/13	317	5.9 ± 0.1
11/14	318	7.5 ± 0.2
11/15	319	5.2 ± 0.2
11/16	320	8.4 ± 0.2
11/17	321	4.8 ± 0.1

Table 5.2. River surface gradient estimates.

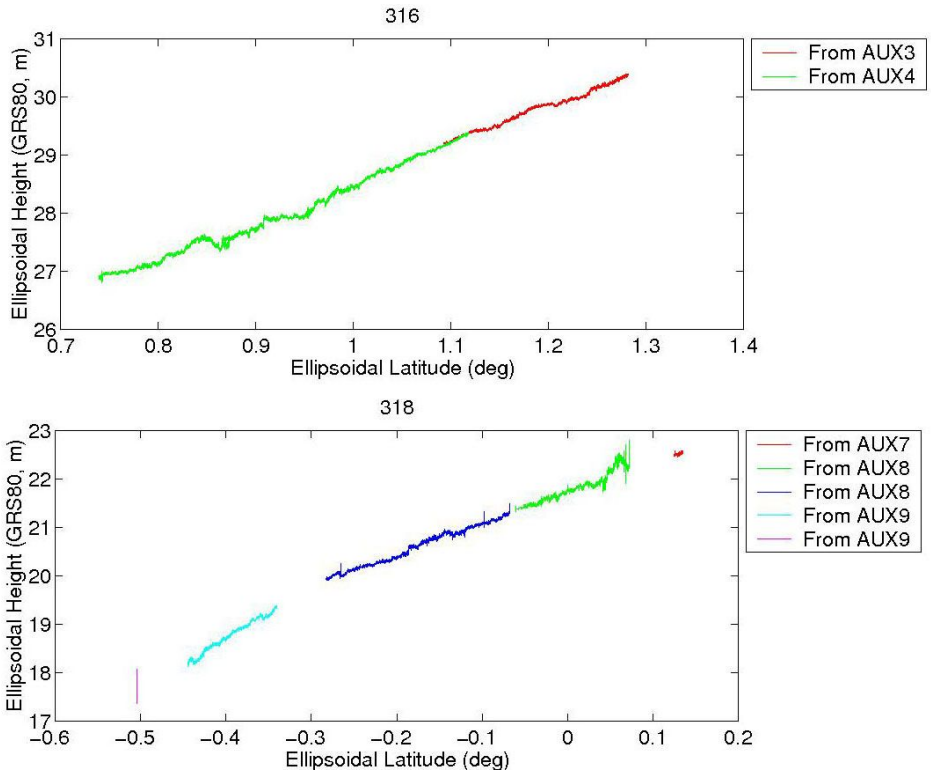

Figure 5.4. The height solutions on November 12 and 14 (DOY 316 and 318).

The reliable river height measurements provided by an altimeter are only available in a few selected area along the river due to the limitation such as the river width etc. Therefore, the river stage gradient estimated with altimeter measurements may not available everywhere along the river. However, the river stage gradient can be estimated with a GPS ship as long as the reference stations can be setup in the desired locations. Even in the area that is inaccessible to the ship, a buoy can be used as the alternative. So the use of GPS water level measurements is clearly beneficial for this type of applications.

5.3 Comparison of water level measurements

One ENVISAT pass (096) passes in the vicinity of the Branco River. The ENVISAT GDR products of Cycles 12 to 25, provided by ESA, were thus used in this study. A comparison of the river stage height between the GPS ship and the ENVISAT river stage height is carried out. Also, the time series of the Caracarai river gauge record and the ENVISAT river stage heights are compared.

Since the height measurements provided by ENVISAT are over the land and the river, instead of the sea surface, it is called the river stage height in this Section. The altimeter corrections that were applied to the river stage height measurements are the dry tropospheric path delay, the ionospheric path delay, the solid Earth tide and the pole tide corrections. They are all provided along with the ENVISAT GDR products. As opposed to the oceans, the modeled wet tropospheric path delay, which was derived from the

European Center for Medium-Range Weather Forecasting (ECMWF), is supposed to be used in place of the radiometer-derived path delay since no valid water vapor contents were measured by the radiometer over lands. However, Birkett et al. (2002) suggest that this correction is inaccurate and should not be used in the Amazon Basin due to, among other reasons, the lack of spatial and temporal radiosonde data in this area. Not using this correction, however, may degrade the quality of the ENVISAT river stage height measurements. As a result, an error source is inevitably introduced because of omitting this correction.

The solid Earth tide and the pole tide corrections were applied to the ENVISAT river stage height measurements. Since the GPS heights and the river gauge record are relative measurements of the river stage, the signals of both the solid Earth tide and the pole tide are insensitive in, and, thus need to be removed from the altimeter measurements.

Figure 5.5 superimposes the color-coded river stage height from ENVISAT and the GPS-ship hourly solution to the elevation obtained from GTOPO30, a global digital elevation model (Gesch, 1998) released by the U.S. Geological Survey (USGS). Two areas, where the ENVISAT track passes the river, are selected to carry out the river stage comparison. The river stage measurements, collected using various techniques: ENVISAT altimeter, GPS, and a river gauge at Caracarai, will be analyzed.

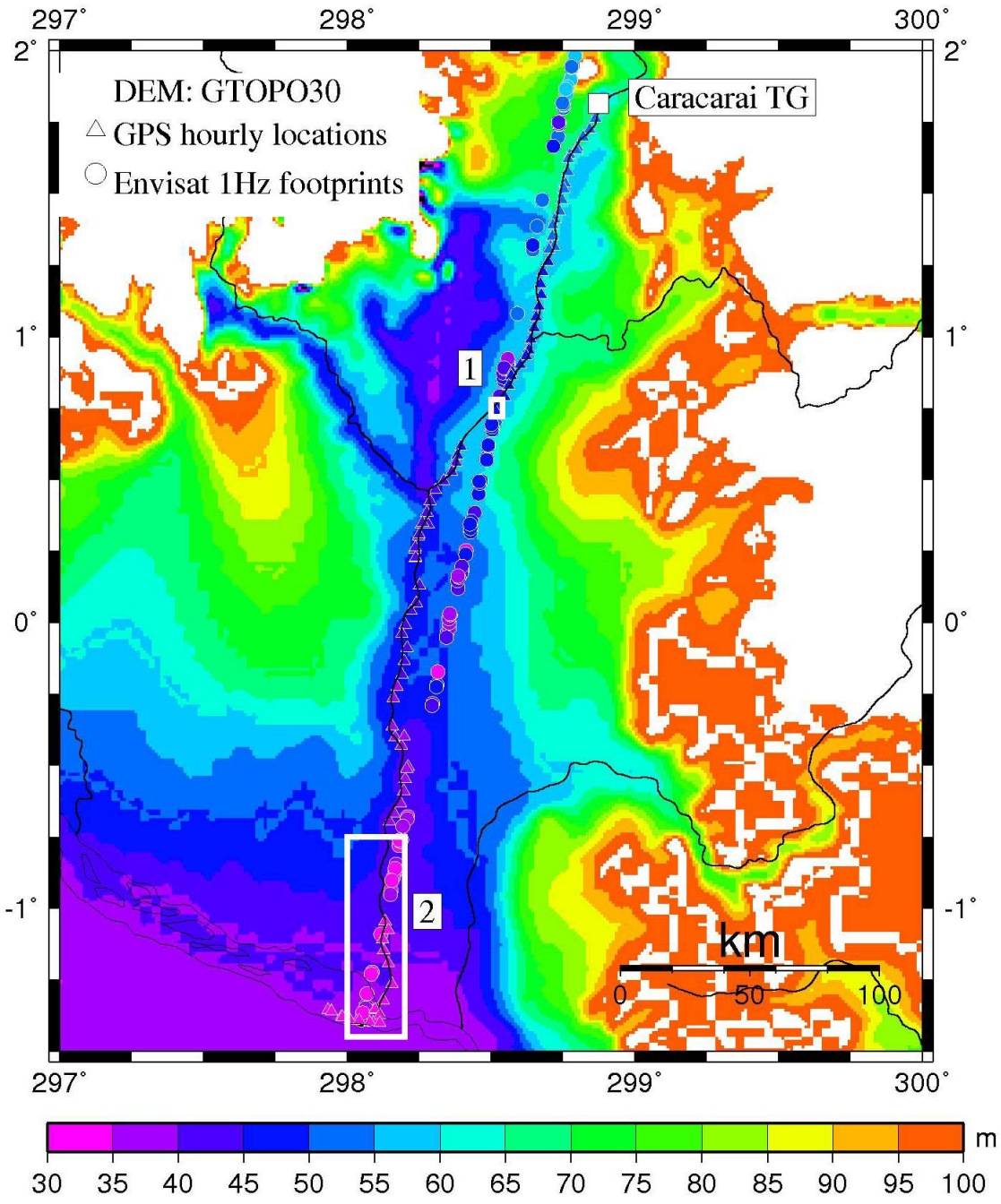

Figure 5.5. The digital elevation model (GTOPO30) in the Branco River watershed, the hourly-averaged GPS ship locations, and the ENVISAT pass 096. Two areas where ENVISAT crosses the river, marked in white boxes, are selected for river stage height comparison.

The high-rate (18 Hz) altimeter range and orbit measurements, obtained from the ENVISAT GDR, are used to determine the 1-Hz river stage height. Frappart et al. (2005) analyzed the ENVISAT GDR in the Amazon Basin with four ENVISAT trackers: OCEAN, ICE1, ICE2, and SEAICE. Although ICE1 is originally designed for ice and general land surface gradient measurement models, they concluded that it is suitable for continental hydrology studies with a median operator as well when calculating the 1-Hz river stage height from the high-rate profile. The high-rate range measurements (from the satellite to the river surface) are more likely to be affected by the terrain and tend to provide jumps near both edges of the river. Hence, the median operator and the median absolute deviation (MAD) are supposedly better than mean and SD since they do not give undue weight to the edging behavior (Croarkin and Tobias, 2005). Nevertheless, other estimators in the class of robust estimators may also preserve this property. Let x be a vector containing the high-rate data, the MAD from the median of the vector x is defined as:

$$MAD(x) = Median(|(x_i - \tilde{x})|) \tag{5.1}$$

where x_i is an element in the vector x, $\tilde{x}$ is the median of all x_i, and Median(·) is the median operator.

Four ENVISAT trackers were tested in the Areas 1 and 2. The result is listed in Table 5.3. The MAD of ICE1 is the smallest among other trackers, which is in agreement with Frappart et al. (2005).

Unit:[m]	OCEAN	ICE1	ICE2	SEAICE
Area 1	0.503	0.178	0.800	0.582
Area 2	0.987	0.658	0.814	0.794

Table 5.3. Mean MAD of each 1-Hz river stage height within the selected areas, derived from different trackers.

The absolute river stage height in the Areas 1 and 2, observed by ENVISAT ICE1 tracker and taken from the GPS ship solution, are presented in Figure 5.6. The bar for ENVISAT height represents the MAD from the median of the high-rate measurements. The bar for GPS ship height is the MAD from the median of the ship data inside the area. The river gauge record is plotted with its mean removed. In the Area 1, the average residual magnitude from the ENVISAT height is about 90 cm (16 cm, the smallest), whereas the residual magnitude of the GPS height is 3 cm, as compared to the mean-removed gauge record, respectively. In the Area 2, the average residual magnitude from the ENVISAT height is about 1.52 m (34 cm, the smallest), whereas the residual magnitude of the GPS height is 3.3 m, when compared to the mean-removed gauge records.

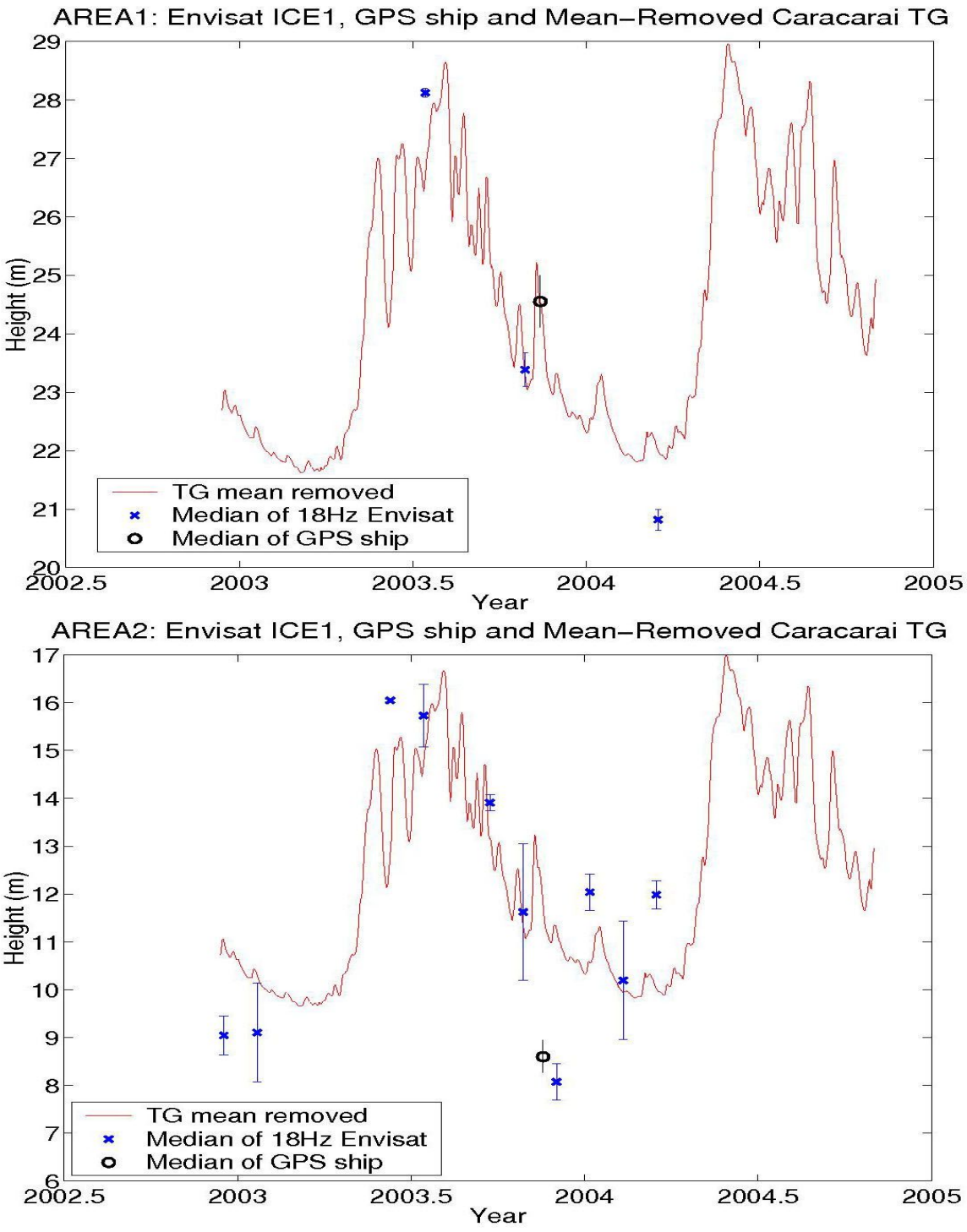

Figure 5.6. The river stage height measured by ENVISAT altimeter, taken from the GPS ship, as well as the mean-removed gauge record in the Areas 1 and 2.

It is worthwhile mentioning that the river stage height observed by the ENVISAT exhibits similar seasonal variation as the river gauge record, despite of the fact that the satellite observations are not collocated with the river gauge. The difference between the ENVISAT measurements and the gauge record is mainly caused by the geographic separation of the testing areas to the gauge location. The river flowing speed and width at different places cause different height variation. In addition, the Area 2 has rapid elevation change and its size is larger than the Area1, and, therefore, the average ENVISAT residual in the Area 2 is larger than that of the Area1.

The height of the GPS ship data is consistent with the gauge record in the Area 1. However, in the Area 2, the GPS ship height is actually closer to the ENVISAT result. It is speculated that the river stage measured by the ENVISAT and by the GPS ship may in fact be correct, since the gauge record is more than 200 km north.

5.4 Summary

This chapter discusses the use of GPS and other satellite-based techniques such as radar altimetry, to supplement the *in-situ* data collection of river stage heights for hydrological applications. The satellite techniques demonstrate a great potential in this type of application since the river stage height can be measured beyond the political barrier. Similar studies such as those by Birkett et al. (2002), Frappart et al. (2005) and Calmant et al. (2005) have shown the potential for using satellite altimetry for this purpose. On the other hand, the GPS technique can be utilized at the desired locations

where satellite altimetry can not always provide the needed data, although a GPS campaign would require local governmental permission. However, GPS provides ellipsoidal heights that can be used to link the time series of the river gauges in order to be consistent with the satellite-based techniques. The GPS technique makes it easier to incorporate river stage heights collected by different sources, and may give an unambiguous view into the entire watershed area across several countries.

The 1-Hz river stage heights measured by ENVISAT, in this Chapter, is determined from the median of the high-rate (18 Hz) orbits and observed ranges provided by GDR. The deviation is measured by the MAD about the median. The analyzed results are consistent with those by Frappart et al. (2005). However, further investigation with the consideration of the altimetric footprint gradient, which was omitted in this study and Frappart et al. (2005), as well as other possible robust estimators other than the median operator, are still needed. The lack of wet tropospheric path delay information also requires more detailed studies.

The river stage height gradient, which is an important input information to quantify sediment transportation and the river's channel behavior, can be estimated by the GPS ship. The estimated river stage gradient is larger than those by Meade et al. (1991) and Birkett et al. (2002). However, the geographic area in this study only covers the Branco River, which is only a small part of the entire Amazon Basin. The gradient estimates may reflect the local gradient. The SD of the gradient estimates are consistent with those of Birkett et al. (2002).

CHAPTER 6

COMPARISON OF ADJUSTMENT MODELS

Generally, two of the major applications discussed in this study compare the averages of two independent data sets. The constant bias, which is defined as the difference between the averages of these data sets, is to be determined. For example, the height of the water level above the reference ellipsoid is to be determined for the linking application. On the other hand, the altimeter range bias, which is a constant and is defined as the offset between altimeter ssh measurements and the *in-situ* observations, is of interest. Therefore, this chapter presents two distinct adjustment models for this type of application along with the corresponding numerical results.

6.1 Gauss-Markov model

The Gauss-Markov model is defined as:

$$y = A\xi + e, \qquad e \sim (0, \sigma_0^2 P^{-1}) \ , \tag{6.1}$$

where y is a nx1 observation vector, whose expectation is a linear combination of the non-stochastic unknown parameter ξ (a mx1 vector) which is to be determined. The random error e is supposed to have zero mean and the dispersion matrix of $\sigma_0^2 P^{-1}$, in which P is the weight matrix whose inverse is assumed to exist. The matrix A is known as the design matrix with $rank(A) = m < n$.

The least-squares solution $\hat{\xi}$ to the model in Eq. (6.1) can be found by minimizing the sum of the squared weighted residuals in $\tilde{e} = y - A\hat{\xi}$. Alternatively, the solution can also be found by using the equivalent condition equation provided that a $k \times n$ matrix B can be found such that the conditions $BA=0$ and $rank(B)+rank(A) = n$ hold. The solution to Eq. (6.1) with the condition equation is then:

$$\tilde{e} = P^{-1} B^T \left(B P^{-1} B^T \right)^{-1} B y \quad . \tag{6.2}$$

The variance component estimate for this model is then:

$$\hat{\sigma}_0^2 = \frac{\tilde{e}^T P \tilde{e}}{n - m} \quad . \tag{6.3}$$

When non-stochastic unknown nuisance parameters η exist, the model described in Eq. (6.1) ought to be revised:

$$y = A\xi + C\eta + e, \qquad e \sim \left(0, \sigma_0^2 P^{-1}\right) \quad , \tag{6.4}$$

with *rank(A)+rank(C)=rank([A,C])*. The nuisance parameters can be eliminated by finding a suitable linear combination between the elements in the observation vector *y* such that *RC=0* with *rank(R)+rank(C)=n*. This is called the Gauss-Helmert model, or "condition equation with unknown parameters":

$$w = Ry = RA\xi + Re\,, \qquad e \sim (0, \sigma_0^2 P^{-1}) \quad . \tag{6.5}$$

Schaffrin and Grafarend (1986) show that the solution to Eq. (6.5) is equivalent to the Gauss-Markov model presented in Eq. (6.1), provided that *RC=0* and the rank condition *rank(R)+rank(C)=n* hold.

6.2 Gauss-Markov model for two independent data sets

This section describes adjustment techniques for a physical phenomenon that has been observed by two independent techniques. For example, it can be the same water level measured by the GPS buoy and by the coastal water level gauge. The constant bias between the means of both data sets is of interest. If there are nuisance parameters, they can be eliminated by finding a suitable matrix *R*. Finally, a Gauss-Markov model can be formed for each data set:

$$\begin{aligned} y_1 &= A_1\xi_1 + e_1\,, \qquad e_1 \sim (0, \sigma_1^2 P_1^{-1}), \\ y_2 &= A_2\xi_2 + e_2\,, \qquad e_2 \sim (0, \sigma_2^2 P_2^{-1}), \qquad Cov\{e_1, e_2\} = 0\,, \end{aligned} \tag{6.6}$$

where ξ_1 and ξ_2 contain the same m parameters to describe the mean of observation y_1 and y_2, respectively. Different design matrices A_1 and A_2 are formed based on the most suitable model for each data set. This can be usually seen in a situation where two data sets are collected for the same physical phenomenon in a distinct way. Therefore, we have to assume the generally different condition matrices B_1 and B_2 must be found for them when forming the equivalent condition equations for both data sets. For instance, both data sets may be collected in different sampling rate. Thus, the least-squares solution can be found:

$$\begin{aligned} \tilde{e}_1 &= P_1^{-1} B_1^T (B_1 P_1^{-1} B_1^T)^{-1} B_1 y_1 \\ \tilde{e}_2 &= P_2^{-1} B_2^T (B_2 P_2^{-1} B_2^T)^{-1} B_2 y_2 \end{aligned} \tag{6.7}$$

The least-squares solutions of $\hat{\xi}_1$ and $\hat{\xi}_2$ can be obtained by substituting $\tilde{e}_1$ and $\tilde{e}_2$ into Eq. (6.6) respectively. Alternatively, normal equations can be formed directly based on:

$$\begin{aligned} \hat{\xi}_1 &= (A_1^T P_1 A_1)^{-1} A_1^T P_1 y_1 \\ \hat{\xi}_2 &= (A_2^T P_2 A_2)^{-1} A_2^T P_2 y_2 \end{aligned} \tag{6.8}$$

with

$$\begin{aligned} D\{\hat{\xi}_1\} &= \sigma_1^2 (A_1^T P_1 A_1)^{-1} \\ D\{\hat{\xi}_2\} &= \sigma_2^2 (A_2^T P_2 A_2)^{-1} \end{aligned} . \tag{6.9}$$

As a result, the relative bias between both data sets can be determined from $\hat{\xi}_2 - \hat{\xi}_1$, and the associated dispersion matrix of the difference vector can be obtained by the law of error propagation:

$$\begin{aligned} D\{\hat{\xi}_2 - \hat{\xi}_1\} &= D\{\hat{\xi}_1\} + D\{\hat{\xi}_2\} \\ &= \sigma_1^2 (A_1^T P_1 A_1)^{-1} + \sigma_2^2 (A_2^T P_2 A_2)^{-1} \end{aligned} \tag{6.10}$$

since the covariance between each element in e_1 and e_2 was assumed to be zero.

6.3 Simplified, but not necessarily equivalent model

Suppose that both data sets were collected for the same physical phenomenon in exactly the same way such that they may share the same design matrix A; then a simplified model could be formed by using the difference of the observations from each data set:

$$\begin{aligned} y_2 - y_1 = A(\xi_2 - \xi_1) + e_2 - e_1, \qquad & e_2 - e_1 \sim (0, \sigma_1^2 P_1^{-1} + \sigma_2^2 P_2^{-1}), \\ & Cov\{e_1, e_2\} = 0. \end{aligned} \tag{6.11}$$

The least-squares solution by forming an equivalent condition model is:

$$\begin{aligned} \widetilde{e_2 - e_1} = & (\sigma_1^2 P_1^{-1} + \sigma_2^2 P_2^{-1}) \\ & B^T (B(\sigma_1^2 P_1^{-1} + \sigma_2^2 P_2^{-1}) B^T)^{-1} B(y_2 - y_1) \end{aligned} \tag{6.12}$$

which is generally not equal to $\tilde{e}_2 - \tilde{e}_1$ as found in Eq. (6.7) unless special conditions such as, e.g.,

$$\sigma_1^2 P_1^{-1} = \sigma_2^2 P_2^{-1} = \sigma_0^2 P^{-1} \tag{6.13}$$

apply. This condition is stringent since it means both data sets have identical stochastic (and functional) variability and also the same number of observations.

The solution of the simplified model is generally different from the use of individual Gauss-Markov models for both data sets as presented in Eq. (6.6). This is because e_1 and e_2 are minimized through the least-squares process without interference among each other when treated individually. In contrast, the object to be minimized in the simplified model is a linear combination of e_1 and e_2. On the other hand, the variance component of one data set can be estimated free from the influence of the other when individual Gauss-Markov models are employed. This will not be the case in the simplified model.

Mäkinen (2002) illustrated the difference between the use of Gauss-Markov models individually in the data sets and the use of the simplified model with three leveling networks. The effect by using different models may reach 22% in some cases and, therefore, it is crucial to choose the correct model if the condition shown in Eq. (6.13) does not hold.

How much difference we can expect in the case of Section 4.4 using the simplified model will now be studied for a typical situation.

6.4 Checking the simplified model solution against the rigorous solution in the case of absolute calibration

A simplified model that uses the difference between the measurements from two independent data sets is defined in Eq. (6.11). In this section, the data from the Lake Erie Calibration Site is used in this simplified model to test the influence of using different models. The simplified model, as seen in Eq. (4.11), used in this section is:

$$h_1 - h_2 = \tau\beta + t\delta + e_1 - e_2, \qquad \begin{aligned} e_1 &\sim (0, \sigma_1^2 P_1^{-1}) \\ e_2 &\sim (0, \sigma_2^2 P_2^{-1}) \\ cov\{e_1, e_2\} &= 0, \end{aligned} \tag{6.14}$$

where the subscripts 1 and 2 represent the altimeter and the water level data sets.

The observation vector is formed by the difference between the altimeter lake surface height measurements (with corrections and gradients applied) and the *in-situ* water level gauge records. The constant bias β and drift δ are to be determined with the least-squares technique. An nx1 vector τ consists of ones and *t* is the vector for elapsed time. It is assumed that the annual signal that presents on both data sets is canceled out by the differencing.

Since the gauge repeated record the water level information every six minutes, one-hour windows is selected and a least-squares fit of the gauge height is produced at the time of closest approach (tca) when the satellite passes the calibration site. The one-hour window is selected based on the same type of gauge in the Great Lakes as discussed in

Cheng (2001). The rms error of the least-squares fit is used in the dispersion matrix for e_2. On the other hand, the dispersion matrix for e_1 is composed of the rms error provided by the altimeter data (JASON-1 from GDR; T/P from the stackfile).

The results are shown in Figures 6.1 and 6.2. It is found that the constant bias estimated for JASON-1 using a simplified model is 109±3 mm, a 5% change as compared to the result derived from the rigorous model (Table 4.4). On the other hand, the constant bias estimated for T/P using a simplified model is 77±6 mm, a 19% change as compared to the result derived from the rigorous model. The reason for the change of the results is because, in part, the condition shown in Eq. (6.13) does not hold for the data sets. The rms errors of the altimeter lake surface height measurements are not consistent with that of the water level gauge and, therefore, result in the different estimates.

On the other hand, the assumption that the annual signal is totally canceled may not be true, especially when two data sets do not have the same sampling rate. An aliasing effect and other signals that are not fully canceled out by the differencing may also contribute to the change of the results.

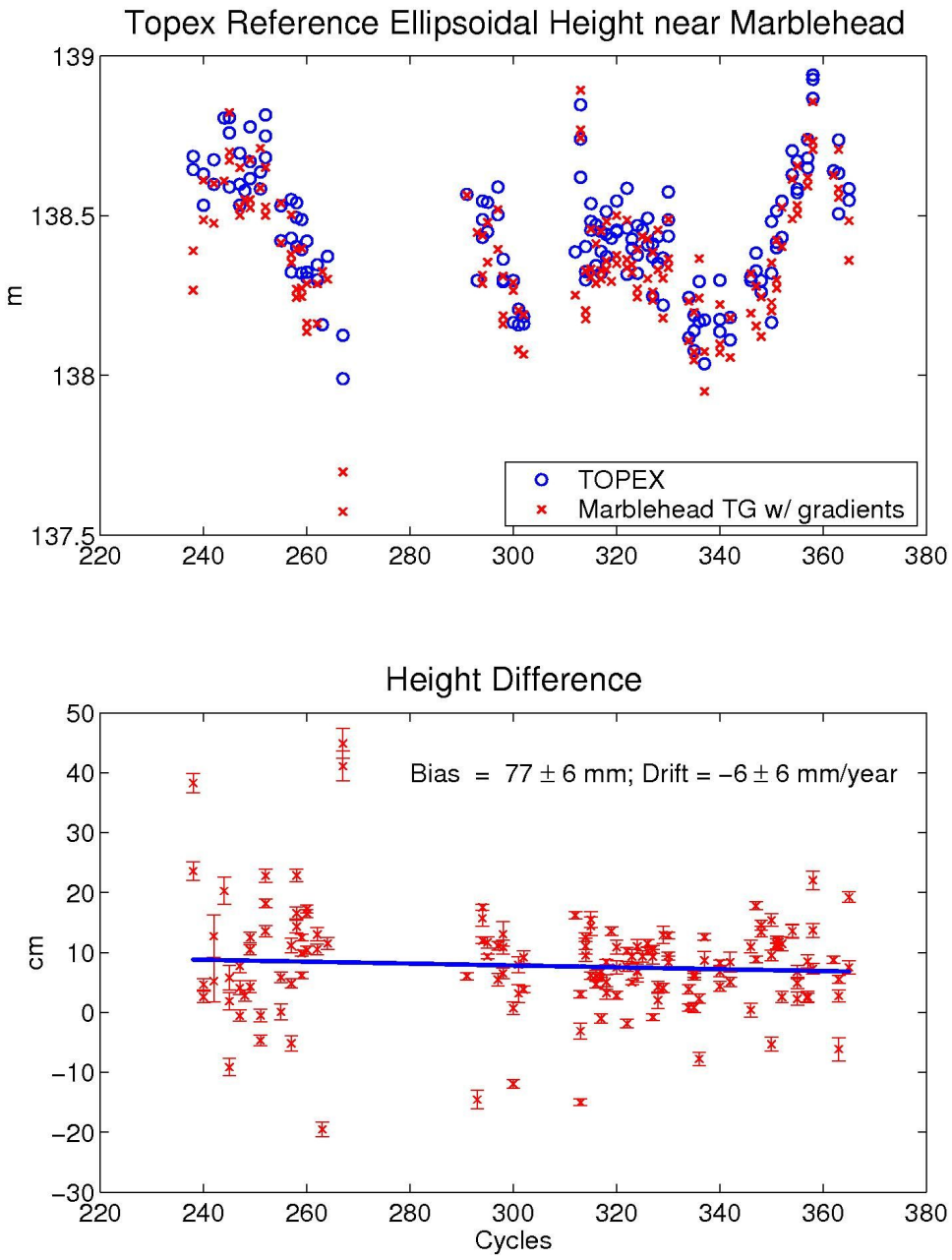

Figure 6.1. The result of using a simplified model using the difference between T/P lake surface height measurements and the gauge records.

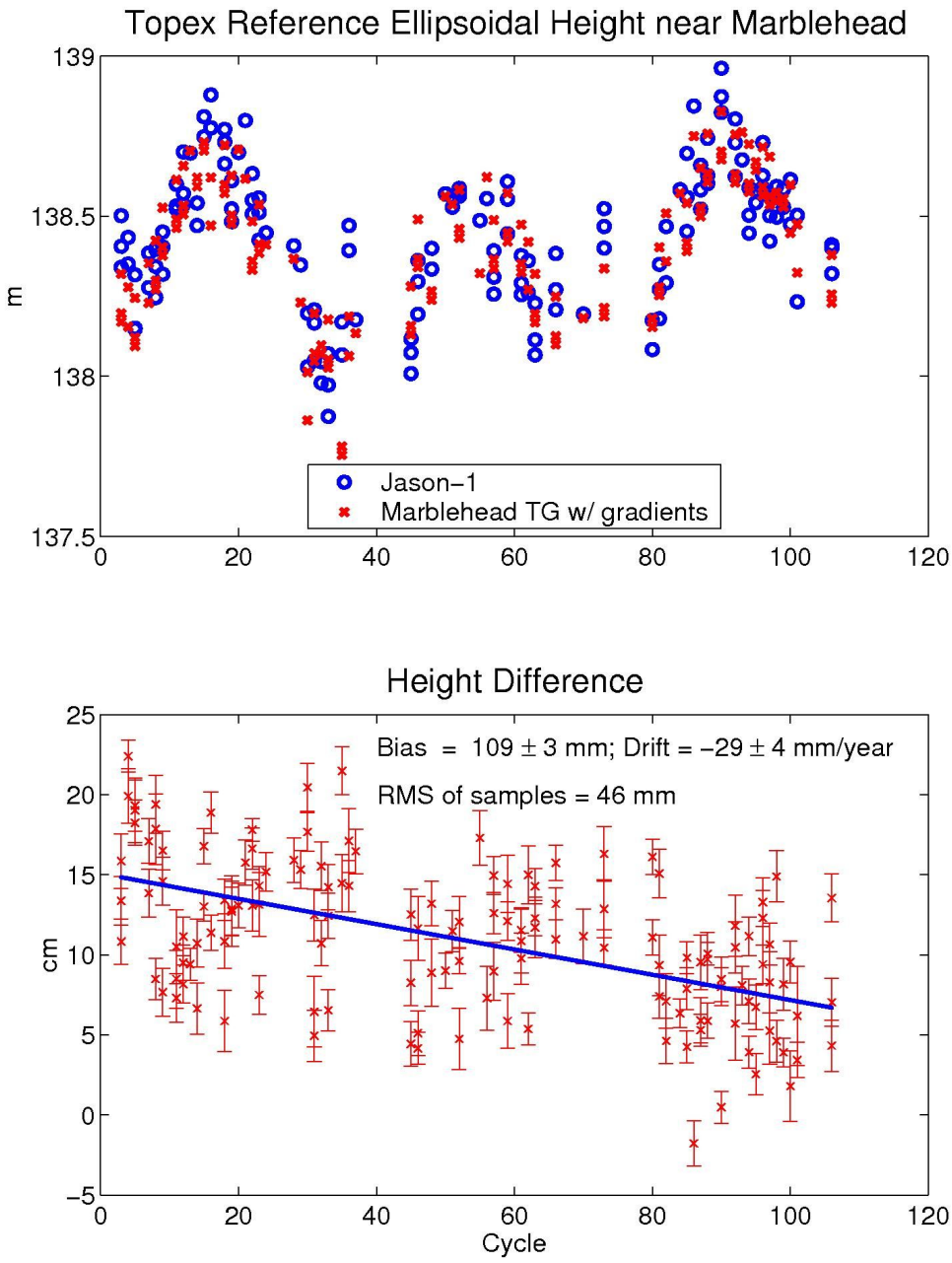

Figure 6.2. The result of using a simplified model using the difference between JASON-1 lake surface height measurements and the gauge records.

6.5 Summary

This chapter briefly presented a typical Gauss-Markov model and the use of it for two independent data sets. A simplified model that uses the difference of the observations from these two independent data sets as the primary observation is also discussed. It is pointed out that the equivalent results can be obtained if the condition shown in Eq. (6.13) holds.

Tests of using the data from the Lake Erie Calibration Site were carried out. The numeric results show that, for the constant bias estimate along, a 5% and a 19% changes can be found when using the simplified model in the cases of JASON-1 and T/P, respectively. The change percentage is smaller than 22% as tested by Mäkinen (2002). It can not be ignored if the rigorous results are desired except the equivalent condition holds.

CHAPTER 7

CONCLUSIONS

The GPS technique is applied in this study to a GPS buoy or a GPS ship in order to collects water level measurements. Different instruments for collecting water level measurements are presented and compared with each other in this study, including coastal water level gauges, bottom pressure gauges, GPS observation and satellite altimetry. An accurate water level is essential to a wide variety of interdisciplinary research fields including glaciology, oceanography, hydrology and geodesy.

Since the epoch-by-epoch solution of a GPS buoy or a GPS-equipped ship is resolved with the DGPS technique, which eliminates the common errors present at the rover and the reference station, such an assumption limits the baseline lengths and, hence, the area for GPS water level applications to be near the shore. As the separation between the buoy and the reference station increases, errors become less common and can be diminished only partially by using DGPS. The analyses in Chapter 2 show that for the baseline longer than 34 km with fewer than 6 satellites, the *a-priori* information about the water level height is needed in order to ensure the correct ambiguities are obtained. The *a-priori* information may be acquired from satellite altimeter ssh measurements,

hydrodynamic models, or the repeated campaigns. For baselines shorter than 34 km, chances are that the ambiguities may be correctly resolved if enough satellites are tracked and the PDOP is smaller than 3, and provided that the buoy sits in calm water. A survey plan before the campaign would be helpful in selecting the optimal observational period with most available satellites.

Accurate ambiguity estimates are essential for cm-level positioning (Leick, 1994). The comparisons in Chapter 2 confirm that. If accurate ambiguity estimates are obtained, the height discrepancy of the buoy is within 4 cm, when comparing the solutions from a 80-km baseline to that of a 20-km one. In addition, if correct ambiguity estimates are obtained, even a 10-second decimated data set produces a height solution that is consistent with the 1-second data set. By lowering the sampling rate, the number of sample reduces rapidly; so does the need of the memory size. However, the solution may end up with incorrect ambiguities due to an inadequate number of samples. As explained in Chapter 2, for example, a 5-second decimated data set with a 34-km baseline may provide vertical jump of ~1 m if the ambiguities are not correctly resolved. Therefore, it is encouraged to collect data in a 1-second interval (or higher) to ensure the quality of the solution.

One of the difficulties in combining the water level record, provided by the traditional coastal water level gauge, to the satellite-based techniques is the lack of a link between the gauge datum and the global reference frame to which the satellite data are collected. Chapter 3 outlines two methods, using the GPS technique, to link the gauge datum to the global reference frame by occupying near the water level gauge: One links the benchmarks with GPS occupations, and the other links the water level with GPS buoy

survey. The pros and cons are discussed but only the latter method is implemented in this study as a generic method to link a bottom pressure gauge in Chapter and a river gauge in Chapter 5 to the global reference frame. A detailed procedure with the associated error budget is provided using the data sets collected from the Cleveland campaign at Lake Erie.

The combination of the water level gauge records with the satellite-based data sets is beneficial. Spatially the gauge records are by the shore whereas the altimeter and GPS buoy measurements are further away from the shoreline and toward the open oceans. Temporally, the longevity of the water level gauge records can fill the temporal gaps found in the satellite-based techniques to help in trend estimation of the global sea level rise, for instance.

Chapter 4 uses GPS water level measurements for altimeter calibration. Two calibration sites at Lake Erie and in the Southwest Pacific were occupied with a GPS buoy and a GPS ship, respectively, to support the global effort for altimeter calibration. The GPS water level measurements may serve as the *in-situ* data for satellite altimeter calibration if the satellite directly passes the buoy. If no direct flight of the satellite altimeter occurred over the location where the GPS buoy deployed, such as in the situations presented at these two sites, the GPS technique (either by a buoy or a ship) can still be used to survey the water surface gradient and to make the connection between an existing water level gauge and the nominal footprint of the altimeter for calibration.

The calibration results for JASON-1 at the Lake Erie Calibration Site are comparable to those from other dedicated sites, such as Harvest and Corsica. However, the results for T/P Side B is slightly larger than the other two sites. This site is arguably

among the first site to employ the use of a coastal water level gauge, 20 km off the satellite ground track, for repeated altimeter calibration. It avoid the need to build a dedicated site on the satellite ground track and, thus, is cost-effective.

The calibration results at the site in Southwest Pacific Calibration Site for ERS-2 and ENVISAT are only preliminary since the GPS data were collected in a 5-second interval with a baseline of ~80 km and an overlapping time of less than one hour. In addition, a simplified adjustment model was used for the results. A campaign with higher sampling rate has been repeated in the are late in 2004 and it is anticipated to improve the results. The impact of using a simplified model on the result at this site remains to be seen.

Chapter 5 presents the potential of the GPS technique for hydrology in conjunction with satellite altimetry and river gauges in observing river stage heights. The use of GPS helps to incorporate river gauge records, possibly collected by different countries in different local datums. Ultimately, the combination of stage data to an unified datum may provide an unambiguous view into the entire watershed area across several countries.

The river stage height gradient is essential to quantify sediment transportation and the river's channel behavior. It was estimated independently with GPS ship measurements along the Branco River. It is found that the gradient is about several cm/km down-stream and the standard deviation of the gradient estimate is better than ±0.4 cm/km, that is consistent with other studies. Unlike using altimeter measurements to estimate river stage

gradient, that are only available in a few certain areas, the advantage of using GPS ship is that the data is available nearly along the entire river, as long as the reference stations can be properly setup along the river.

The processing criteria for ENVISAT in the rivers and the inundation areas are certainly different from those in the oceans. The lack of the wet tropospheric path delay correction for ENVISAT is certainly a cause for these discrepancies. Further attention should be paid to an alternative to the wet tropospheric path delay in the Amazon Basin, as well as the altimeter footprint gradient in the altimeter retracking process in order to obtain more realistic altimetric river stage heights.

The choice of a suitable adjustment model is important. The impact of using the rigorous model against a simplified one may reach 5% and 19% when the real data from the Lake Erie Calibration Site were used for JASON-1 and T/P, respectively. Therefore, it is important to check whether the equivalent condition described in Chapter 6 holds true or not, if it is intended to use a simplified model.

Overall, this study is trying to demonstrate the versatile utilization of GPS water level measurements, collected by a buoy or a ship. The GPS technique helps to improve the existing means of water level collections: Two examples have been shown in this study, namely the calibration of satellite altimeters and the linking of the water level datum to the global reference frame. As new systems such as GALILEO, and the improvement of the current system with new civilian codes and new satellite designs, become available in the near future, it can be envisioned that the water level measurements provided by the integrated GNSS will have even better accuracy, improved capabilities, and for other interdisciplinary applications.

REFERENCES

Alsdorf, D., C. Birkett, T. Dunne, J. Melack, and L. Hess. 2001. Water level changes in a large Amazon lake measured with spaceborne radar interferometry and altimetry. *Geophy. Res. Lett.* 28 (14):2671-4.

Alsdorf. D.E., J.M. Melack, T. Dunne, L.A. Mertes, L.L. Hess, and L.C. Smith. 2000. Interferometric radar measurements of water level changes on the Amazon flood plain. *Nature.* 404:174-7.

Andrews Space & Technology. 2001. GLONASS–Summary. Available online at http://www.spaceandtech.com/spacedata/constellations/glonass_consum.shtml (Accessed on May 11, 2005).

Benveniste, J., M. Milagro-Perez, L. Rempicci, B. Greco, P. Femenisa, and, A. Martini. 2002. ENVISAT altimeter cross-calibration plan and early results. Abstract in EGS XXVII General Assembly, April 21-6, in Nice, France.

Bevis, M., W. Scherer, and M. Merrifield. 2002. Techinical issues and recommendations related to the installation of continuous GPS stations at tide gauge. *Marine Geodesy*. 25:87-99.

Birkett, C.M., L.A. Mertes, T. Dunne, M.H. Costa and M.J. Jasinski. 2002. Surface water dynamics in the Amazon Basin: Application of satellite radar altimetry. *J. Geophy. Res.* 107 (D20) 8059, doi:10.1029/2001JD000609,2002.

Bisnath, S., D. Dodd, D. Wells, S. Howden, D. Wiesenburg, and G. Stone. 2003. Water level recovery with an RTK GPS-equipped buoy. Paper presented at the U.S. Hydro 2003 Conference, March 23-27, in Biloxi, Mississippi, USA.

Blackwell, J., and S. Hilla. 2000. *PAGE-NT User's Manual*. National Geodetic Survey, National Oceanic and Atmospheric Administration, Silver Spring, Maryland, USA.

Bonnefond, P., P. Exertier, O. Laurain, Y. Menard, A. Orsoni, G. Jan, and E. Jeansou. 2003. Absolute calibration of Jason-1 and TOPEX/POSEIDON altimeters in Corsica. *Marine Geodesy*, 26:261-84.

Bonnefond, P., B. Haines, and S. Nerem. 2004. Local to global CalVal experiments: Report of the Splinter Session. Report presented at the OSTST Meeting, November 4-6, in St. Petersburg, Florida, USA.

Bordi, J.J. 1999. Analysis of the Precise Range and Range-Rate Experiment and Its Applications to Precise Orbit Determination. *Ph. D. dissertation*. CRS-99-01. Center for Space Research, University of Texas at Austin, Austin, Texas, USA.

Born, G.H, M.E. Parke, P. Axelrad, K.L. Gold, J. Johnson, K. W. Key, and D.G. Kubitschek. 1994. Calibration of the TOPEX altimeter using GPS buoy. *J. Geophys. Res*., 99 (C12):24517-26.

Bouin, M.-N., V. Ballu, S. Calmant, K. Cheng, C. Shum, and L. Testut. 2003. Absolute height of sea surface by trajectory of GPS antennae over submerged pressure gauges. Poster presented at the AGU Fall Meeting, December 8-12, in San Fransisco, California, USA.

Brakenridge, G.R., S.V. Nghiem, E. Anderson, and S. Chien. 2005. Space-based measurement of River Runoff. *EOS Trans AGU* 86 (19):185-8.

Braun, A., K. Cheng, B. Csatho, and C. Shum. 2004. ICESat laser altimetry in the Great Lakes. Paper presented at the 60th Annual Meeting of the Institute of Navigation, June 7-9, in Dayton, Ohio, USA.

Calman, J. 1987. Introduction to Sea-Surface Topography from Satellite Altimetry. *Johns Hopkins APL Technical Digest*, 8 (2):206-11,

Calmant, S., F. Seyler, A. Braun, M. Cauhope, and M.-P. Bonnet. 2005. ICESat laser altimetry over Amazon Rivers: Validation and multi-techniques cross-calibration. In progress.

Calmant, S., K. Cheng, G. Jan, C. Kuo, C. Shum, Y. Yi, V. Ballu, and M.-N. Bouin. 2004. Comparison of sea surface heights derived from satellite altimetry and from ocean bottom pressure gauges: The SW Pacific MOTEVAS Project. *Marine Geodesy* 27:597-613.

Calmant, S., B. Pelletier, P. Lebellegard, M Bevis, F W. Taylor, and D A. Phillips. 2003. New insights on the tectonics along the New Hebrides subduction zone based on GPS results. *J. Geophys. Res.* 108 (B6):2319-40.

Cardellach, E., E. Behrend, G. Fuffini, and A. Rius. 2002. The use of GPS buoys in the determination of oceanic variables. *Earth Planets Space* 52:1113-6.

Chelton, D.B., J. Ries, B. Haines, L.-L. Fu, and P. Callahan. 2001. Satellite altimetry. In *Satellite Altimetry and Earth Sciences: A Handbook for Techniques and Applications* edited by L.-L. Fu and A. Cazenave, 1-131, Academic Press, San Diego, California, USA.

Cheng, K. 2004. *GPS Buoy Campaigns for Vertical Datum Improvement and Radar Altimeter Calibration.* Report No. 470. Geodetic Science and Surveying in the Department of Civil and Environmental Engineering and Geodetic Science, The Ohio State University, Columbus, Ohio, USA.

Cheng, K. 2001. Radar Altimeter Absolute Calibration Using GPS Water Level Measurements. *M.S. Thesis.* Department of Civil and Environmental Engineering and Geodetic Science, The Ohio State University, Columbus, Ohio, USA.

Cheng, K., C. Shum, C. Han, Y. Yi, and D. Martin. 2001. Application of GPS-buoy water level instrument for radar altimeter calibration. In *Gravity, Geoid, and Geodynamics 2000 : GGG2000 IAG International Symposium,* International Association of Geodesy Symposia, Sym. 123. Edited by M.G. Sideris. Berlin: Springer.

Christensen, E.J., B.J. Haines, S.J. Keihm, C.S. Morris, R.A. Norman, G.H. Purcell, B.G. Williams, B.D. Wilson, G.H. Born, M. E. Parke, S.K. Gill, C.K. Shum, B.D. Tapley, R. Kolenkiewicz, and R.S. Nerem. 1994. Calibration of TOPEX/POSEIDON at Platform Harvest. *J. Geophys. Res.* 99 (C12):24465-85.

Clark, J.E. 2004. GPS III Program: Goals and Status. Presented at the IEEE Position, Location and Navigation Symposium 2004, April 24-7, in San Diego, California, USA.

Cohen, J.E., C. Small, A. Mellinger, J. Gallup, and J. Sachs. 1997. Estimates of coastal population. *Science* 278:1211-2.

Coordinating Committee on Great Lakes Basic Hydraulic and Hydrologic Data. 1995. *Establishment of International Great Lakes Datum (1985).* Available online at http://chswww.bur.dfo.ca/danp/igld1985.html (Accessed on April 20, 2005).

Croarkin, C. and P. Tobias, editors. 2005. *NIST/SEMATECH e-Handbook of Statistical Methods*. Available online at http://www.itl.nist.gov/div898/handbook/ (Accessed on April 19, 2005).

Dillinger, W., M. Cline, R. Foote, S. Hilla, J. Ray, R. Snay, and Soler, T. 2003. Analysis of nine years of North American CORS data. *EOS Trans. AGU.* 84 (46), Fall Meeting Suppl. Abstract G31B-0701, 2003.

Douglas, B.C. 2001. An introduction to sea level. In *Sea Level Rise, History and Consequences*. International Geophysics Series, Vol. 75. Edited by B.C. Douglas, M.S. Kearney, and S.P. Leatherman. San Diego: Academic Press.

Douglas, B.C. 1997. Global sea level rise: A redetermination. *Surveys in Geophysics.* 18:279-92.

El-Rabbany, A. 2002. *Introduction to GPS: The Global Positioning System*. Boston/MA: Artech-House, Inc.

Emery, K.O., and D.G. Aubrey. 1991. *Sea Levels, Land Levels, and Tide Gauges.* New York: Springer-Verlag.

European Commission. 2003. *The Galileo Project, GALILEO Design Consolidation*. Guildford/U.K.: ESYS plc.

European Space Agency. 1997. Mission in Operation: ERS (ESA Remote Sensing Satellit). Available online at http://www.esoc.esa.de/external/mso/ers.html (Accessed February 1, 2005).

Filloux, J.H. 1980. Pressure fluctuations on the open ocean floor over a broad frequency range: New program and early results. *Journal of Physical Oceanography* 10(12): 1959-71.

Frappart, F., S. Calmant, M. Cauhope, F. Seyler, and A. Cazenave. 2005. Preliminary results for ENVISAT RA-2 derived water levels validation over the Amazon Basin. Submitted to *Remote Sensing of Environment* .

Fu., L.L., E.J. Christensen, C.A. Yamarone, M. Lefebvre, Y. Menard, M. Dorrer, and P. Escudier. 1994. TOPEX/POSEIDON Mission Overview, *J. Geophys. Res.,*99 (C12):24369-81.

Garcia-Lopez, R.V. 1997. *Determination of Vehicle Acceleration by Using the GPS Phase Acceleration.* Report No. 440. Geodetic Science and Surveying in the Department of Civil and Environmental Engineering and Geodetic Science, The Ohio State University, Columbus, Ohio, USA.

Gaspar, P., S. Labroue, F. Ogor, G. Lafitte, L. Marchal, and M. Rafanel. 2002. Improving nonparametric estimates of the sea state bias in radar altimeter measurements of sea level. *J. Atmos. & Oceanic Tech.* 19:1690-707.

Gaspar, P., F. Ogor, P.Y. Le Traon, and O.Z. Zanife. 1994. Estimating the sea state bias for the TOPEX and POSEIDON altimeters from crossover differences. *J. Geophys. Res.* 99 (C12):24981-94.

Gesch, D.B. 1998. Accuracy assessment of a global elevation model using shuttle laser altimeter data. In *Geoscience and Remote Sensing Symposium Proceedings, 1998. IGARSS '98. 1998 IEEE International*. IEEE, doi:10.1109/IGARSS.1998.702752.

Gesch, D., and R. Wilson. 2001. Development of a seamless multisource topographic/bathymetric elevation model of Tampa Bay. *Marine Technology Society Journal* 35, 4:58-64.

Goad, C.C. 1998. Short distance GPS models. In *GPS for Geodesy*, 2nd edition. Edited by P.J. Teunissen and A. Kleusberg. Berlin: Springer-Verlag.

Gopalapillai, S., A.G. Mourad, and M. Kuhner. 1975. Satellite altimetry applications to geodesy, oceanography and geophysics. *Ocean. Proceedings: Annual Conference – Marine Technology Society.* 508–514. New York: Institute of Electrical and Electronics Engineers.

Guman, M.D. 1997. Determination of Global Mean Sea Level Variations Using Multi-Satellite Altimetry. *Ph. D. dissertation.* Department of Aerospace Engineering and Engineering Mechanics, The University of Texas at Austin, Austin, Texas, USA.

Guzkowsak, M.A., C.G. Rapley, J. K. Ridley, W. Cudlip, C.M. Birkett, and R.F. Scott. 1990. Developments in inland water and land altimetry. *ESA Contract*, CR-7839/88/F/FL.

Haines, B., P. Bonnefond, G. Born, P. Exertier, S. Gill, E. Jeansou, D. Kubitschek, G. Jan, O. Laurain, Y. Menard, and A. Orson. 2002a. Calibrating the JASON-1 measurement system: Initial results from the Corsica and Harvest verification experiments. Presented at the AGU Fall Meeting, December 6, in San Francisco, California, USA.

Haines, B., D. Kubitschek, G. Born, and S. Gill. 2002b. Monitoring Jason-1 and TOPEX/POSEIDON from an offshore platform: The Harvest Experiment. Paper presented at the Jason-1 Science Working Team Meeting, October 21-23, in New Orleans, Louisiana, USA.

Hayne, G.S. 1999. *Topex Altimeter Range Stability Estimate Update.* NASA GSFC Wallop Flight Facility, Observational Science Branch, Wallops Flight Facility, Wallops Island, Virginia, USA. Available online at ftp://topex.wff.nasa.gov/RngStbUp.txt (Accessed on April 20, 2005).

Hayne, G.S., and D.W. Hancock. 2000. *Topex Side B Sigma0 Calibration Table Adjustment,* NASA, Goddard Space Flight Center, Wallops Flight Facility.

Hein, G.W., H. Blomenhofer, H. Landau and E. Taveira. 1992. Measuring sea level changes using GPS in buoys. In *Sea Level Changes: Determination and Effects,* Geophysical Monograph 90, IUGG Vol. 11. Edited by P.L. Woodworth, D.T. Pugh, J.G. DeRonde, R.G. Warrick, and J. Hannah. Washington, DC: American Geophysical Union and International Union of Geodesy and Geophysics.

Hein, G.W., H. Landau, and H. Blomenhofer. 1990. Determination of instantaneous sea surface, wave heights, and ocean currents using satellite observations of the Global Positioning System. *Marine Geodesy* 14:217-24.

Heiskanen, W.A., and H. Moritz. 1967. *Physical Geodesy*,Institude of Physical Geodesy, Technical University Graz, Austria :reprinted.

Hess, K. 2001. *Generation of Tidal Datum Fields for Tampa Bay and the New York Bight,* NOAA Technical Report NOS CS 11, National Oceanographic and Atmospheric Administration, USA.

Hofmann-Wellenhof, B., H. Lichtenegger, and J. Collins. 1997. *GPS Theory and Practice*. 4th edition. New York: Springer-Verlag Wien New York.

Institut de Recherche pour le Développement. 2003. *Rapport de Mission Branco*, in French. Available online in http://www.mpl.ird.fr/hybam/campagnes/br_33.pdf (Accessed on June 13, 2005).

Jekeli, C. 2000. *Heights, the Geopotential, and Vertical Datums.* Report No. 459. Geodetic Science and Surveying in the Department of Civil and Environmental Engineering and Geodetic Science, The Ohio State University, Columbus, Ohio, USA.

Kaula, W.M. 1969. *The Terrestrial Environment: Solid Earth and Ocean Physics, Application of Space and Astronomic Techniques.* Report of a Study at Williamstown, Massachusetts, August 1969, to the National Aeronautics and Space Administration. Cambridge, Massachusetts, USA.

Kelecy, T.M., G.H. Born, M.E. Parke, and C. Rocken. 1994. Precise mean sea level measurements using the Global Positioning System. *J. Geophys. Res.* 99 (C4):7951-9.

Key. K, M. Parke, and G. Born. 1998. Mapping the sea surface using GPS buoy. *Marine Geodesy* 21:67-79.

Koch, K-R. 1987. *Parameter Estimation and Hypothesis Testing in Linear Model*. Springer-Verlag:Berlin.

Kruizinga, G.L. 1997. Validation and Applications of Satellite Radar Altimetry. *Ph.D. dissertation.* Department of Aerospace Engineering and Engineering Mechanics, The University of Texas at Austin, Austin, Texas, USA

Kuo, C.Y., C.K. Shum, and A. Braun. 2004a. Crustal vertical motion inferred by tide gauges and satellite altimetry. Paper presented at the 60th Annual ION Meeting, June 7-9, in Dayton, Ohio, USA.

Kuo, C.Y., C.K. Shum, A. Braun, and J.X. Mitrovica. 2004b. Vertical crustal motion determined by satellite altimetry and tide gauge data in Fennoscandia. *Geophysical Research Letters* 31:doi:10.1029/2003GL019106.

Langley, R.B. 1993. The GPS observables. *GPS World*, 4(4):55-9. Paper presented in the 12th European Frequency and Time Forum (EFTF'98), March 10-2 in Warsaw, Poland.

Lebedev, M. 1998. GLONASS as instrument for precise UTC transfer.

Leendertse, J., and S. Liu. 1978. A three-dimensional turbulent energy model for non-homogeneous estuaries and coastal sea systems. In: *Hydrodynamics of Estuaries and Fjords.* Edited by J. Nihoul. Amsterdam: Elsevier.

LeProvost, C., F. Lefevre, F. Lyard, and L. Roblou. 2002. FES2002–A New Version of the FES Tidal Solution Series, LEFOS Internal Report.

Leick, A. 1994. *GPS Satellite Surveying,* second ed., New York:Wiley.

Llewellyn, S.K., and R.B. Bent. 1973. *Documentation and description of the Bent ionospheric model*, AFCRL-TR-73-0657.

Li, R., K.W. Bedford, C.K. Shum, J.R. Ramirez, A. Zhang, and K. Di. 2002. Digitalization of coastal management and decision making supported by multi-dimensional geospatial information and analysis. Paper presented at NSF National Conference for Digital Government Research, May 20-2, in Los Angeles, California, USA.

Liebsch, G., K. Novotny, and R Dietrich. 2002. Comparison of multimission altimetric sea-surface heights with tide gauge observations in the Southern Baltic Sea. *Marine Geodesy* 25:213-34.

Lisitzin, E. 1974. *Sea Level Changes*, Elsevier Oceanographic Series, 8, New York.

Lorell, J., E. Colquitt, and R.J. Anderle. 1982. Ionospheric correction for SEASAT altimeter height measurement., *J. Geophys. Res.* 87 (C5):3207-12.

Mader, G., D. Martin, and T. Schöne. 2001. *GPS Water Level Measurements,* Mid-term Report SSG2.194. IAG Travaux 2001. Available online on http://op.gfz-potsdam.de/altimetry/SSG_buoys/index.html (Accessed on April 10, 2004).

Mader. G. 1999. GPS antenna calibration at the National Geodetic Survey. *GPS Solutions*, 3 (1):50-8.

Mader, G.L. 1986. Dynamic positioning using Global Positioning System carrier phase measurements. *Manuscr. Geod.* 11:272-77.

Mäkinen, J. 2002. A bound for the Euclidean norm of the difference between the best linear unbiased estimator and a linear unbiased estimator. *J. Geodesy*. 76:317–22.

Manville, A., and M. Craymer. 2005. Present-day tilting of the Great Lakes region based on tide gauges. *Geol. Soc. Am. Bull.* 117 (7):1070-80.

Martinez-Benjamin, J., M. Martinez-Garcia, J. Garate, J. Martin-Davila, J. Ferrandiz, M. Vigo-Aguiar, M. Ortiz-Castellon, J. Talaya, B. Perez, G. Kruizinga, B. Haines, O. Colombo, B. Chao, C. Shum, M. Parke, S. Han, and K. Cheng. 2000. The T/P CATALA altimeter calibration campaign. Presented at the Spring AGU Meeting, May 30-June 3, in Washington D.C., USA.

Meade, R.H., J.M. Rayol, S.C. Conceicao, and J.R. Natividade. 1991. Backwater effects in the Amazon River Basin of Brazil. *Environmental Geology and Water Sciences* 18 (2):105-14.

Menard, Y., P. Escudier, L.-L. Fu, and G. Kunstmann. 2000. Cruising the ocean from space with JASON-1. In EOS, Transactions. *Amer. Geophys. Un.* 81(34):318,390-1.

Menard, Y., L. Fu, P. Escudier, F. Parisot, J. Perbos, P. Vincent, S. Desai, B. Haines, and G. Kunstmann. 2003. The Jason-1 mission. *Marine Geodesy*, 26:131-46.

Milbert, D. 2002. VDatum Transformation Tool (new Version 1.05), The Geo Community Spatial News, Available online on http://spatialnews.geocomm.com/features/vdatum/. (Accessed on October 20, 2003).

Moritz, H. 1992. Geodetic Reference System 1980. *Bulletin Geodesique,* 66, (2): 187-92.

Morris, C.S., and S.K. Gill. 1994. Evaluation of the TOPEX/POSEIDON altimeter system over the Great Lakes. *J. Geophys. Res.* 99 (C12):24527-40.

Murphy, C.M., P. Moore, and P.L. Woodworth. 1996. Short-arc calibration of the ERS-1 and TOPEX/Poseidon altimeters utilising in-situ data. *J. Geophys. Res.* 101 (C6): 14191-200.

National Geodetic Survey. 2004. CORS Coordinates. Available online at http://www.ngs.noaa.gov/CORS/metadata1/ (Accessed on January 7, 2005).

National Geodetic Survey. 2003a. International Great Lakes Datum of 1985. Available online at http://www.ngs.noaa.gov/TOOLS/IGLD85/igld85.shtml (Accessed on January 7, 2005).

National Geodetic Survey. 2003b. What are datasheets. Available online at http://www.ngs.noaa.gov/cgi-bin/datasheet.prl?Explain=DATASHEET, (Accessed on January 7, 2005).

National Geodetic Survey. 2001. Technical information page for G99SSS, GEOID99 and DEFLEC99. Available online on http://www.ngs.noaa.gov/GEOID/GEOID99/tech.html (Accessed on January 7, 2005).

National Oceanographic Data Center. 2003. Datasets and products: World Ocean Atlas 2001. Available online at http://www.nodc.noaa.gov/OC5/WOA01/pr_woa01.html (Accessed May 1, 2004).

Neilan, R.E., A. Moore, J. Dow, G. Gendt, and R. Weber. 2004. International GPS Service–Ten years history, new directions for GNSS and space geodesy. Poster presented at AGU Fall Meeting, December 13-7, in San Francisco, California, USA.

Niu, X. C. Kuo, V. Velissario, R. Li, K.W. Bedford and C.K. Shum. 2003. Multi-source coastal data analysis. Paper presented at 2003 National Conference on Digital Government Research, May 18-21, in Boston, Massachusetts, USA.

Park, Y., and B. Saint-Guily. 1992. Sea level variability in the Crozet-Kerguelen-Amsterdam area from bottom pressure and Geosat altimetry, In *Sea Level Changes: Determination and Effects*, 117–131. Edited by P.L. Woodworth et al. Geophysical Monograph 69, IUGG, Volumn 11, IUGG. Washingtom, DC: American Geophysical Union: International Union of Geodesy and Geophysics.

Parker, B., D. Milbert, K. Hess, and S. Gill. 2003. National VDatum–The implementation of a national vertical datum transformation database. Paper presented at the U.S. Hydro 2003 Conference, March 23–27, in Biloxi, Mississippi, USA.

Peltier, W. 2002. Global glacial isostatic adjustment: Palaeogeodetic and spatial-geodetic tests of the ICE-4G (VM2) model. *J. Quaternary Science.* 17 5–6:491–510.

Ponte, R.M. 1993. Variability in a homogeneous global ocean forced by barometric pressure. *Dyn. Atmos. Oceans.* 18:209–34.

Resti, A., J. Benveniste, M. Roca, G. Levrini, and J. Johannessen. 1999. The ENVISAT radar altimeter system (RA-2). *ESA Bulletin* 98.

Rocken, C, T.M. Kelecy, G.H. Born, L.E. Young, G.H. Purcell Jr., and S.K. Wolf. 1990. Measuring precise sea level from a buoy using the Global Positioning System. *Geophysical Research Letters* 17 (12):2145–8.

Schäfer, W., and W. Schumann. 1995. PRARE-2 Building on the lessons learnt from ERS-1. *ESA Bulletin.* 83:38–40.

Schaffrin, B., and E. Grafarend. 1986. Generating classes of equivalent linear models by nuisance parameter elimination. *Manuscripta Geodaetica* 11:262–71.

Schöne, T. 2000. *GPS Water Level Measurements,* Final Report SSG2.194. Presented at the EGS General Assembly, Apr. 26, in Nice, France.

Schöne, T., M. Forberg, R. Galas, and C. Reigber. 2002. GPS-buoy for lifetime RA drift monitoring. AGU Fall Meeting 2002, *EOS Trans. AGU*, 83 (47), Fall Meeting Suppl., Abstract OS52A0189, 2002.

Schueler, T., B. Zimmermann, B. Riedl, and G.W. Hein. 2003. Radar altimeter calibration of the Envisat satellite: An autonomous system of high-precision for instantaneous sea surface height determination. In *Proceeding of NTM 2003*– National Technical Meeting, 397–406. January 22–24, in Anaheim, California, USA.

Schutz, B.E., G. Kruizinga, D. Kuang, P.A. Abusali, C.K. Shum, R. Gutierrez, S. Nelson, and E. Rodriguez. 1995. Galveston Bay experiment for altimeter calibration. Paper presented at American Geophysical Union Fall Meeting*,* December 11–15, in San Francisco, California, USA.

Schwab, D.J., K.W. Bedford, and F.H. Quinn. 1996. Overview of the Great Lakes coastal forecasting system. *Proc. 11th International Conference on IIPS for Meteorology, Oceanography, and Hydrology*, Amer. Meteor. Soc., 132–133, Boston, Massachusetts, USA.

Schwarz, C.R. 1990. *North American Datum of 1983.* NOAA professional paper, NOS 2, National Geodetic Survey. Rockville, Maryland, USA.

Seeber, G. 1993. *Satellite Geodesy.* Berlin, New York: Walter de Gruyter.

Shum, C., and M. E. Parke. 1999. *Current GPS-buoy sea level research,* Draft. The Ohio State University, Columbus, Ohio, USA.

Shum, C., Y. Yi, K. Cheng, C. Kuo, A. Braun, S. Calmant, and D. Chambers. 2003. Calibration of Jason-1 altimeter over Lake Erie. *Marine Geodesy* 26:335–54.

Smith, D.A., and D.R. Roman. 2001. GEOID99 and G99SSS: 1-arc-minute geoid models for the United States. *J. Geodesy* 75:169–90.

Snay, R.A. 1999. Using the HTPD software to transform spatial coordinates across time and between reference frames. *Surveying and Land Information Systems*, 59 (1):15–25.

Snay, R., M. Chin, D. Conner, T. Soler, C. Zervas, J. Oyler, M. Craymer, M. Piraszewski, S. Gutman, C. Shum, K. Cheng, and C.-Y. Kuo. 2002. Great Lakes Continuous GPS (CGPS) Network for geodynamics, meteorology, and safe navigation. Poster presented at the Weikko A. Heiskanen Symposium in Geodesy, October 1–5, in Columbus, Ohio, USA.

Snow, K. 2002. *Application of Parameter Estimation and Hypothesis Testing to GPS Network Adjustment*. Report No. 465. Geodetic Science and Surveying in the Department of Civil and Environmental Engineering and Geodetic Science, the Ohio State University, Columbus, Ohio, USA.

Snow, K.B., and B. Schaffrin. 2004. GPS-network analysis with BLIMPBE: A less biased alternative to least-squares adjustment. Paper presented at the 60th Annual Meeting of the Institute of Navigation, June 7–9, in Dayton, Ohio, USA.

Snow, K.B. and B. Schaffrin. 2003. Three-dimensional outlier detection for GPS networks and their densification via the BLIMPBE approach. *GPS Solutions* 7:130–9.

Soler, T., J.D. Love, L.W. Hall and R.H. Foote. 1992. GPS results from statewide high precision networks in the United States. *Proc. 6th DMA,* 2:573–82.

Tapley, B.D., J.B. Lundberg, and G.H. Born. 1982. The SEASAT altimeter wet tropospheric range correction, *J. Geophys. Res.,* 87 (C5):3213–20.

Tapley B.D., C. K. Shum, J.C. Ries, S.R. Poole, P.A. Abusali, S.V. Bettadpur, R.J. Eanes, M.C. Kim, H.J. Rim, and B.E. Schutz. 1997.The TEG-3 geopotential model. In: Proc Gravity Geoid and Marine Geodesy 1996 International Symposia. IAG Symp 117. Edited by K. Schwarz. Springer: New York.

Thurman, H.V. 1991. *Introductory Oceanography*. 6th edition. New York: Macmillan Publishing Company.

Trupin, A., and J. Wahr. 1990. Spectroscopic analysis of global tide gauge sea level data. *Geophys. J. Int.* 100:441–53.

Urban, T.J. 2000. The Integration and Applications of Multi-Satellite Radar Altimetry. *Ph.D. dissertation.* Department of Aerospace Engineering and Engineering Mechanics. The University of Texas at Austin, Austin, Texas, USA.

U.S. Naval Observatory. 2005. Block II Satellite Information. Available online at ftp://tycho.usno.navy.mil/pub/gps/gpsb2.txt (Accessed on April 20, 2005).

U.S. Navy 2005. Navy GEOSAT Follow-ON Altimetry Mission. Available online at http://gfo.bmpcoe.org/gfo (Accessd on September 18, 2005).

Watson, C., R. Coleman, N. White, J. Church, and R. Govind. 2003. Absolute calibration of TOPEX/Poseidon and Jason-1 using GPS buoys in Bass Strait, Australia. *Marine Geodesy* 26:285–304.

White, N., R. Coleman, J. Church, P. Morgan, and S. Walker. 1994. A southern hemisphere verification for the TOPEX/Poseidon satellite altimeter mission. *J. Geophys. Res.* 99 (C12):24505–16.

Woodworth, P.L., D.T. Pugh, J.G. DeRonde, R.G. Warrick, and J. Hannah. 1992. *Sea Level Changes: Determination and Effects.* Preface. Washington, DC: American Geophysical Union and International Union of Geodesy and Geophysics.

Wunsch, C. 2001. Global problems and global observations. In *Ocean Circulation and Climate: Observing and Modelling the Global Ocean.* 47–58. Academic Press. San Diego, California, USA.

Yi, Y, 2000. OSU Stackfile, Department of Civil and Environmental and Geodetic Science, The Ohio State University, Columbus, Ohio, USA.

Young, L.E., S.C. Wu, and T.H. Dixon. 1986. Decimeter GPS positioning for surface element of sea floor geodesy system. *Proc., International Symposium on Marine Positioning*, Reston, Virginia, USA, October 14–17.

Zhao, C., C.K. Shum, Y. Yi. 2003. Calibration results of GFO. In *Satellite Altimetry for Geodesy, Geophysics and Oceanography*. International Association of Geodesy Symposia. Vol. 126. Edited by C. Hwang, C. Shum, and J. Li. Springer: New York.

Zilkoski, D., and D'Onofrio, D. 1996. *Geodetic Phase of NOS' San Francisco Bay Demonstration Project.* National Geodetic Survey, National Oceanographic and Atmospheric Administration, USA. Available online on http://www.ngs.noaa.gov/initiatives/HeightMod/Geodetic/sfbay_geodetic.html (Accessed on October 10, 2003).

Zilkoski, D.B., J.H. Richards, and G.M. Young. 1992. Results of the general adjustment of the North American Vertical Datum of 1988. *Surveying and Land Information Systems,* 52, (3):133–49.